Eötvös Loránd University
Faculty of Science

Master's Thesis

Technical and Clinical Examination of Plasma Anodized Titanium Implant Surface Treatment

Author:
Ambrus Karai,
Materials Science MSc student

Supervisor:
Sándor Olasz,
PhD student at BME ATT

2015, Budapest

Nyilatkozat

- Név: Karai Ambrus
- ELTE Természettudományi Kar, szak: anyagtudomány MSc
- Neptun azonosító: J4AD39
- Szakdolgozat címe: Technical and clinical examination of plasma anodized titanium implant surface treatment

A szakdolgozat szerzőjeként fegyelmi felelősségem tudatában kijelentem, hogy a dolgozatom önálló munkám eredménye, saját szellemi termékem, abban a hivatkozások és idézések standard szabályait következetesen alkalmaztam, mások által írt részeket a megfelelő idézés nélkül nem használtam fel.

Aláírás: _____

Dátum: _____

Declaration of Authorship

- Author: Ambrus Karai
- Eötvös Loránd University
- Faculty of Science
- Materials Science MSc
- Thesis title: Technical and clinical examination of plasma anodized titanium implant surface treatment

I hereby certify that this thesis has been composed by me and is based on my own work, unless stated otherwise. No other person's work has been used without due acknowledgement in this thesis. All references have been quoted according to the standard rules.

Signed: _____

Date: _____

Abstract

Technical and Clinical Examination of Plasma Anodized Titanium Implant Surface Treatment

by Ambrus KARAI

Plasma electrolytic oxidation of commercial pure titanium with textured surface was investigated in this work for the purpose of the development of dental implant's surface. With complex literature investigation no former article was found about this topic. The aim of this thesis is to develop a hybrid treatment for titanium which is able to induce osseointegration, thus shorten the healing time and enhance lifespan of an implant by increasing its adhesion to the bone. It was proven that an implant's porous surface in the range of 1...10 μm can influence osseointegration. The PEO treatment is clinically suitable to develop morphology in this range. Laser textured surfaces can promote ordered cell proliferation and cell adhesion with 10...150 μm feature size on the surface. For this purpose *only PEO treated* and *laser textured than PEO treated* surface were prepared. Composition and morphology of the surfaces created by the two method were similar. 1...5 μm micro-holes appeared on the surface during the PEO treatment accompanied by bioactive anatase formation and phosphorous incorporation. The laser textured coating had surface features in the size of 100 μm. With the clinical evaluation it was shown that the surface which was only PEO treated seems to be equivalent to the market leader implant manufacturer, the Noble BioCare's TiUnite surface.

Contents

List of Figures

List of Tables

Chapter 1

Introduction

1.1 Prequel

As the start of my third semester on the university I had to begun working on my thesis. First of all, I had to choose a topic. I knew that I wanted to work on a topic which connected to applied technology. The interdisciplinarity and practical sides of medical implants got my attention. This subject incorporates physics of metals and ceramics, electrochemistry, colloidics, materials testing, control theory, health science, quality control and some business knowledge. I consulted with Sándor Olasz at the Budapest University of Technology and Economics, Department of Materials Science and Engineering. His specialities include biomaterials and implant development. He accepted my ask for supervising my thesis, offered me a topic about the plasma anodization of dental implants and suggested me project tasks.

1.2 Aim of the thesis

The aim of this thesis is to develop technology parameters for the plasma electrolytic oxidation of titanium for biomedical applications. The four project tasks in order:

1. Summarize the technical literature about the passivation and surface modification of titanium implants regarding those biocompatibility properties.
2. Design experiments for the plasma anodization of titanium samples with different parameters. Execute the experiments.
3. Examine the plasma anodized samples and compare the results with the datas from the literature.

4. Evaluate the results of the material testings and make proposals for optimizing the technology parameters and for the biocompatibility validation processes.

Chapter 2

Theoretical summary

2.1 Historical overview of dental restoration

Various devices for replacing missing body parts are being used for many thousand years. The substitution of missing teeth have always been a special case, because beside the funtional role it may fully serve aesthetically. Ancient civilisations replaced missing teeth with prosthesis made from mood, seashell, stone, carved ivory. Transplanting teeth from animals and humans also occured. Gold was being used because of its corrosion resistance and durability. Of course, these solutions often led to inflammation or rejection causing the loss of implant. Ceramic implants was introduced in the 18th century, these were fixed with low-melting point metals. In the 19th century other materials appeared for dental substitution like amalgam (mercury-based alloy), plaster, gold and zinc alloys, polymer resins. At the end of the century J. Maggiolo introduced a new technique: a tooth-root-shaped implant was cast from 18 carat gold, that was surgically implanted into the jawbone, and after a healing period porcelain crown was attached to the metallic root. The first threaded, self-drilling capable implant appeared in the late 1930s. Until that time various materials came up as implants, like Vitallium (65 w% Co, 30 w% Cr, 5 w% Mo), sapphire ($\alpha - Al_2O_3$) and even methyl methacrylate. The success rates of these implant were low, infection and incapsulation often appeared. New cast alloys with improved properties has appeard the latter 20th century, they showed smaller density, greater stiffness, greater strength and reduced costs. Cobalt-chromium, nickel-chromium, pure titanium, noble alloys and base metal alloys came into production, a wide range of dental products fabricated from them: inlays, outlays, crowns, fixed and removable substitutions, all-metal and metal-ceramic implants. Nowadays titanium and its alloys are the only metals that are being used for dental implantation. Per-Ingvar Brånemark considers the "father of modern dental implantology". In the 1970s

he developed a novel implantation system (see Figure 2.1) and indroduced a multi-stage surgical technique. In the first step of this technique the implant is placed into the jaw and depending on bone quality left there for months. During this time the implant integrates with the surrounding tissues while it is protected from external impacts. In the second stage the implant is uncovered and the abutment and the prosthesis is placed on it. [1–3]

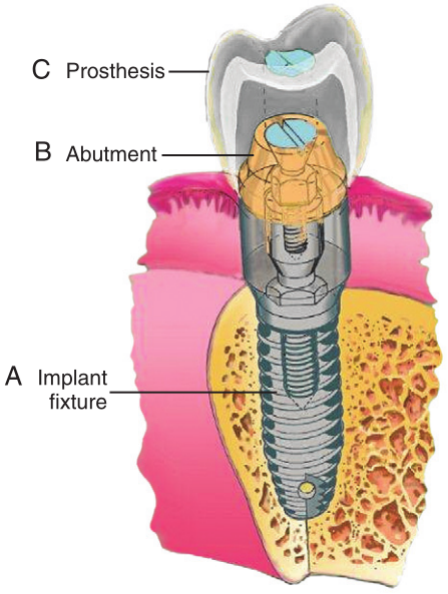

FIGURE 2.1: The Branemark implant system [3]

2.2 Biological aspects

2.2.1 Biocompatibility and biological response

Today various biomaterials are being used for teeth restoration, they come from both three material groups (metals, ceramics and polymers) and those composites. A *biomaterial* is a non-viable material that has the task to backup or replace one or more functions of the living organism. It has a close or direct contact with the body. A biomaterial may function as an artificial organ, rehabilitation device, implant replacing natural tissue, drug-delivery system or biosensor. [4]

When a medical device is inserted into the body it creates a new surface between the tissues. The interacting sites have a dynamic nature, thus the implant must show biological and structural durability. An implant is *biocompatible* if it has no harmful

effects on the body and performs biofunctionality. It must fulfil this on both macroscopic and microscopic levels. [2, 3]

The exact definition of biocompatibility according to David F. Williams [5]:

> "Biocompatibility refers to the ability of a biomaterial to perform its desired function with respect to a medical therapy, without eliciting any undesirable local or systemic effects in the recipient or beneficiary of that therapy, but generating the most appropriate beneficial cellular or tissue response in that specific situation, and optimising the clinically relevant performance of that therapy."

A biocompatible dental implant must satisfy the following requirements [6]:

- corrosion resistance,
- mechanical strength,
- Young's modulus similar to bone tisse,
- capable for sterilisation,
- radiodensity,
- electric passivity.

There is always some chance the implant will induce adverse reactions, thus biocompatibility is related to risk management. Allergic reactions to the components of the implant is dose independent. Toxic effects depend on the lowest dose of a substance that induce harmful reactions. Other unwanted responses: chemical burn, pulp irritation and damage, thermal injury, tissue irritation. These are the results of some kind of degradation process. In case of metals it means wear for mechanical forces, dissolution for chemical potential gradient, and corrosion for electrochemical potential gradient. The biological response for corrosion depends on the composition of the implant, amount of released species, shape of the implant and its location in the body, the environment-metal interface and the implant's surface quality. [2]

Intraorally all metals and alloys corrode some extent, some element release and current flow is allways present. Forceful electrochemical degradation leads to poor esthetics, compromise of physical and mechanical properties and increased irritation. Low level of particle release may slow enough to last for months or years. Presence of muliple phases

and non-noble elements in the implant's material increse the risk of corrosion. Recognized noble dental implant elements are gold, platinum, palladium, iridium, rhodium, osmium, and ruthenium. [1]

According to tissue reactions in the presence of medical implant biocompatible materials could be divided into three groups. (1) A connective tissue forms on the *biotolerant material*, which separates the implant from the living tissues. Release of substances in a non-toxic concentration occurs. These materials are not suitable for dental implants. Biotolerant materials are the Vitallium, steel alloys and various plastics. (2) In case of *bioinert material* a stable oxid layer forms on the surface which causes the passivation of the implant. There is no release of toxic substances. Titanium, tantalum, aluminium oxide cheramics belong here. Their mechanical properties limit the usage in implantology. (3) *Bioactive material* creates a direct mechanical and chemical link with the tissues. Ceramics have this effect, like hydroxyapatite ($Ca_5(PO_4)_3(OH)$), tricalcium phosphate ($Ca_3(PO_4)_2$) and various bioglasses. Because of the low mechanical strength, these materials are not capable to act as medical implants on their own, rather being used as a coating to modificate the implant's surface. [6]

2.2.2 Osseointegration

Bioactive materials has the feature to stimulate the formation of bone when inserted to an osseus site of the living body. This is the so-called *osseointegration*. In this process an interface zone appears between the contact surfaces. The requirements of the interface zone are the chemical, mechanical and thermal stabiliy so it will not influence the bulk material's quality. The driving force behind the formation is the electric potential differece of the surfaces. This is well represented by the surface tension. Hydrophilic layer induces molecular processes that leads to bioadhesion, which has the following steps [6, 7]:

1. The implant's surface adsorbs OH^- ions in nanoseconds.
2. The hydration followed by natrium, calcium, chloride and phosphate ion adsorption.
3. Within 30 seconds to hours the surface covered with extracellular matrix proteins. These come from blood and other tissue fluids. The desoprtion of these proteins in native or denatured, intact or fragmented forms are responsible for the host reactions.
4. From hours to several days cells interact with the proteins via collagen fibers. This initiate cellular adhesion, migration and differentiation.

The integration of a dental implant into the human body depends on the following parameters [8]:

- implant material
- implant design
- implant surface
- status of the bone
- surgical technique
- implant loading conditions

Bone-formation is highly effected by surface characteristics: microscopically rough and pure surface supports the osseointegration [3]. This is the *osteoconductive* phenomenon, which is "the is the ability of a biomaterial to foster the in-growth of bone cells, blood capillaries and perivascular tissue into the gap between implant and existing bone" [9].

In the followings I focus on the most common implant material and the features of the implant's surface.

2.3 Material and surface

2.3.1 Titanium

In a previous section I introduced the biological requirements of a dental implant. The success of the implantation is highly affected by the integration of the implant's material with the host tissues. Titanium became a reachable choice for biomedical applications after it was provided well in the advancing post-World War II technologies of aerospace and military industry. Titanium and its various alloys show better biocompatibility and lower modulus compared to convenctional stainless steels and cobalt-based alloys. Nowadays titanium is the most commonly used metallic biomaterial for dental implantology. [10]

2.3.1.1 Pure titanium

Titanium is a transition metal, its atomic number is 22, standard atomic weight is 49.9, the electron configuration is $[Ar]4s^2 3d^2$, it has 4 valence electrons. The electronegativity is 1.54, the standard electrode potential at 25 °C for the $Ti^{2+} + 2e^- \rightarrow Ti$ reduction

reaction is E_0=-1.63 V. Its 4.5 g/cm^3 density considered relatively low. In addition it shows radiodensity. Titanium's occurence in the Earth's crust is 0.6%, its most common ore forms are rutile (TiO_2) and ilmenite ($FeTiO_3$). High flexural strength, bonelike Young's modulus and high corrosion resistance via fast, stable oxide formation on surface makes titanium the best choice as an endosseous dental implant. Titanium exists in many oxidation states and solves oxygen easily. They form TiO, TiO_2, Ti_2O, Ti_2O_3, Ti_3O, Ti_3O_2, Ti_3O_5. The TiO_2 is the most stable: titanium is in the +IV oxidation state and the Gibbs free energy of formation is highly negative. TiO_2 has three allotropes: rutile, anatase and brokite. Anatase and rutile consists a titanium surrounded by six oxygen atoms in an octahedral configuration. In the presence of oxygen a passive, 2...6

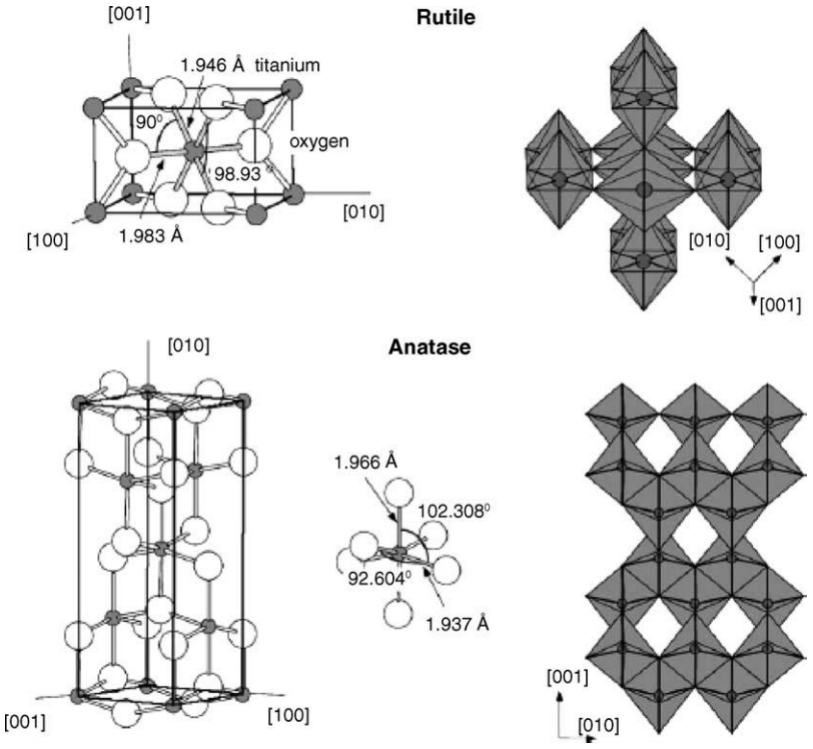

FIGURE 2.2: Allotropes of titanium dioxide: rutile and anatase [10]

nm thick ceramic layer forms within nanoseconds on the surface of titanium, and may be amorph, partially or fully chrystalline. At room temperature the anatase and brookite metastable transform into the thermodinamically stable rutile, though the anatase-rutile transformation is kinetically inhibited. [10, 11]

It was reported [12, 13] that the crystallographic matching between the (110) plane of anatase and the (0001) plane of HA is better than the matching between the (101) plane of rutile and (0001) of HA. Anatase increases the formation of HA in a biological environment. On the other hand rutile improves dissolution resistance: it can inhibit ionic diffusion with its closed packed structure [13].

2.3.1.2 Titanium alloys

Beta transus temperature exists for titanium: at 882.5 °C a phase transformation proceeds, from hexagonal-closed packed α-phase to body-centered cubic β-phase. Both phase can be stabilized with alloying elements by changing the beta transus temperature. α-stabilizers increase the transus temperature. Aluminium, oxygen, nitrogen and carbon belong here. Aluminium is the principal α-stabilizer, below 9 w% it increses tensile strength, creep strength and elastic modulus. β-stabilizers decrease the transus temperature, these components are the molybdenum, vanadium, niobium, tantalum. Vanadium can minimize the $TiAl_3$ formation, increases corrosion resistance and strenght. Most commonly commercial pure (cp) titanium being used, these are the Grade 1...4 alloys in the ASTM standards. These differs only in their impurity content. Alloyed titanium are classified by its alpha and beta phase content. According to this pure α, near α, α-β and metastable β alloys exist. Ti6Al4V (6 w% Al, 4 w% V) alloy considered an α-β Ti-alloy. Because of its increased strength, cheap alloying elements and easy processing make the most commonly used titanium alloy. Titanium shows a high affinity for interstitial elements: carbon, iron, nitrogen and oxygen increases strength but reduces ductility. The extra low interstitial (ELI) grade titanium alloys have increased ductility because of the low level of dissolved oxygen on the interstitial sites. Hydrogen content is always minimized in titanium because it begins to precipitate at several hundred ppm, leads to the embrittlement of the implant, thus increases the risk of stress cracking. Titanium is very reactive and has a high melting temperature, its primary fabrication is expensive. [14]

In biological environment the Ti6Al4V alloy can release cytotoxic vanadium and aluminium which is connected to neurological disorders. Overcoming these effects there are efforts to develop Si, Fe, Zr, Nb, Mo containing titanium alloys. [15–18]

TABLE 2.1: Properties of titanium alloys [19]

Alloy	**ASTM name**	**Nominal composition by weight percent**	**Ultimate tensile strength**	**Yield strength**	**Young's modulus**	**Elongation**
cp-Ti	Grade 2	0.03%N, 0.30%Fe, 0.25%O	345 MPa	275 MPa	103 GPa	20%
cp-Ti	Grade 4	0.05%N, 0.50%Fe, 0.40%O	550 MPa	485 MPa	103 GPa	15%
Ti6Al4V	Grade 5	6%Al, 4%V	900 MPa	830 MPa	114 GPa	14%
Ti6Al4V ELI	Grade 23	6%Al, 4%V	830 MPa	760 MPa	114 GPa	15%

2.3.2 Surface quality

The structure of an implant's surface has a huge effect on its lifespan. The connecting interface influence the cellular reactions through osteoblast (bone building cell) proliferation and differentation, tissue regeneration. According to physiology processes the implant's surface has two main feaures. *(a) Purity and cleanliness* provide the optimal surface tension. Foreign atoms lead to incresed surface tension (which cause lowered protein adsorbtion), unwanted biological responses by the host and could catalyze oxidation. In most cases contamination ouccures at surface machining, treatment and implant storage. *(b) Morphologically* distributed, porous surface regenerates faster, shows better bone adhesion. Macropores mechanically stabilise the implant. Micropores are smaller than 100 μm accelerate cell migration to the interface. It is proven that a rough surface shows better osseointegration than a smooth, however this property is still not fully understood. [6]

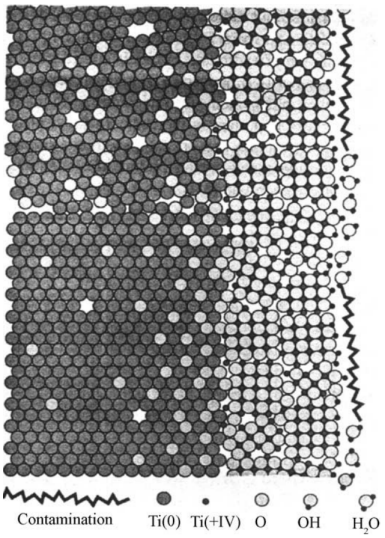

FIGURE 2.3: The surface of titanium in a schematic view [10]

Neupane et al. [20] reported after studying in cell culture the electrochemically anodized titanium dioxide surface:

> "The roughest surface has the lowest contact angle and highest surface energy values. The contact angle values are a reasonable option for wettability characterization taking into account the importance of surface interaction between the biological fluids and biomaterials. Materials with a higher surface energy (i.e. hydrophilic surfaces) produced increased differentiation of osteoblast cells when compared to substrates with a lower surface energy

> because surfaces with more electron-acceptor sites encouraged osteoblastic differentiation."

High surface roughness leads to mechanical interlocking between the implant and bone-ongrowth. On the other hand it increases the risk of inflammatory processes and ionic leakage. It was reported that a moderately rough surface, S_a=1...2 μm can limit these adverse reactions. [21]

2.4 Surface modification of titanium implants

Various technologies was developed for optimising the surface of titanium implants. This is necessary in terms of surface roughness and passivity. A microscopically rough and pure implant surface possesses osteoconductive properties. In addition early high bone-to-implant area ratio is also necessary for a successful implantation. [21] On the other hand a few nanometre width, electrochemically passive protective oxide layer forms by itself on the titanium's surface which can deteriorate in body fluid. The goal is to thicken and homogenise the passive surface. [4]

2.4.1 Chemical treatments

2.4.1.1 Acid etching

Strong acids and their combinations are used on TiO_2 to create homogeneous, micro-roughened surface in the scale of 0.5-2 μm which is beneficial for cell adhesion. The used acids are HCl, HNO_3, H_2SO_4 and HF. The latter has a high ability to dissolve the passive surface of titanium, in addition the fluoride incorporation to the surface structure leads to enhanced cell differentiation. HCl can easily dissolve titanium salts and keep intact the passive layer, thus it is excellent for removing contamination. The acid etching induce a few nanometre thick oxide layer which slowly grows in air. Acid treatment can lead to hydrogen incorporation under the oxide layer what causes the embrittlement of the surface region. [4]

2.4.1.2 Hydrogen peroxide treatment

Immersion of titanium into H_2O_2 leads to the formation of amorphous Ti-peroxy gel on the surface. The heat treatment at 300 °C transforms the amorphous phase to a crystalline state. Below 600 °C mainly anatase phase forms, above 700 °C the rutile phase dominates. The thickness of the layer linearly depends on immersion time. [10]

Wälivaara et al. [22] thermally evaporated 2000 Å thin titanium onto a silicon wafer. They incubated the samples in 10 mmol/dm^3 and 100 mmol/dm^3 H_2O_2 for 0, 26 and 74 hours, than immersed them into blood plasma for 10 minutes. They showed that the hydrogen peroxide facilitates the Ca^{2+} and Mg^{2+} deposition on the surface by the formation of non-toxic and stable $Ti(IV)O_2^-$, $Ti(IV)O_2^{2-}$ or $Ti(III)O_2$. In addition connective tissue components bind easier and faster to the surface with the suppression of inflammatory activity.

2.4.1.3 Alkali treatment

The alkali treatment enables the creation of bone-like apatite layer on titanium substrate. The titanium samples are immersed in 5...10 M NaOH or KOH solution and heat treated at 800 °C on low pressure. During this the negatively charged $HTiO_3^-$ species interact with the alkali ions producing bioactive porous and crystalline alkalinic titanate hydrogel in addition of anatase and rutile formation. [10]

Su et al. [23] investigated the effect of heath treatment after alkali treatment. They immersed Ti6Al4V disks into 10 M NaOH solution for 24 hours than heated them to 200...800 °C. At about 400 °C the sodium hydrogen titanate was converted into amorphous sodium titanate, which promotes bioactive behaviour. At 800 °C crystallization occured, rutile appeared with Al and V. Cell-culture studies showed that cell population was the highest in case of heat treatment at 600 °C for 1 hour.

2.4.1.4 Sol-gel coating

The sol-gel method is a chemical process in which the hydrolysis and polycondensation step take place in parallel. Metal alkoxide precursor ($M(OR)_n$) is dissolved in alcohol and with the addition of water the hydrolysis begins, alkoxide ligands replace hydroxyl ligands:

$$M(OR)_4 + H_2O \rightarrow HO - M(OR)_3 + ROH$$

Via the condensation reaction two hydrolysed molecule link together:

$$_3M - OR + HO - M(OR)_3 \rightarrow (OR)_3 - M - O - M - (OR)_3 + ROH$$

When the number of interconnecting $M - O - M$ bonds are large enough they behave as a sol. These colloidal particles can link together to form a three-dimensional network. This is the gelation of the sol, which structure and properties can be modified with

the aging step of the process. In this step condensation continues with dissolution and precipitation of monomers, shrinking may occur. The sol-gel method is used to deposit thin ceramic films with good control of chemical composition and microstrucure, it requires simple equipments and lower production costs. [10]

Catauro et al. [24] showed that a ZrO_2/PCL hybrid coating can improve the bioactivity of titanium. They investigated [25] the corrosion and mechanical properties of this bioactive sol-gel coating. The hybrid organic-inorganic coating was synthesized from the solution of zirconium propoxide ($Zr(OC_3H_7)$) and the solution of polycaprolactone (PLC). Sol was prepared by stirring after the addition of reactants. Grade 4 titanium disks were dip-coated into the sol, than were heat treated for 1 day at 45 °C. Nanoindentation showed that the Young modulus depends on the amount of used PLC, it is the range of 200...250 MPa. Corrosion tests showed that the ZrO_2/PCL does not affect significantly the passivation of the substrate because of the solubility of PLC in the electrolyte.

Zhang et al. [26] deposited a high-purity, dense and uniform fluoridated hydroxyapatite (FHA) coating on Ti6Al4V substrate with dip-coating method. They prepared the sol from calcium nitrate tetrahydrate ($Ca(NO_3)_2 \cdot 4H_2O$), phosphorous pentoxide (P_2O_5) and hexafluorophosphoric acid (HPF_6) by a soluting-refluxing protocol. The deposition and heat-treatment at 500...700 °C was repeated 4 times to achieve the 1.5 µm thickness. The FHA coating showed better adhesion to the substrate due to the incorporation of F into the HA structure. In addition the substrate/coating interface layer became more ductile.

2.4.2 Blasting

Alumina, titania or HA ceramic particles are blasted with high pressure to a material's surface removing contamination. With the selection of the particle size the surface could be smoother or rougher influencing the surface activity. Studies were made with 25 and 75 µm particle size alumina. After 12 weeks of insertion time in rabbit models it was shown that the bone removal torque was higher for the implants blasted with 75 µm particles with the average roughness of 1.4 µm. Blasting particles can form remnants on the implant's surface with the potential risk of inflammatory host tissue reactions. [4]

Mano et al. [27] sprayed apatite powder on grade 4 titanium samples. The surface roughness decreased from 1.67 µm to 1.30 µm. Six weeks after the implantation new bone directly contacted with the titanium through the apatite layer in 50 µm thickness. No inflammatory reactions occured. The contact ratio in case of the untreated titanium sample was 40 %. It increased to 90 % on the apatite blasted samples.

Leinenbach and Eifler [28] compared corundum grit blasting with other surface treatment methods on Ti6Al4V and Ti6Al7Nb samples. The 0.5...1 µm sized aluminium oxide particles increased the surface roughness from 0.040 µm to 5.120 µm. Axial fatigue tests showed that grit blasting largely decrease the fatigue life of titanium alloys.

2.4.3 SLA

The SLA stands for sandblasted, large-grit, acid-etched. This is a hybrid treatment, the particle blasting procedure followed by an acid etching step removing particle remnants and refining the surface. Strong acids and their combinations are used on TiO_2 to create homogeneous, micro-roughened surface in the scale of 0.5-2 µm which is beneficial for cell adhesion. The used acids are HCl, HNO_3, H_2SO_4 and HF. The latter has a high ability to dissolve the passive surface of titanium, in addition the fluoride incorporation to the surface structure leads to enhanced cell differentiation. HCl can easily dissolve titanium salts and keep intact the passive layer, thus it is excellent for removing contamination. The acid etching induce a few nanometre thick oxide layer which slowly grows in air. Acid treatment can lead to hydrogen incorporation under the oxide layer what causes the embrittlement of the surface region. [4, 10]

Guo et al. [29] compared machined, TiO_2 blasted, TiO_2 blasted than HF treated cp-Ti surfaces. The machined surface's S_a value was 0.5 µm, it was increased in case of the grit blasted samples to 1.3...1.45 µm. HF treated surface was in the range of 1.2...1.4 µm. The TiO_2 blasted and HF treated surface had a randomly textured surface in the range of 100 nm. Cell-culture and in vivo experiments showed that cell propagation was highly increased on the SLA treated samples.

2.4.4 Powder plasma spraying

With powder plasma spraying ceramic powders are injected into a plasma jet that melt and carry the particles to the implant's surface where they condense and fuse together. About a 50 µm thick film forms on the surface with 7...20 µm average roughness. Alumina and zirconia powders are being used clinically. It was shown that the plasma spraying of titanium implants increased the tensile strength at the bone/implant interface. Metal ion release by the dissolution and wear from the coating may occur. [21]

Hung et al. [30] plasma sprayed HA particles onto Ti6Al4V ELI samples of disks, cylinders and dental implants. Corundum grit blasting preceded the apatite deposition. The plasma sprayed surface contained almost entirely HA. Its roughness was about 6.20 µm,

thickness was 50...130 μm, degree of crystallinity was 55%. Adhesion strength almost reached 42 MPa. Increasing the amount of secondary gas (hydrogen) or decreasing the powder feeding rate resulted a denser and more uniform coating with a higher adhesion strength. The crystallinity reached 75% after immersing the samples to SBF for 28 days without Ti, Al or V release.

Palanivelu et al. [31] deposited a hydroxyapatite/Al_2O_3-TiO_2 (HA/AT) bilayer onto commercial pure titanium with plasma spraying. They found that the bilayer's microhardness (728 HV) was 3 times grater than the HA coating (236 HV) and 1.3 times greater than the AT coating (556 HV). The bilayer's roughness was 11 μm, it was 9 μm in case of the HA and AT coatings. The HA/AT coating exhibited a better corrosion resistance: the corrosion current (I_{corr}) was -544 nA/cm^2, -484 nA/cm^2 and -240 nA/cm^2 for the HA/AT, AT, HA, respectively. After the immersion of the samples into SBF solution for 14 days a thin apatite layer formed on the surfaces. It indicates that the coatings were biocompatible.

2.4.5 Laser texturing

The laser texturing of titanium implants enables to modify the surface's microgeometry. The ablation pattern on the surface improves cell ongrowing by increasing the surface energy and the wettability of the surface and enhances the interlock between bone/implant interface. The application of micro-grooves on the surface result in ordered cell proliferation within the grooves which improve healing. [32, 33]

Pfleging et al. [32, 34] used ArF excimer laser to create textures on Ti6Al4V specimens. They showed that dimple texturing of the surface increases its surface energy and the texturing itself shifts the specimen's corrosion potential to noble.

The effect of dimples in the dimension of 100...160 μm on cp-Ti in vivo studied by Jianguo Li et al. [35] Push-out tests on the specimens showed that the shear strength significantly increased at the bone/implant interface compared to the control specimens.

J. Chen et al. [36] did short-time cell culture studies on laser textured Ti6Al4V specimens. The linear grooves were 13 μm wide, 10 μm deep and groove spacing were 20...60 μm. Longitudinal cell guidance and enhanced cell adhesion was observed on the micro-grooved surfaces.

2.4.6 Anodic oxidation

A protective oxide layer can be formed on the titanium surface with the potentiostatic ((constant votlage) and galvanostatic (constant current) anodization. The titanium workpiece is immersed as an anode into an ionic solution, typically H_2SO_4, HNO_3, H_3PO_4 and HF. The applied DC voltage during anodization is at the range of 10...100 V, thus redox reactions occur at the bulk/oxide and oxide/electrolyte interface with enhanced oxide formation. The main reactions at the anode:

- at the titanium/titanium oxide interface:

$$Ti \rightarrow Ti^{2+} + 2e^{-}$$

- at the titanium oxide/electrolyte interface:

$$2H_2O \rightarrow 2O^{2-} + 4H^{+}$$
$$2H_2O \rightarrow O_2 + 4H^{+} + 4e^{-}$$

- at both interfaces:

$$Ti^{2+} + 2O^{2-} \rightarrow TiO_2 + 2e^{-}$$

If the applied electric field is high enough ions pass through the oxide layer, current will flow and the oxide layer is growing. The oxide layer's resistivity is increasing with its thickness, so the applied voltage drops. The final oxide thickness is about 1000 nm, nearly linearly depends on the applied voltage. The thickened oxide layer increases the titanium's corrosion resistance, decreases ion release from titanium alloys and enables the colouration of the surface via optical intereference. The anodic oxide layer exhibit

FIGURE 2.4: Colored titanium orthopedic screws. Source: Medimetal Ltd., www.medimetal.com/en

amorphous phases at lower voltages, anatase and rutile phases appear at higher voltages. The coating properties can be varied on a wide range with the parameters of anode potential, current density, electrolyte composition and concentration, temperature, treatment time. [4, 10, 37]

When the applied voltage on the anode half-cell exceeds the breakdown potential than electric discharges appear on the surface accompanied by high temperature and pressure. This is the so-called plasma electrolytic oxidation.

Munirathinam and Neelakantan [13] created titania nanotubes on pure titanium with anodic oxidation. The electrolyte in their work was solution of 0.1 mol/dm^3 citric acid and 0.5wt% NaF. The potentiostatic anodization were performed at 20 V for 0.5...3 hours. A set of samples were than heat treated at 600 °C for 3 hours. A tubular surface was formed on the substrate, the size of the holes increased with treatment time. The inner diameters were in the range of 85...105 nm for the as-formed surfaces and 68...73 nm for the heat treated surfaces. The porosity were in the range of 35...50%. The as-formed surfaces were amorphous, in case of the heat treated surfaces the amount of rutile phase increased with the anodization time. For both the heat treated and as-formed samples the surface roughness was 0.5...1.5 μm. Contact angle measurement showed that the surface energy was decreased in case of the heat treated samples from 30 mJ/m^2 to 20 mJ/m^2. Polarization measurement resulted a passive behaviour for every surfaces with the passive current density of 0.5...5·10^{-7} A/cm^2.

2.5 Plasma electrolytic oxidation

The plasma electrolytic oxidation (PEO) is an electrochemical process in which a valve metal is set as the anode, and with the applied high voltage a hard and passive oxide layer forms on the metal's surface. The method evolved from the anodic oxidation, the layout of the equipment and the redox reactions are similar:

- the oxidation of metal at the anode:

$$\mathrm{Ti} \rightarrow \mathrm{Ti}^{2+} + 2\mathrm{e}^-$$

- the reduction reaction at the cathode:

$$2\mathrm{H_2O} + \mathrm{e}^- \rightarrow \mathrm{H_2} + 2\mathrm{OH}^-$$

In addition of the redox reactions non-Faradic processes also occur at the electrodes, these mechanisms are still under research. With plasma anodization higher voltages in

AC-mode and higher current densities applied thus plasma discharges appear on the working electrode's surface accompanied by increased gas liberation. In practice Mg, Al and Ti-alloys are used to set as the anode (working electrode) and stainless steel acts as the cathode (counter electrode). The electrolyte usually contains calcium acetate, sodium phosphate, potassium phosphate, β-calcium glycerophosphate. The growing oxide layer is able to absorb species from the electrolyte, thus it is possible to modify the surface with various elements. The created metallic oxide layer becomes thicker and more porous. Characteristic spongy surface with enhanced bioactivity and increased corrosion resistance could be achieved by the PEO. Smaller friction coefficient and the yield of hardness and wear resistance is the result of the porous surface. The coating comprise of amorphous and crystalline phases. [38, 39]

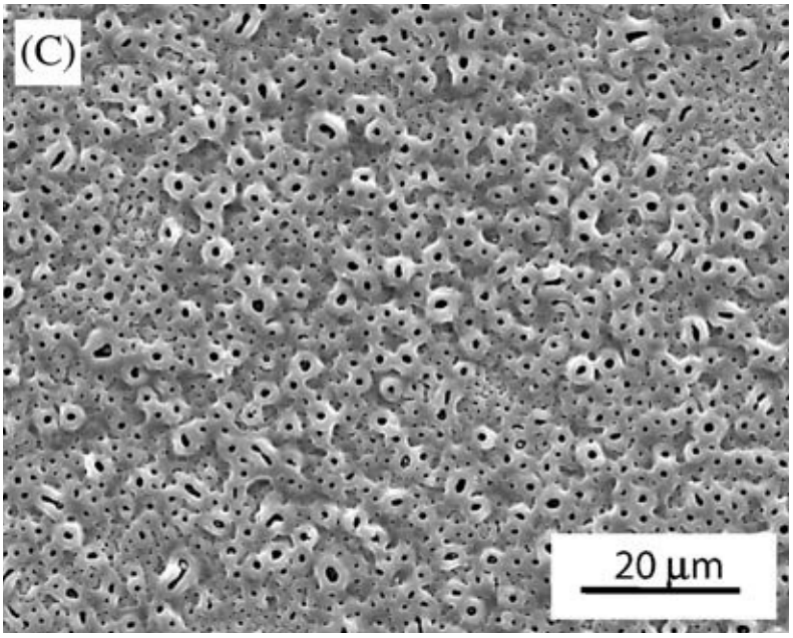

FIGURE 2.5: PEO treated surface of grade 2 titanium [40]

The PEO treated titanium surface depends on the following parameters:

- substrate's material,
- electrolyte composition, pH, temperature,
- applied voltage, current density, waveform, frequency, duty cycle,
- treatment time, number of treatments.

This process appears under various names in literature: plasma electrolytic oxidation (PEO), microarc oxidation (MAO), microarc electrolytic oxidation (MEO), plasma anodization, micro-plasma oxidation, spark anodization.

The coating formation of PEO is still unclear, there are many theorems about the oxide growth [41]. It is commonly acknowledged that during the process the metal substrate oxidizes, an oxide coating forms on the surface, the oxide coating reaches its dielectric breakdown potential due to the applied high voltage, it melts, than ejects through the discharge channel and solidifies on the coating surface accompanied with intensive gas liberation. The electrical transient during PEO plays a key role. Analysing the voltage during the process in constant current mode (galvanostatic) gives us informations about the occurring transient states. Figure 2.6 shows the voltage as the function of time during the plasma anodising of an aluminium alloy. It is visible that the curve could be divided into four sections. At the I. stage the fast Faradaic growth of the oxide layer occurs, the resistivity of the layer increases rapidly, thus the voltage must be increased to keep the current at a constant rate. At stage II. the speed of oxidation is decreased by dissolution, the voltage increase is lower. At the border of the II. and III. stage the plasma discharges appear. In the IV. stage the process steps into the final stage, the coating grows in a slower rate thus the voltage increases slower. The large defects are mainly develops in the final stage. The average discharge diameter increases with processing time, it falls in the range of 0.01...1.35 μm and last for 10...100 μs. With the grow of the oxide layer the population of the sparks are decreasing, they change color and become intense. The discharge behaviour and exact mechanism is still unclear in PEO treatment. It is highly affected by the current regime, the electrolyte and the substrate material. [38]

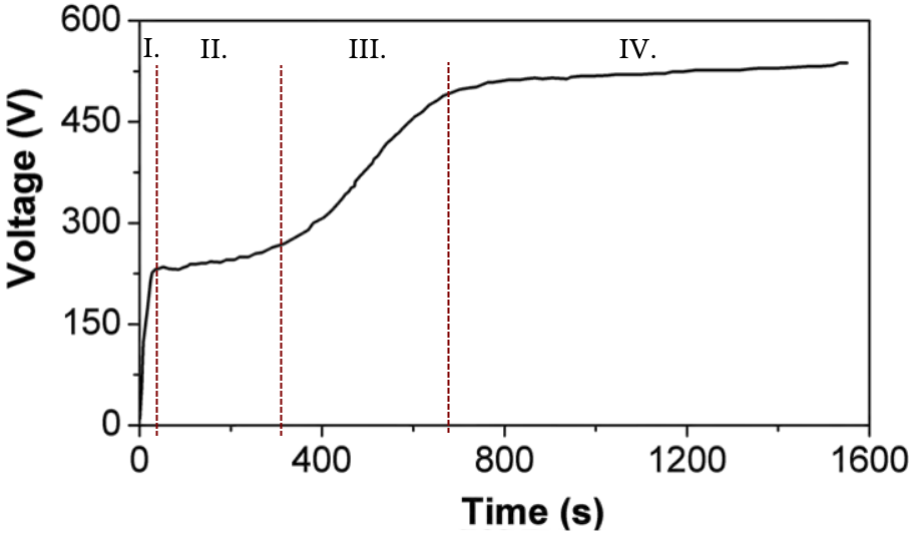

FIGURE 2.6: Voltage transient recorded during the plasma anodization of Al alloy in a solution of 1 g/l KOH at 4.67 A/dm^2 current density. Figure reproduced from [38]

Chen et al. [42] coated cp-Ti samples with PEO in an electrolyte containing P and Ca. Treatment carried out with current of 0.5 A/cm^2 and 420 V for 60 min. The coating

consisted Ca and P, XRD analysis showed anatase and rutile on the surface. With short time treatment anatase and rutile containing surface was achieved by Shokouhfar et al. [43]. They treated the samples with 350 V on 1 kHz with 40% duty cycle for 3 minutes. Aliasghari et al. [44] plasma anodized Ti6Al4V samples galvanostatically at 0.5 A/cm^2 rms for 1 hour. They found that the PEO treated surface contained anatase, rutile and Ti_2O_5.

Chapter 3

Experimental design ratio, building a self-made PEO equipment

In this present work I am going to compare the surface characteristics of three different coatings. These are the laser textured surface, the plasma anodized surface and the plasma anodized and laser textured surface. Although plasma anodization is a widely researched coating technology of dental implants, there are no previous study on combining the PEO and the laser texturing process in this field. The PEO enables to create a bioactive coating on the implant's surface. The proper dimension of the grooves made by the laser texturing might enhance the cell proliferation on the contact site and increase the mechanical interlock between the bone/implant interface. Combining this two technology might increase the intracellular matrix/coating contact area, thus extend the lifespan of a dental implant and reduce healing time after the surgery. For the experiments I obtained 4 mm thick Grade 2 titanium plates. Disk samples in 19 mm diameter were cut with a Trumpf TLF 5000 Turbo CO_2 laser.

3.1 PEO equipment building

The experiments were carried out on an equipment what I built for this purpose. A power source operated on 1 A rms (root mean square) constant current mode, its maximum power load was 600 VA. An external function generator provided the square wave signal. The electrolytic cell consisted a custom built glass container with a sample access on its side and a platinum web hanging inside as the counter electrode. The sample holder plastic tube allows to treat surfaces in the size of 227 mm^2. A digital multimeter was

connected parallel to the cell for measuring the rms voltage. A schematic diagram is represented at Figure 3.1.

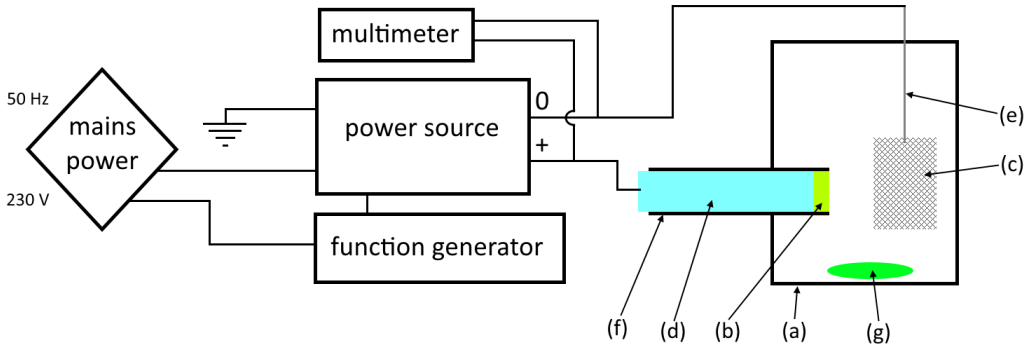

FIGURE 3.1: Schematic diagram of the plasma anodizing equipment: (a) glass container, (b) Ti sample as the anode, (c) Pt web as the cathode, (d) Al rod outlet, (e) Pt wire outlet, (f) plastic tube, (g) magnetic stir bar.

3.2 Pre-experiments: parameters and evaluation

3.2.1 Laser texturing

The aim of the pre-experiments was to create dimples and linear grooves on the titanium's surface. An SPI G4 fiber laser was used for the process. It's wavelength is 1070 nm with a peak-power of several hundred watt in impulse mode. Positioning of the laser spot was made by a scanner equipped with a 255 mm focal lens. The laser texturing was done in an ambient environment, scanning speed for creating dimples and linear grooves was 4500 mm/s and 1500 mm/s, respectively. The laser's focus was set on the surface and the scanning was done 20 times. The examination was made with a Keyence VHX-2000 digital microscope. The resulting pictures can be found at Appendix A. It is visible that the dimples are 40 µm deep, 100 µm in diameter and 150 µm apart (Figure A.1). The linear grooves are 40 µm deep and 150 µm apart (Figure A.2). Gold and blue colourisation of the surface indicated by intensive oxidation during the laser texturing. This oxide layer uneven and thick so the texturing was tested in argon atmosphere with the same parameters. It was found that the grooves and dimples became shallow. This might because of the absence of the highly exothermic formation titanium oxide, which could burn out material from the surface. Pickling of the surface became necessary for oxide removal.

3.2.2 Plasma anodization

The PEO pre-experiments were done in an electrolyte containing phosphoric acid and calcium hydroxide. The frequency was set to 1 kHz, duty cycle was 50%. During the plasma anodization it was experienced that the power source could be loaded with 400 V rms at most, otherwise the resistors warmed up rapidly. Immediately after switching on the power intensive micro-bubble formation appeared near the sample's surface, than the surface colourized to grey. For about 5 minutes the voltage continuously increased, than it stabilised at about 400 V rms and the plasma discharges appeared on the sample's surface. Through the process the size, duration and intensity of the discharges increased. After about 10 minutes of plasma anodization the process reached its late period, the sparking times became longer and intensive, their population decreased. Intensive sparking could last for many seconds, which could lead to "burn" of the surfaces (Figure A.3). It was observed in case of the PEO treatment of the linearly grooved surface that plasma sparks appeared 3...4 minutes later.

3.3 Parameters of experiments

3.3.1 Laser texturing

At first every sample went through a laser polishing process, which refined the surface. After that the selected samples were laser textured with the same laser equipment as used in the pre-experiments. The scanning speed for the texturing was set to 1500 mm/s for linear grooves and 6000 mm/s for dimples to increase the distance between them. The process was done in an ambient atmosphere, laser focused on the sample's surface and scanning was done 25 times.

3.3.2 Pickling

After the laser texturing every specimen went through an acidic pickling process for 20 minutes at room temperature. The solution contained 30w% HNO_3 and 3w% HF.

3.3.3 Plasma anodization

The literature showed that anatase can be achieved with PEO treatment at 350...450 V, 0.5 A/cm^2 with element incorporation from the electrolyte.

The PEO treatment was done in an electrolyte containing 0,1 mol/dm^3 H_3PO_4 and 0,007 mol/dm^3 $Ca(OH)_2$. The pH level of the solution was 2. Voltage was set to 400 V rms, frequency of the square wave was 1 kHz with 50% duty cycle. The rms current density with the constant current power mode was 0,44 A/cm^2. The treatment lasted for 10 minutes on the P and T2 samples (laser textured for dimples), and for 15 minutes on the T1 samples (laser textured for linear grooves).

3.4 Sample nomenclature

Table 3.1: Sample nomenclature

Label	**Type**	**Treatments as in order**
C	control	laser polishing pickling for 20 min
P	PEO-treated	laser polishing pickling for 20 min PEO for 10 min at 400 V, 1 kHz, 50%
T1	laser textured and PEO-treated	laser polishing laser texturing with 1500 mm/min, 25 times pickling for 20 min PEO for 15 min at 400 V, 1 kHz, 50%
T2	laser textured and PEO-treated	laser polishing laser texturing with 6000 mm/min, 25 times pickling for 20 min PEO for 10 min at 400 V, 1 kHz, 50%

Chapter 4

Results

4.1 Voltage transient diagram

Measuring the voltage through the plasma anodization was done via checking the multimeter in various time intervals. On Figure 4.1 it is visible that both three surfaces tend to reach 400 V. The voltage on the T2 surface is lower in the first 3 minutes of the process, than it behave as the T1 surface. The voltage increase on the P and T1 surfaces is higher at the beginning. It was visually visible that the sparking started a few minutes later on the T1 sample.

A video of the process can be viewed here: https://youtu.be/uGF2z8dpfgE

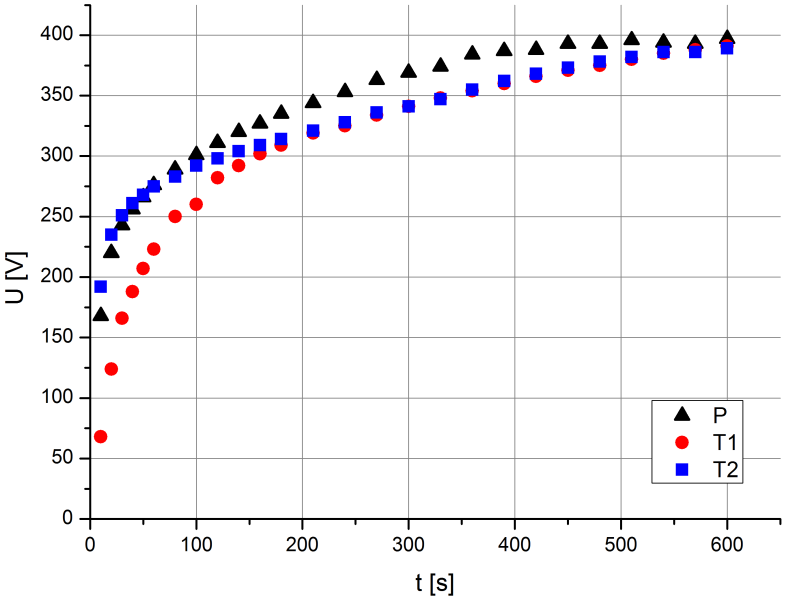

FIGURE 4.1: Voltage diagram of the PEO treatment

4.2 Optical microscopy

Surface morphology and roughness was investigated with a Keyence VHX-2000 digital microscope at the Bay Zoltán Ltd. for Applied Research.

Images can be found at Appendix A. After laser polishing the titanium samples' surface became smooth and free of any contaminations (Figure A.4).

The linear grooves of laser texturing are 30 µm deep and 200 µm apart. Two barbs are formed align between two grooves during the ablation (Figure A.5). The dimples on the T2 samples became shallow, the depth is 10 µm and are 200 µm apart, diameter is 110 µm (Figure A.6).

The acidic pickling discoloured the surface and removed oxides from it. The grooves and dimples became deeper: 50 µm and 30 µm, respectively (Figures A.7, A.8, A.9). The height of the barbs are 35 µm on the T1 sample and 20 µm on the T2 sample.

After the PEO process the samples' surface became spongy, the size of the micro-holes are about to 5 µm (Figure A.10). The laser textured surfaces were coated evenly by the micro-holes by the PEO treatment. Significant change in the surface roughness is not visible compared to the C samples (Figures A.11, A.13). The coating became dense and crack-free, micro-holes inside the dimples are visible (Figure A.14).

4.3 Scanning electron microscopy

Surface morphology was investigated with a Philips XL 30 scanning electron microscope (SEM), element composition was analysed with a built-in energy-dispersive X-ray spectroscope (EDS). Before the secondary electron imaging the samples were ultrasonically cleaned for 3 minutes in ethanol and distilled water. Measurements were done at the Budapest University of Technology and Economics, Department of Materials Science and Engineering.

SEM images can be found at Appendix B. The images of sample C show the laser polished surface, it is visible on Figure B.1a. Micro-cracks due to rapid cooling appeared on the surface (Figure B.1b). Surface composition was measured with EDS, represented on Figure B.2. The surface contains mainly titanium. Some nitrogen incorporated into the top layer of the sample during the laser polishing, while high atomic content of carbon is present due to contamination during sample handling.

On sample P a highly porous surface was created with the plasma anodization (Figure B.3). The size of the micro-holes are in the range of 1...4 µm (Figure B.3b).

The grooves of sample T1 are visible on Figure B.3. Number of the micro-holes decrease on the barb, solid parts are bigger (Figure B.7). According to the EDS measurement this area contains the highest amount of titanium (Figure B.8). The surface is rich of oxygen, highest atomic ratio was measured on the barb (Figure B.9). The phosphorous content is about to 10at%, which drops to 5at% in the grooves (Figure B.10). High content of carbon was also measured there.

Images of T2 samples shows a crack-free, continuous surface. The population of micro-holes on the barb is lower (Figure B.12). Again, as were on sample T1, the solid parts are bigger there. The barbs both on T1 and T2 samples contain oxygen in a higher content. The size of the micro-holes is the highest between two dimples. Oxygen content is somewhat lower inside the dimple (Figure B.15), phosphorous incorporation was the highest between the dimples (Figure B.13). On Table 4.1 the composition of the surface's regular sites were summarized.

No calcium was detected on the samples' surfaces by the EDS.

TABLE 4.1: Surface composition (based on Figure B.2, B.4, B.8, B.13)

Element	**C**	**P**	**T1**	**T2**
C at%	25.24	-	-	-
N at%	15.15	-	-	-
P at%	-	7.72	11.30	11.35
O at%	-	67.12	60.48	65.75
Ti at%	59.61	25.16	28.22	22.90

4.4 X-ray diffraction

Phase composition of the surface was analyzed by a Bruker AXS D8 Discover X-ray diffractometer (XRD) with a wavelength of CuK_{α}=0.15418 nm. The scanning range was between 10° and 90 ° with a stepping angle and stepping time of 0.02° and 3 seconds, respectively. The XRD measurements were done at the Hungarian Academy of Sciences, Institute of Technical Physics and Materials Science.

The diffractograms are in Appendix C. On the XRD diagram of sample C only the titanium has peaks (Figure C.1). On the plasma anodized P sample beside titanium the anatase phase appears on the diffractogram (Figure C.1). It has an intensive peak at around 25°. The dimpled T2 sample has a similar diffractogram, except that that diffraction peak is somewhat lower. Some rutile phase forms with anatase on the surface of sample T1 (Figure C.3).

4.5 Profilometry

The profilometry measurements were done with a Mahr MarTalk stylus profilometer system at the University of Miskolc, Institute of Metallurgy. For the roughness characterization the one-dimensional arithmetic average roughness (R_a) and the average distance between the highest peak and lowest valley (R_z) were taken into account.

The R_a roughness of the samples are around 5 µm, except the T1 sample's which was doubled. The T1 and T2 samples' R_z values represent the depth of the dimples and grooves.

TABLE 4.2: Surface roughness parameters

sample	$\mathbf{R_a}$ [µm]	$\mathbf{R_z}$ [µm]
C	4.249	24.800
P	4.731	24.546
T1	11.276	62.665
T2	5.605	35.216

4.6 Electrochemical characterization

The electrochemical measurements were performed in a glass-made measurement cell containing the sample as the working electrode, a platinum web as the counter electrode, and a Luggin capillary connected to a saturated calomel electrode (SCE) as the reference electrode. Artificial plasma solution (Table 4.3) was used as electrolyte, its temperature was maintained at 37 °C. A VoltaLab PGZ 301 measuring equipment was used for the power control and data record. According the ISO standard [45] the samples were ultrasonically cleaned in ethanol for 15 minutes than immersed into the artificial plasma for 2 hours. After the preparation open-circuit potential (OCP) was measured for 1200 seconds on 176 mm^2 area of the samples. The recorded potential was the mean amplitude for the electrochemical impedance spectroscopy (EIS). The EIS analysis was performed with a 20 mV amplitude sinusoidal wave ranging from 100 kHz to 10 mHz. The measurements were done at the Engineering Division of the Bay Zoltán Ltd. for Applied Research.

The E_{OCP} is the measured potential of the sample when no external load connected to it. In this case the anodic and cathodic currents are equal on the surface, there is neither dissolution, nor formation for infinite time. Anodic OCP exhibit higher dissolution and ion leakage, that may cause adverse reactions.

TABLE 4.3: Composition of artificial plasma according to ISO 10993-15:2000 [45]

Component	**Concentration [g/l]**
NaCl	6,800
CaCl	0,200
KCl	0,400
$MgSO_4$	0,100
$NaHCO_3$	2,200
Na_2HPO_4	0,126
NaH_2PO_4	0,026

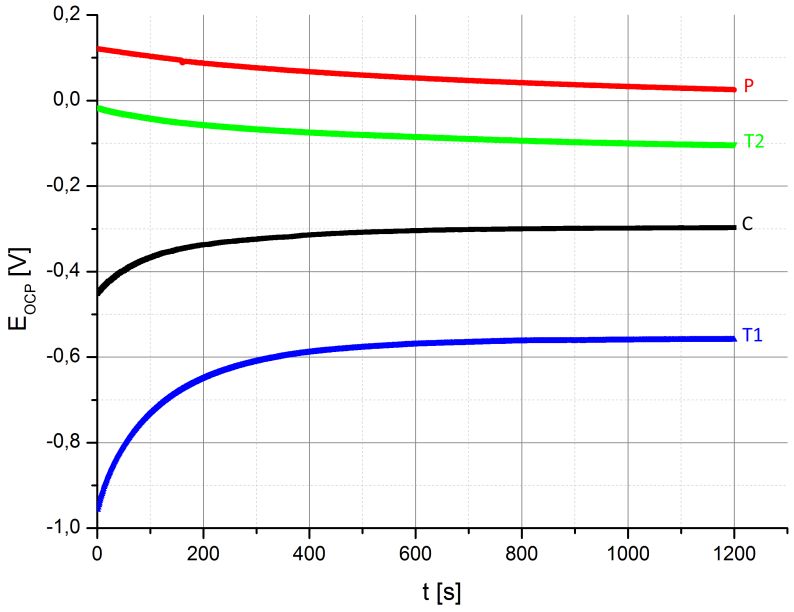

FIGURE 4.2: Diagram of the OCP measurements

The results of the OCP measurements are represented on Figure 4.3. The control sample's surface was nobleized after the PEO treatment: the E_{OCP} shifted from -0.297 V to 0.024 V. The laser dimpled T2 sample's OCP is -0.102 V. The linearly grooved T1 surface became more anodic, its OCP is -0.559 V. the anodic zones would exhibit higher active dissolution and ion liberation, which may lead to adverse effects.

Scribner ZView 2 software was used to evaluate the EIS measurements. Representing the results on a Nyquist plot it is visible that every sample have a high slope (Appendix D), which indicates passive behaviour. After fitting a curve and setting up an equivalent circuit diagram it is possible to quantify the coating. The overall resistance of the surfaces were $R_C \approx 420$ kΩ, $R_{T1} \approx 120$ kΩ, $R_{T2} \approx 960$ kΩ. The results are in coincidence with the OCP measurements: the T1 surface's corrosion resistance reduced, the T2's was increased compared to the untreated C surface. Although the Nyquist plot of the P sample indicates noble behaviour, its overall resistance was determined with high error.

4.7 Contact angle

Contact angle measurements were performed on a KSV Contact Angle Measurement optical tensiometer system at the University of Miskolc, Institute of Metallurgy. 5 µL artificial blood plasma dripped on the surfaces, the measurements lasted for 200 seconds. The achieved equilibrium contact angles were taken into account.

TABLE 4.4: Contact angles

Sample	**Contact angle**
C	77°
P	70°
T1	73° and 131°
T2	83°

In case of sample T1 the contact angle was measured parallel and perpendicular to the grooves. From the top view of the sample and the result showed that the surface behaves anisotropic because of the linear grooves (Figure 4.3, Table 4.4).

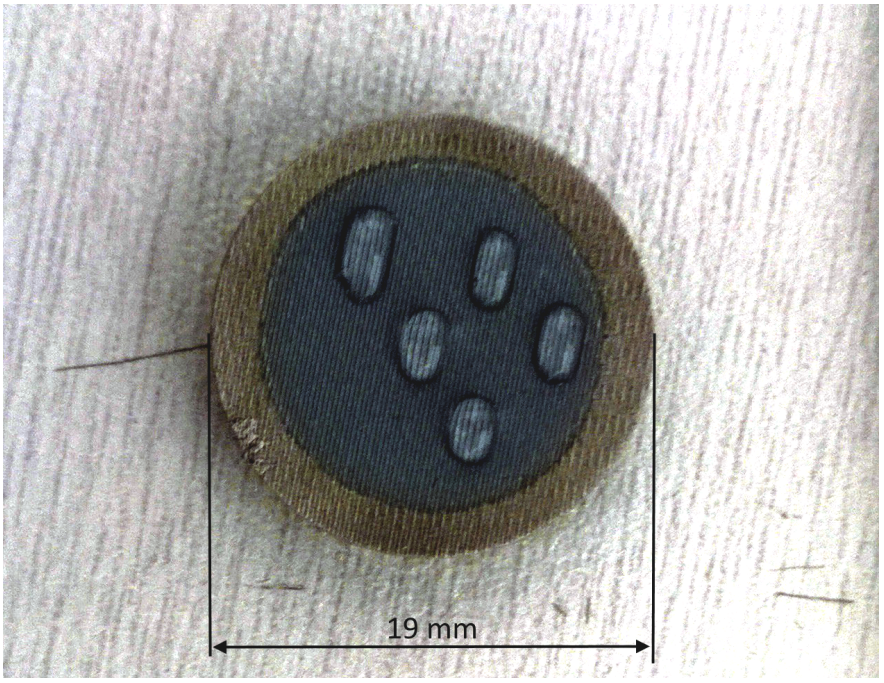

FIGURE 4.3: Top view of sample T1 with droplets on it

It is visible that the PEO treatment and the laser dimpling do not alter the contact angle significantly. On the linearly grooved surface the liquid spread transversally hindered, the contact angle was almost doubled compared to the longitudinal direction. The Cassie-Baxter wetting theory must be taken into account for further conclusions.

4.8 Clinical evaluation

Before go on market with any type of medical device, the clinical evaluation has exceptional importance in the technical file in accordance with 93/42/EEC, the requirements of medical devices directive (MDD). The correct clinical evaluation must be performed proper to the MEDDEV 2.7.1 annex of the directive above. In this study the geometry of implant is neglected, only the surface properties taken account and I concentrate on the biocompatibility. The MEDDEV 2.7.1 guideline allow the comparison upon literature if the implant's material is equal to the reference product. In this study the reference implant is the Nobel Active product family's TiUnite surface treatment, developed in 2007 by Nobel BioCare Inc. The aim of this master's thesis is the correct comparison of the TiUnite process and my self-made pilot plant product from point of view of expected biological, clinical response. In accordance with the requirements of the MEDDEV guideline from some multi-center clinical studies it can be declared that the so-called cumulative survival rate (CSR) of the Nobel Active dental implants are around 95% within 1 year [46] which is accepted in the medical industry. In the following my self-made samples will be compared to the TiUnite PEO process.

Literature investigation in the ScieneDirect database:

- keyword: "tiunite", 181 results found, 20 read, 2 relevant: [47, 48]
- earlier obtained relevant articles: [49, 50]

The chosen articles are similar, the authors compare 2 or 4, commercially available dental implants. All contain evaluation of in vivo experiments and surface analysis by SEM. It is identical that the TiUnite treated implants' pore size is in the range of 1...10 µm. Kohal et al. [47] did profilometric measurements on the surface, they found that the S_a and S_z value was 1.31 µm and 12.38 µm, respectively. These are the two-dimensional expansion of R_a and R_z. The XPS analysis by Kang et al. [50] showed that the TiUnite implant's surface consists 17.5at% Ti, 55.1at% O, 9.5at% P, 17at% C and 0.9% N.

The Nobel Active implants are made of ISO 5832-2 grade 4 titanium which in chemical composition and mechanical properties [51] are similar to my product's material (ASTM B265 grade 2 titanium). The TiUnite is a property PEO treatment of Nobel BioCare which produces a similar surface by morphology and composition to my surface treatment, thus their clinical response may be identical. Upon these the Nobel BioCare's TiUnite surface seems to be equivalent to my PEO treated samples.

Chapter 5

Discussion

In accordance with my project tasks I made a complex literature investigation about the up-to-date surface treatment of dental implants. I noticed that although there are countless of articles about the bioactivation of titanium, only a few method steps into the applied field. I did further investigation in the topic of plasma electrolytic oxidation which upon I built an own PEO equipment. The purpose of the experiments is to develop a surface treatment which might be usable in human implantology, namely reproduce the plasma electrolytic oxidation on my equipment.

I compared the samples which was prepared with my custom-built equipment to the properties of market leader Noble Active implants. In addition I combined the plasma electrolytic oxidation with laser texturing. My PEO treated samples were favourable in terms of osseointegration by comparison them with the Noble BioCare's TiUnite. Further pre-clinical examinations are required for the laser surface treated samples. There were articles about that linearly laser treated surface on titanium can induce enhanced cell adhesion and longitudinal cell guidance.

The plasma electrolytic oxidation performed on high voltages are preferred by osseointegration because of the higher amount of developed anatase [42–44]. I did anodisation treatments on 130 V at the Poligrat GmbH in München. The samples what I created there did not contain any crystalline oxide allotrope. With the optimization my goal was to examine the effect of current regime on high voltage and to execute the PEO treatment on a textured surface. While I was working on my thesis I gained valuable experiences: I built a working PEO equipment on which I can perform further experiments. For improving the size and population of the micro-holes the current density must be increased, which can be influenced with the conductivity of the electrolyte. Extending the PEO treatment increase the porosity of the surface and induce its bioactivity, thus plasma anodizing on a lower voltage must be considered to avoid the intensive and long

sparks. Thorough preparation, namely grinding and the optimal pickling solution can remove protrusions thereby prevent "burn" of the surface. This "burn" effect limits the usage of the plasma electrolytic oxidation. My aim is to avoid of the "burning" effect of the surface. The exact process of this effect is unclear, it requires researches in which the ZIGG GmbH indicates as partner.

Chapter 6

Conclusion

This thesis demonstrates plasma electrolytic oxidation with a self-made PEO equipment of untreated and laser textured grade 2 titanium surfaces. The conclusions are the following:

- with visual inspection the on the linearly laser textured surface the second stage of the PEO process delays, the sparks appear later compared to the untreated surface because of the thicker oxide layer.
- Determined by scanning electron microscopy the plasma electrolytic oxidation is effective inside the dimples and grooves of the laser textured surfaces. The size and population of the micro-holes decrease there in some extent and EDS analysis showed that a fewer amount of element incorporates from the electrolyte.
- The laser texturing does not alter the overall phase composition of the surface. Observed by XRD measurements it mainly contains anatase.
- Profilometry measurements showed that the roughness increase on the 100 μm wide laser grooved surface by the dense, oxide rich barbs.
- Plasma electrolytic oxidation and in combination with laser textured dimples increase corrosion resistance. Linearly laser textured surface combined with PEO treatment shift the surface's open circuit potential to anodic and reduce its overall resistance.
- With the assembly of the PEO equipment, the experiments and the materials examinations I gained valuable experiences which is a foundation of further researches.

Acknowledgements

Would like to thank the following people:

- **Sándor Olasz**, at the Budapest University of Technology and Economics, Department of Materials Science and Engineering, the supervisor of this thesis for the continuous motivation, guidelines and the practical and theoretical support;
- **Ferenc Hajdú** at the Bay Zoltán Ltd. for Applied Research for his selfless technical help in the experiments and the electrochemical measurements;
- **János Csizmazia** at the Bay Zoltán Ltd. for the encouragements and the creative brainstormings;
- **Péter Hartmann** at the Hungarian Academy of Sciences, Institute for Solid State Physics and Optics for lending the power source;
- **Zsolt Endre Horváth** at the Hungarian Academy of Sciences, Institute of Technical Physics and Materials Science for performing the XRD measurements;
- **Gábor Lassú** at the University of Miskolc, Institute of Metallurgy for performing the profilometry measurements;
- **Dr. Péter Baumli and Ali Alazzawi** at the University of Miskolc, Institute of Metallurgy for performing the contact angle measurements;
- **Dr. Olaf Böhme** at the Poligrat GmbH in München for the practical advices;
- **János Dobránszky** at the Budapest University of Technology and Economics, Department of Materials Science and Engineering for revising my thesis;
- **Péter Magyar** and **Zoltán Csordás** at the Bay Zoltán Ltd. for the sample preparations;
- my family for the motivation and support in my education.

Appendix A

Microscopy images

The images were taken with a Keyence VHX-2000 digital microscope.

A.1 Pre-experiments

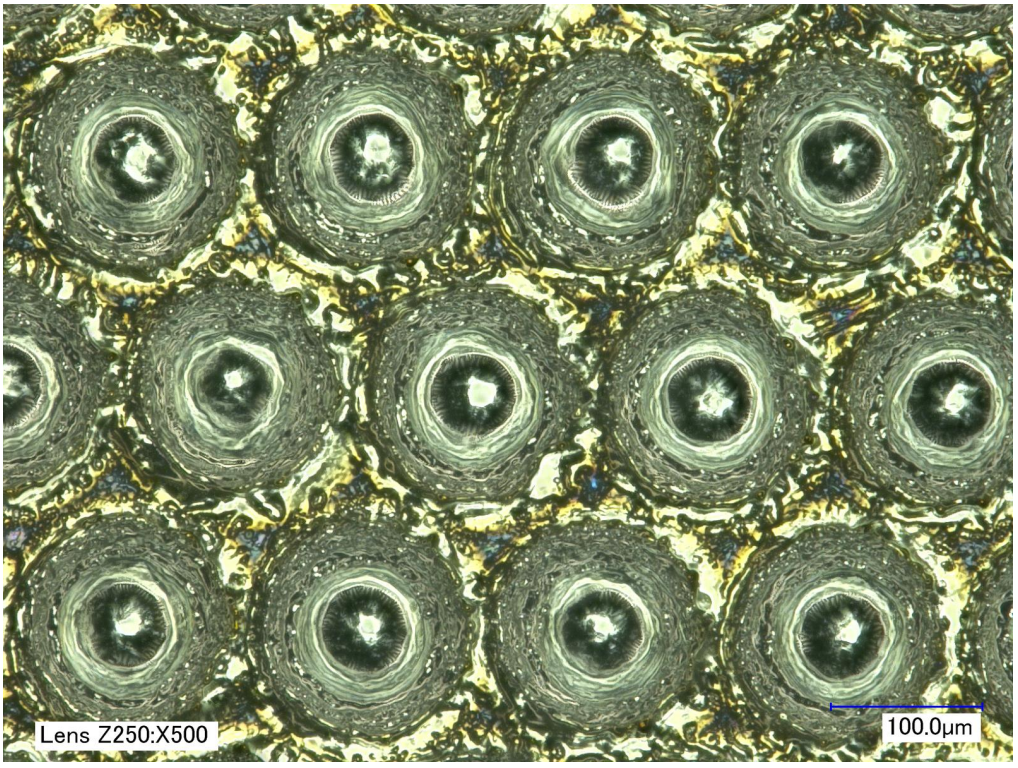

(A) Image of the surface, magnification: 500x

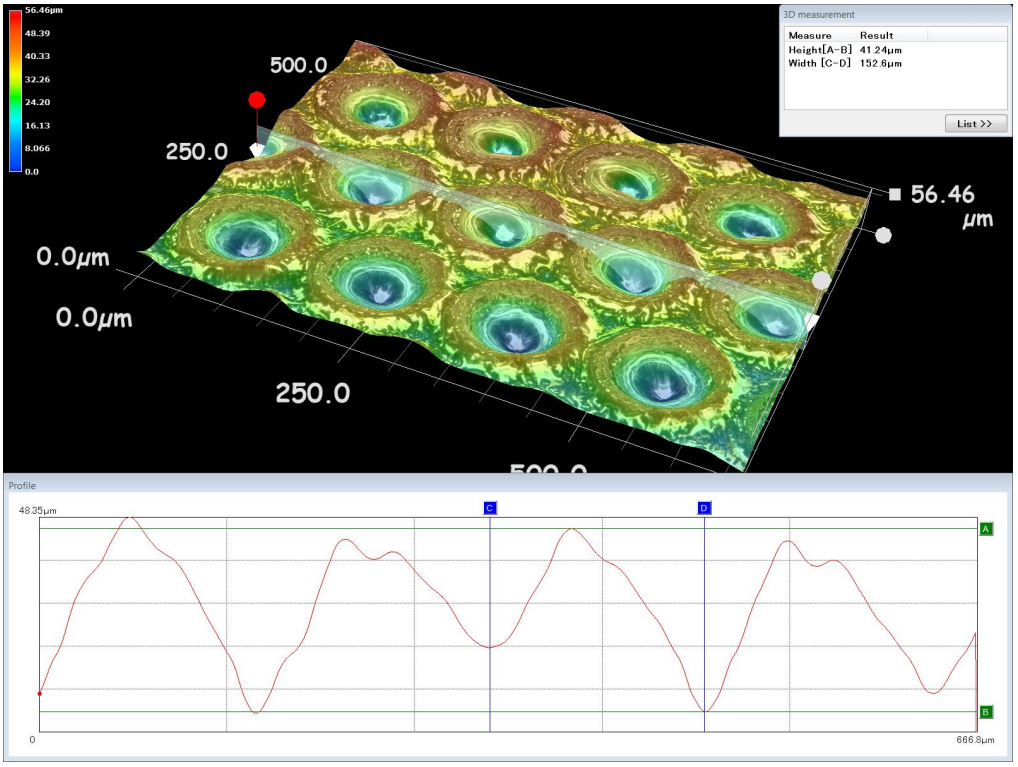

(B) 3D image and a section of the surface, magnification: 500x

FIGURE A.1: Pre-experiment: dimpled surface

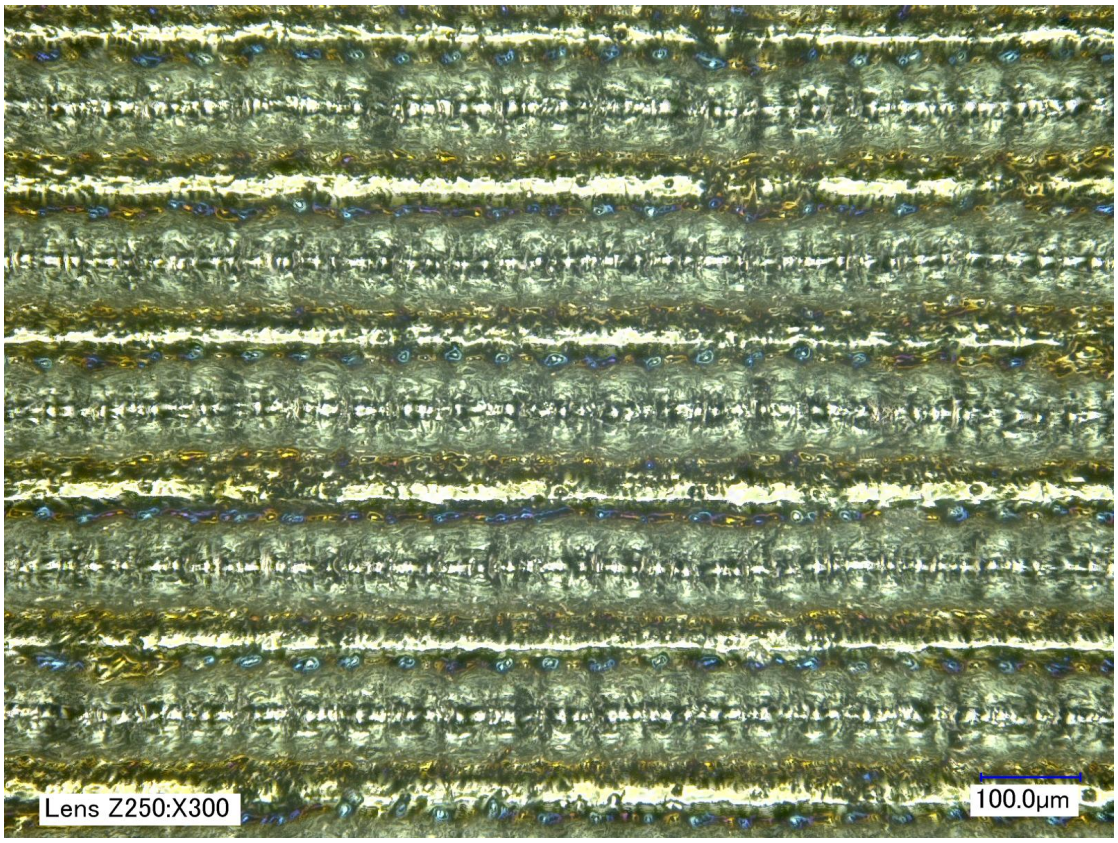

(A) Image of the surface, magnification: 300x

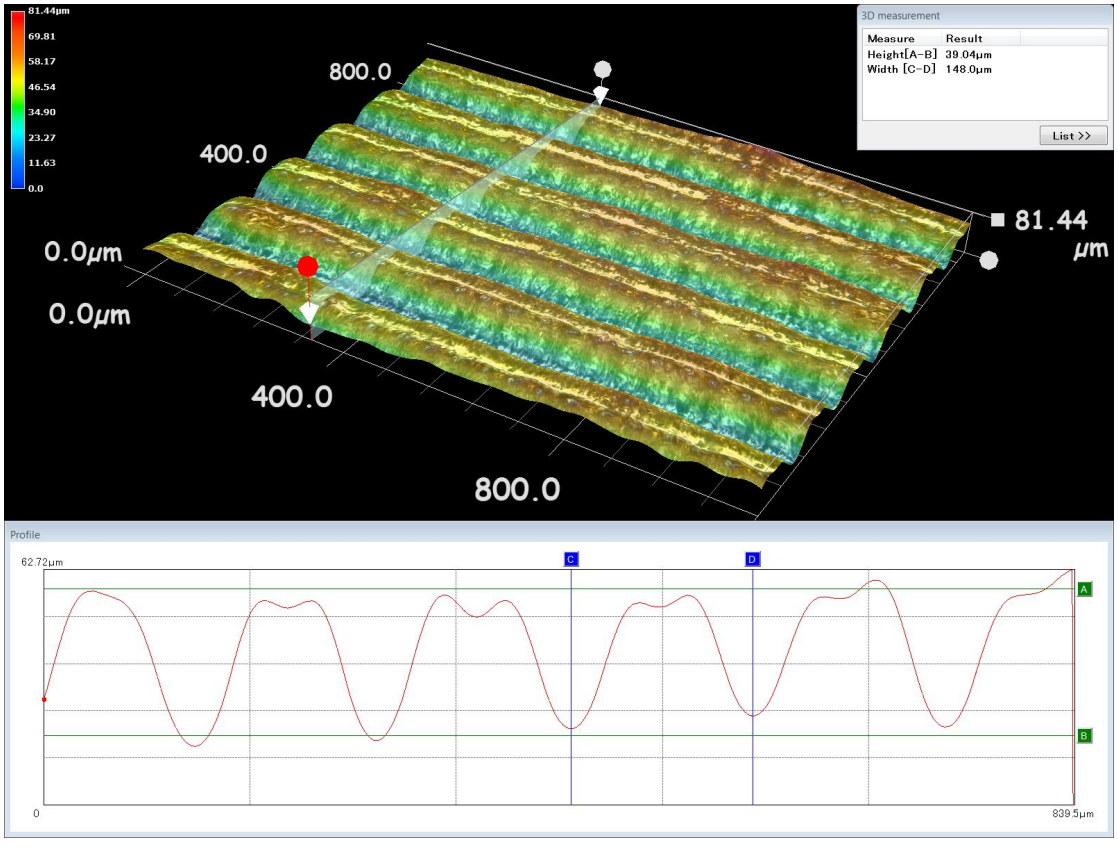

(B) 3D image and a section of the surface, magnification: 300x

FIGURE A.2: Pre-experiment: linearly grooved surface

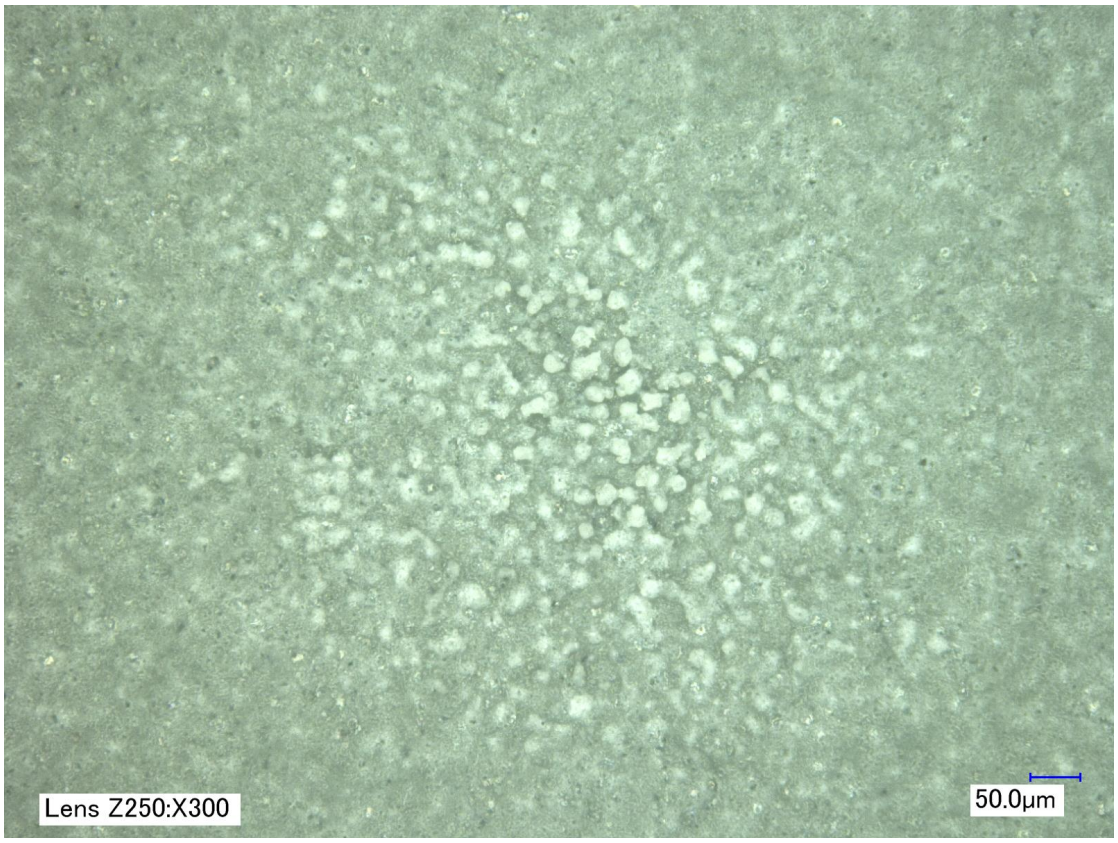

(A) Image of a "burned" part of the surface, magnification: 300x

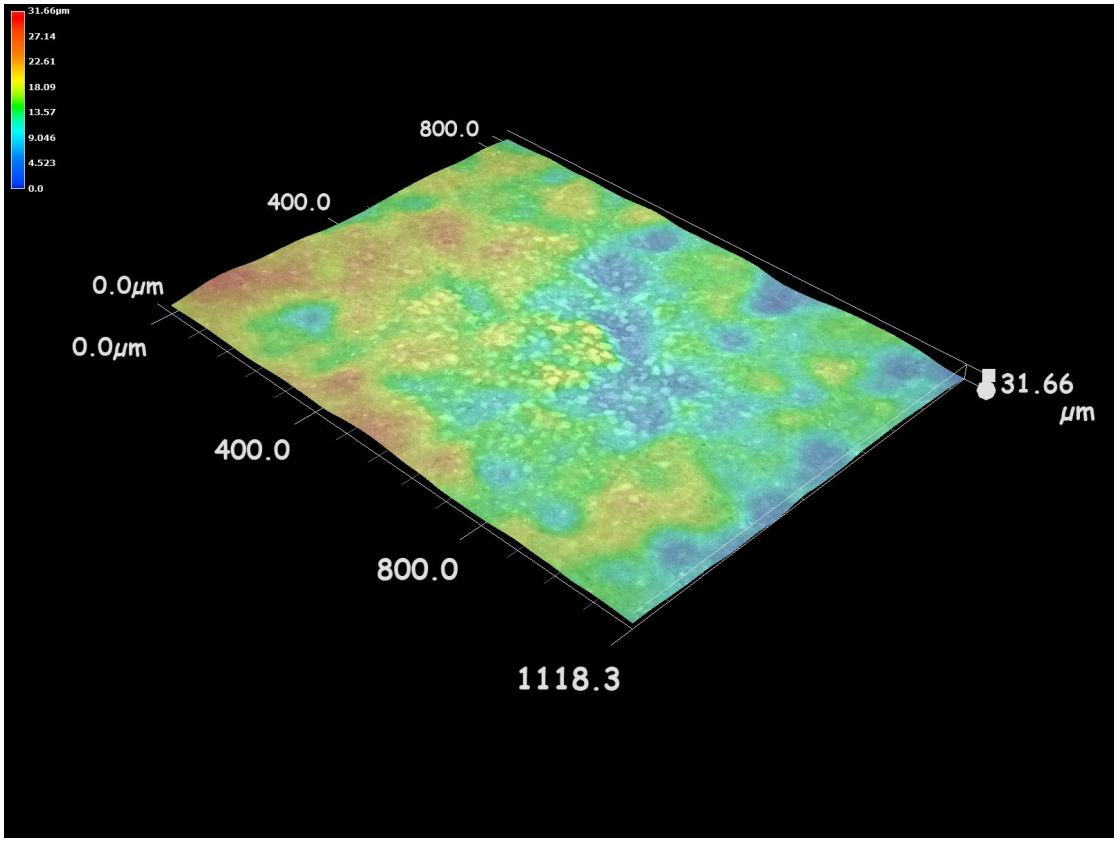

(B) 3D image of a "burned" part of the surface, magnification: 300x

FIGURE A.3: Pre-experiment: surface after PEO treatment

A.2 Samples before pickling

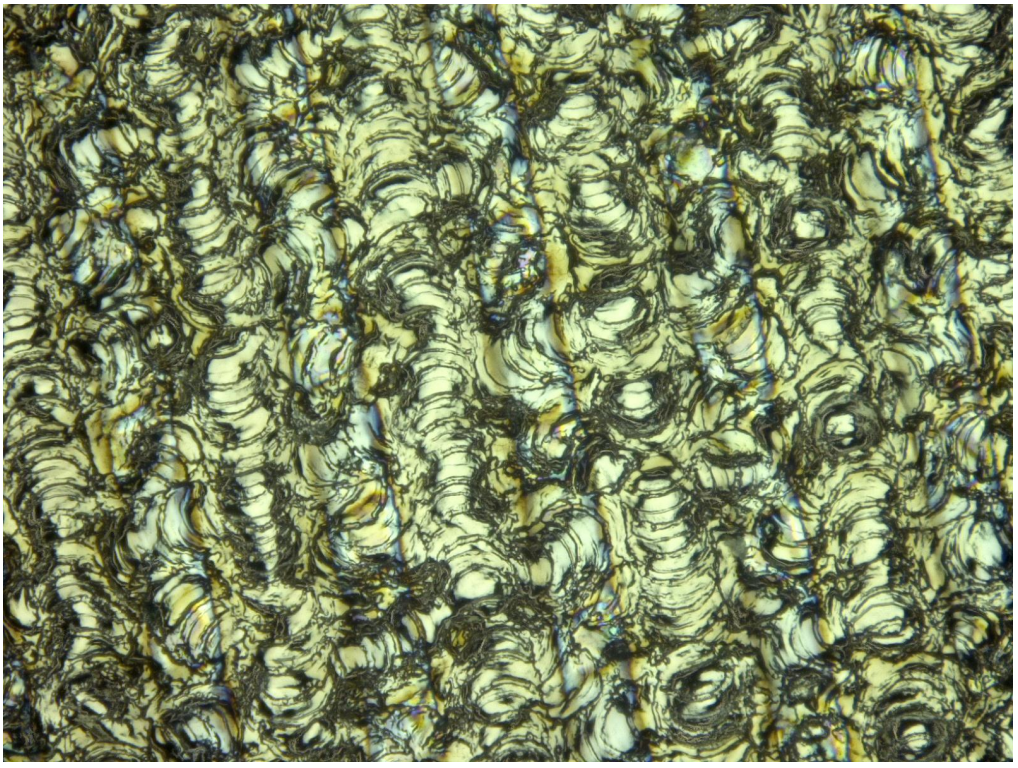

(A) Image of the surface, magnification: 300x

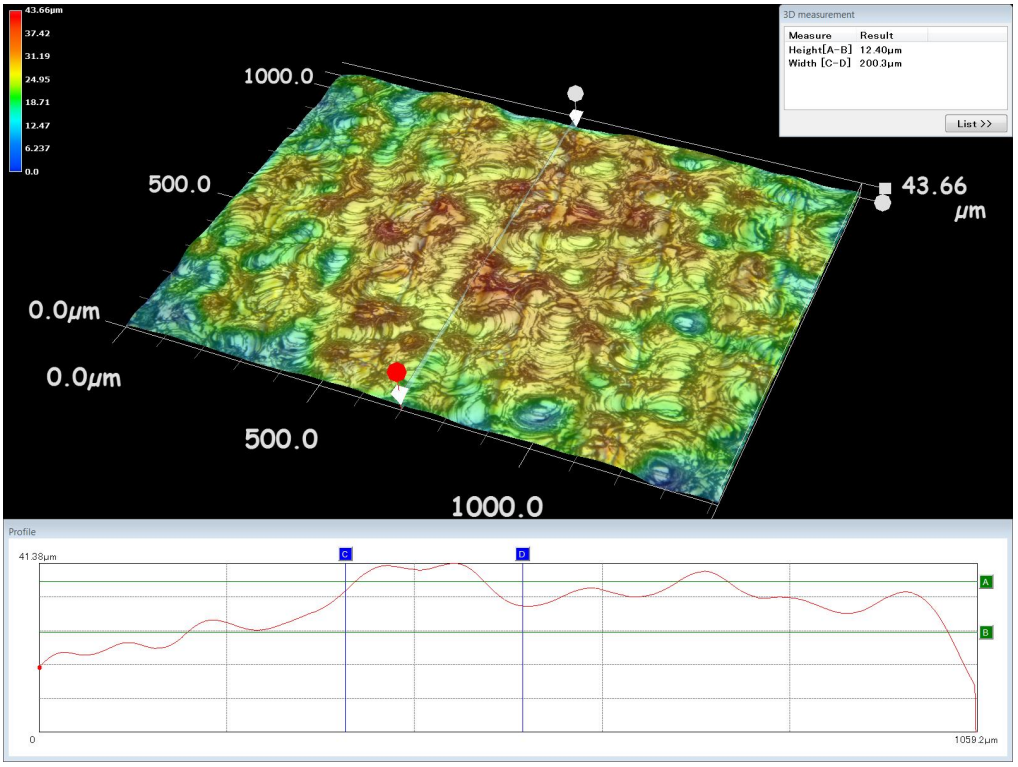

(B) 3D image and a section of the surface, magnification: 300x

FIGURE A.4: Surface after laser polishing

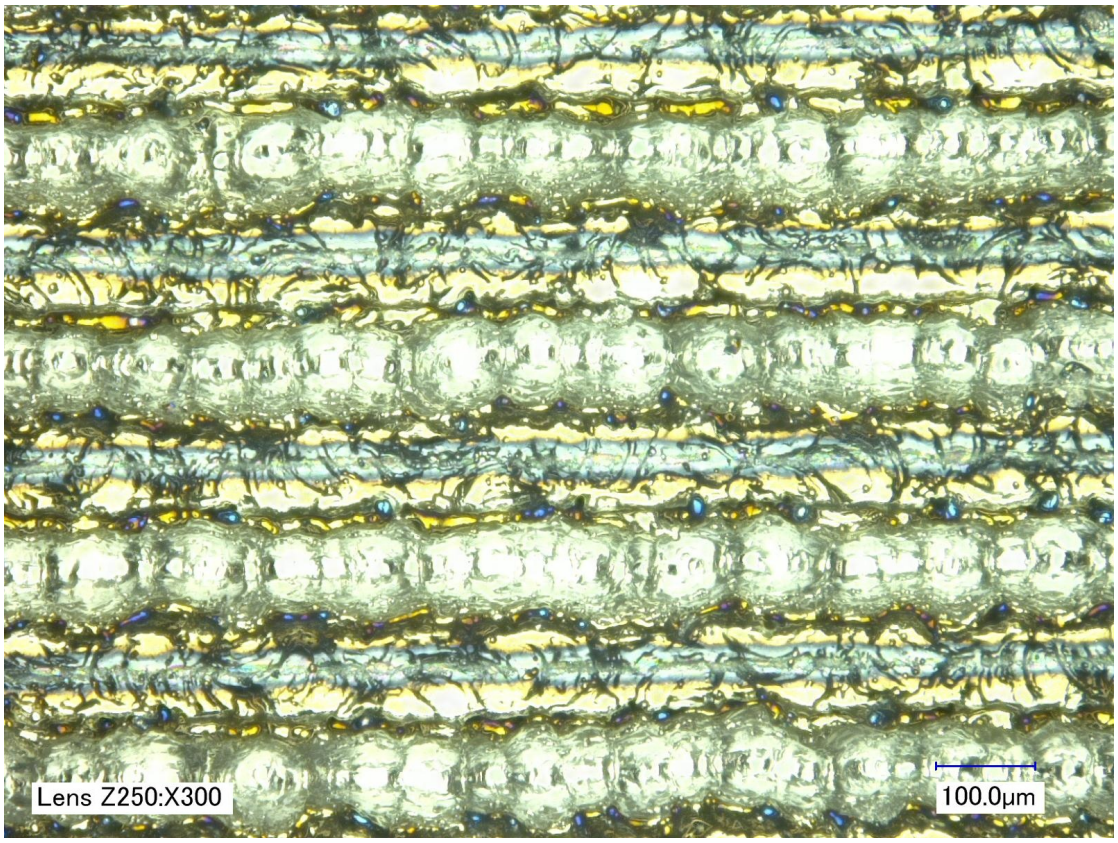

(A) Image of the surface, magnification: 300x

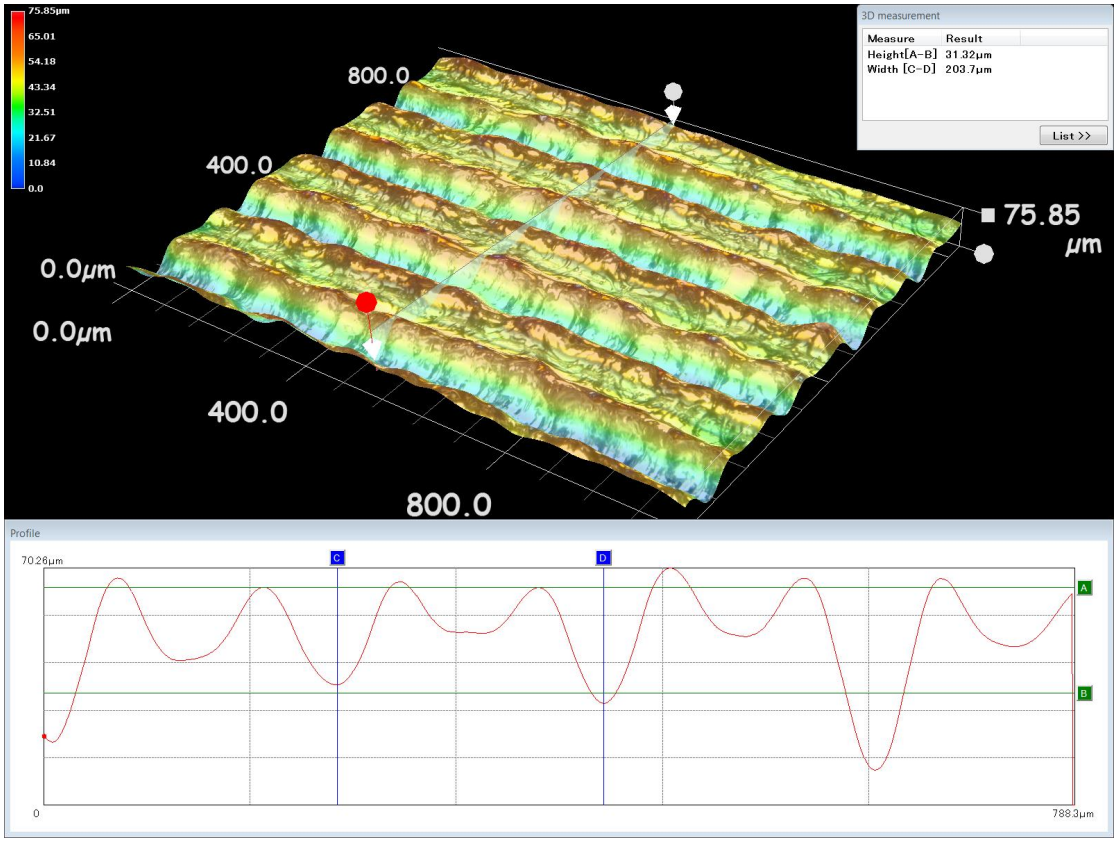

(B) 3D image and a section of the surface, magnification: 300x

FIGURE A.5: Laser textured surface: linear grooves

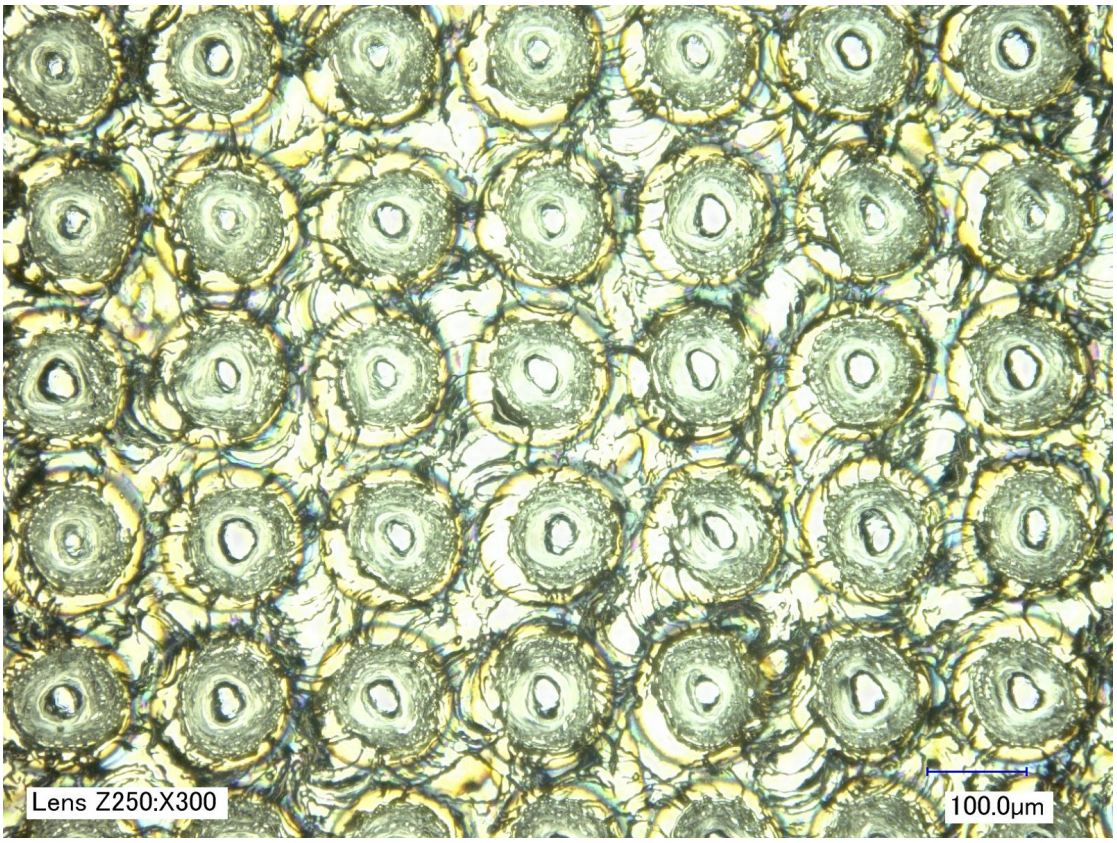

(A) Image of the surface, magnification: 300x

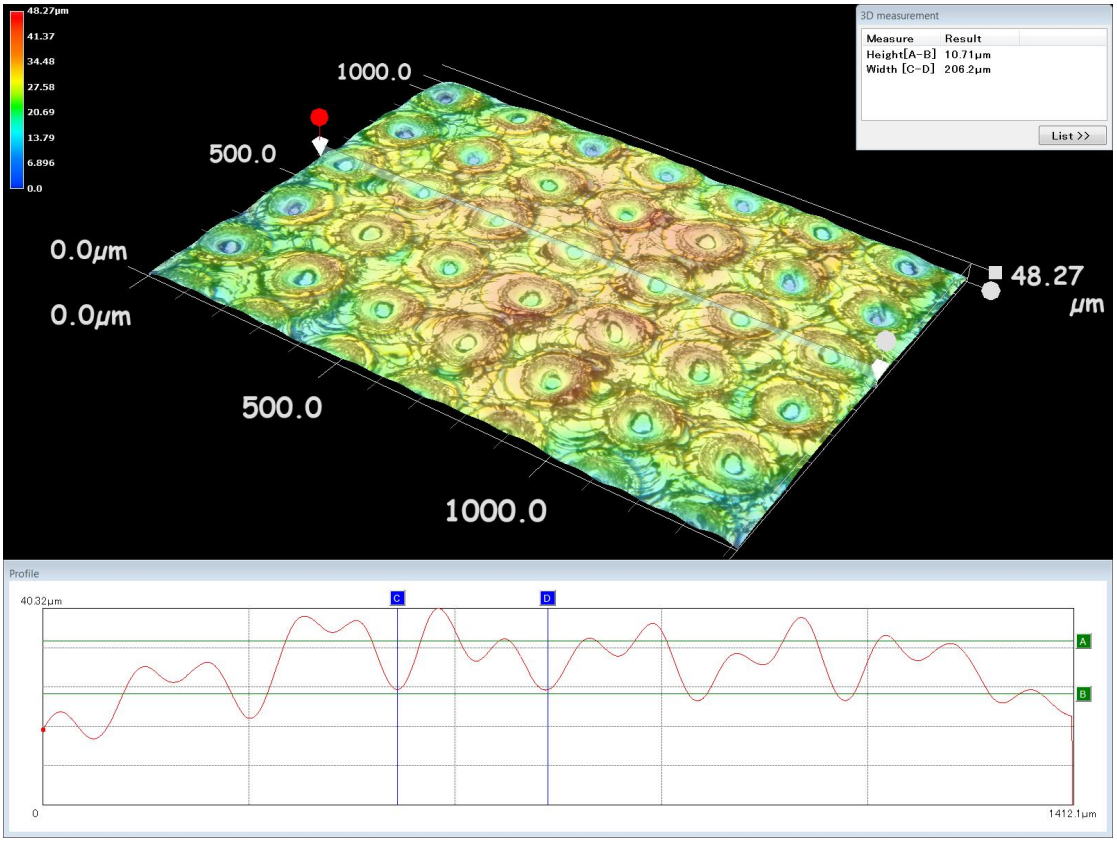

(B) 3D image and a section of the surface, magnification: 300x

FIGURE A.6: Laser textured surface: dimples

A.3 Samples after pickling

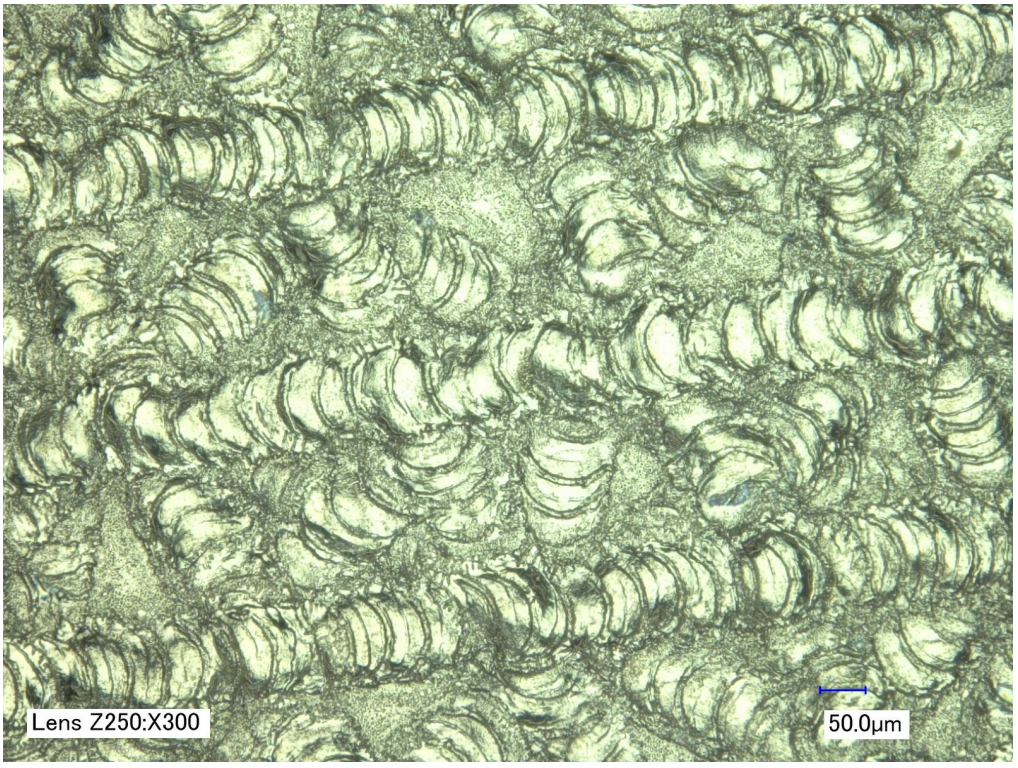

(A) Image of the surface, magnification: 300x

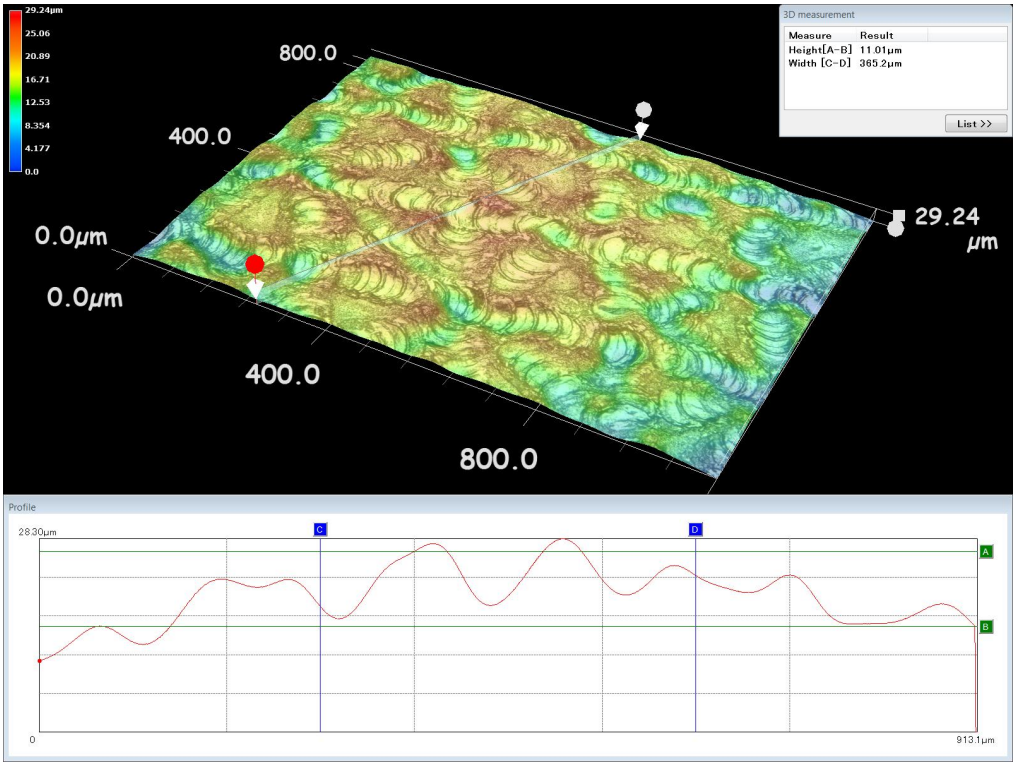

(B) 3D image and a section of the surface, magnification: 300x

FIGURE A.7: P surface after pickling

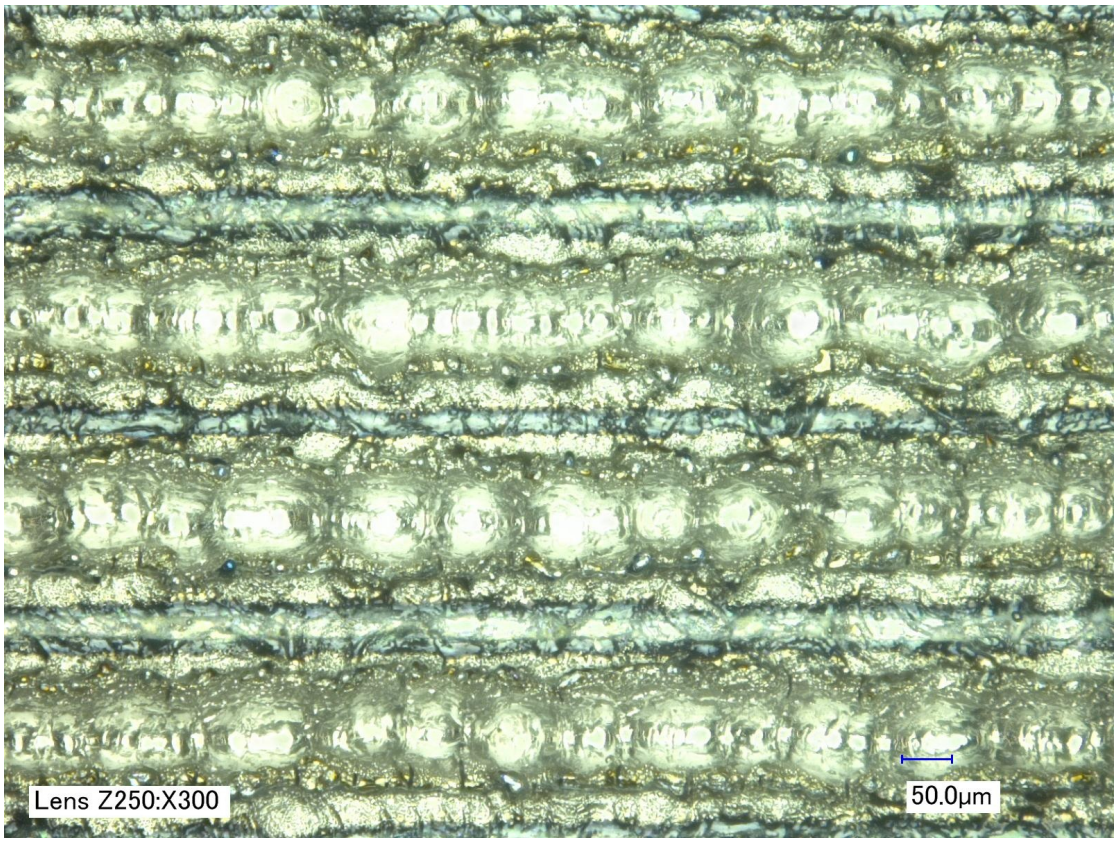

(A) Image of the surface, magnification: 300x

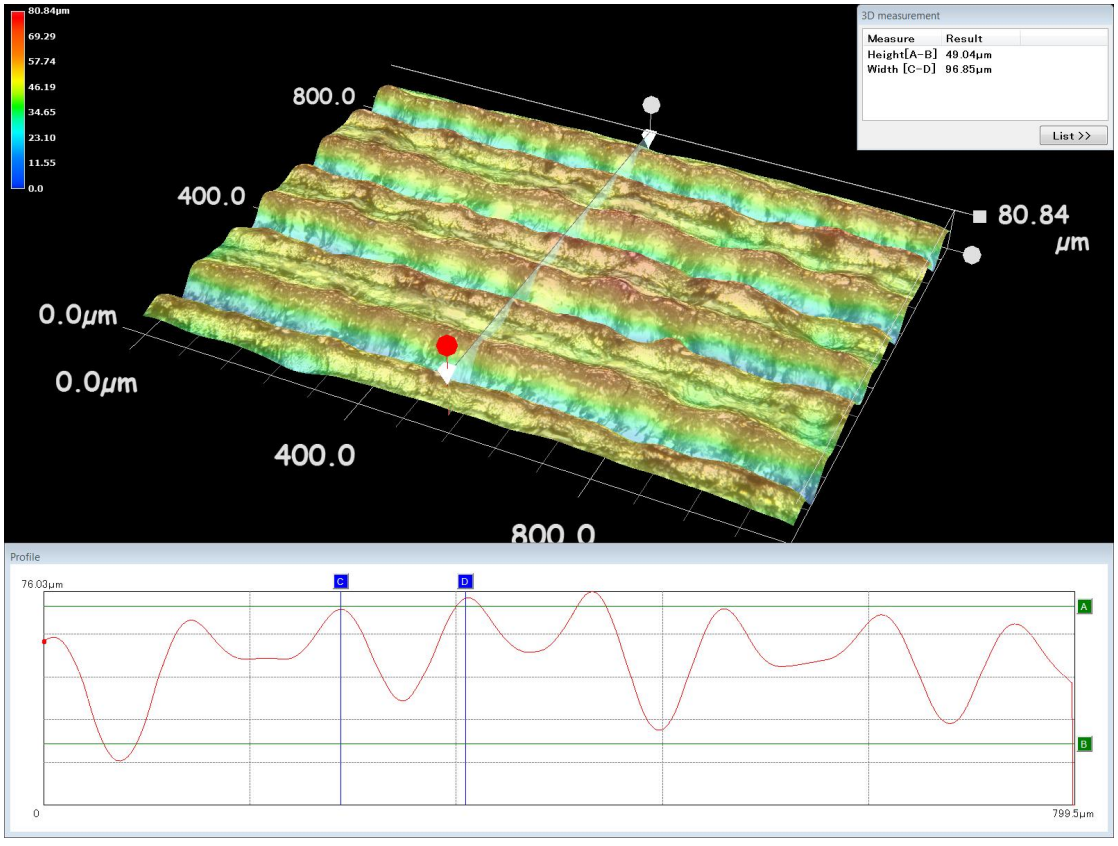

(B) 3D image and a section of the surface, magnification: 300x

FIGURE A.8: T1 surface after pickling

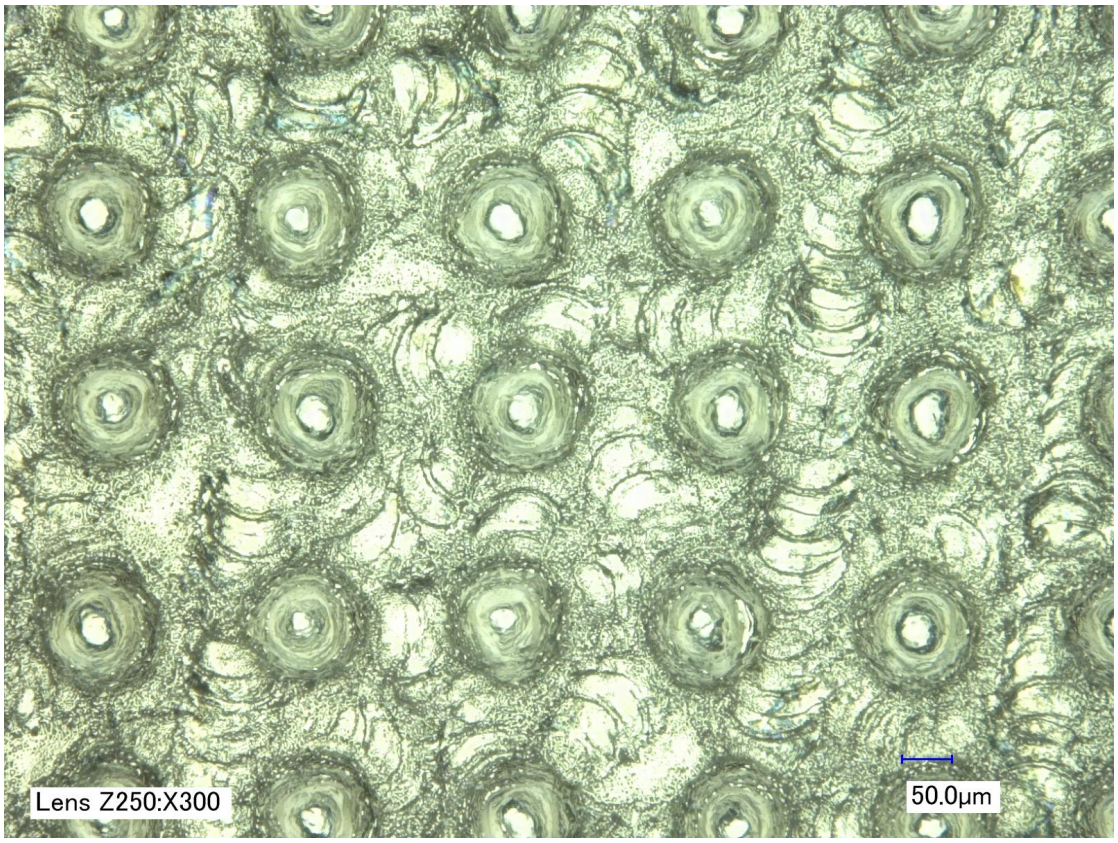

(A) Image of the surface, magnification: 300x

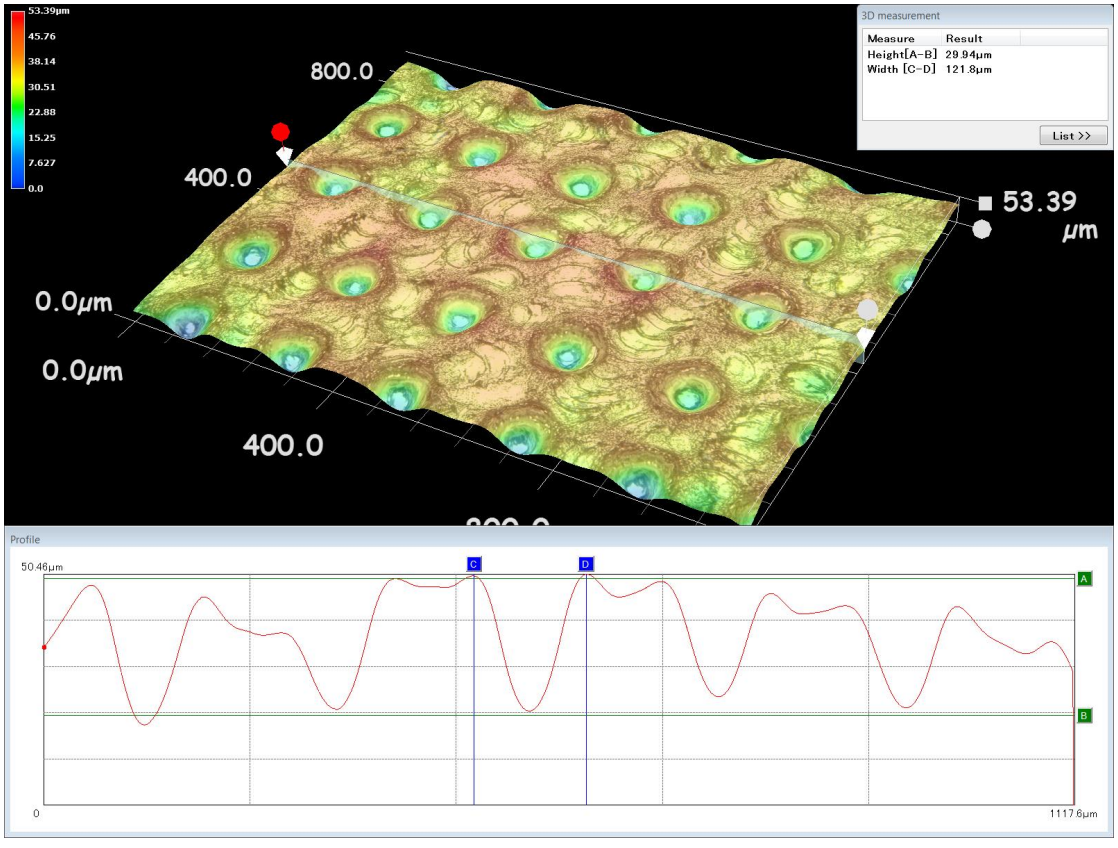

(B) 3D image and a section of the surface, magnification: 300x

FIGURE A.9: T2 surface after pickling

A.4 Samples after the PEO treatment

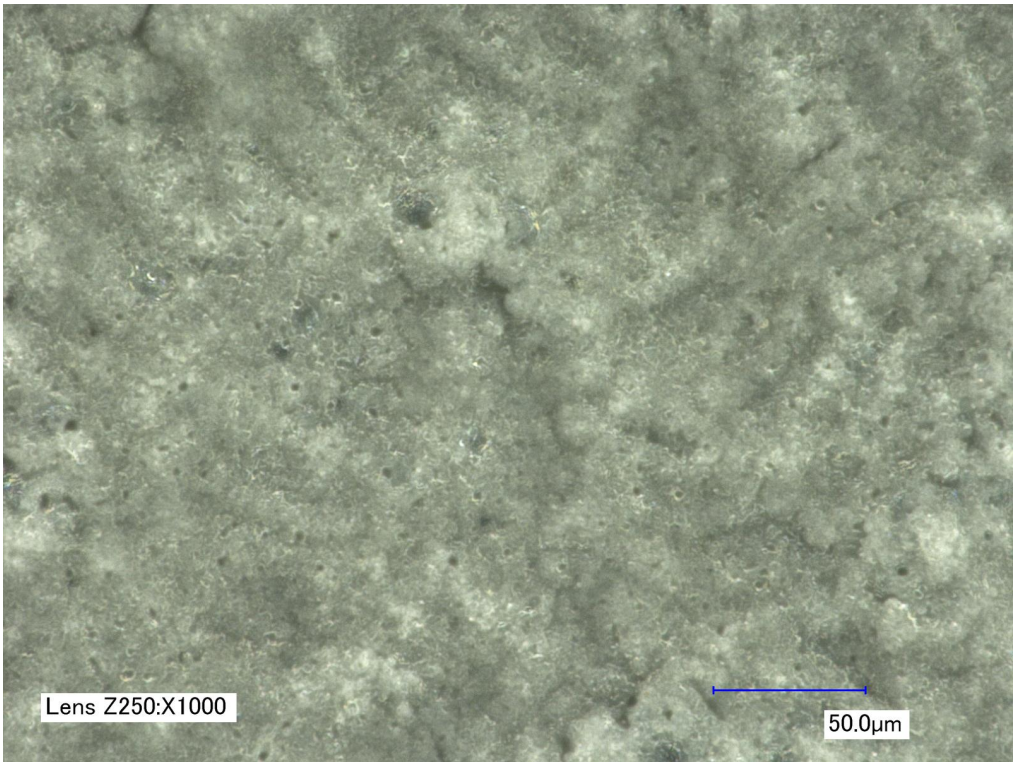

(A) Image of the surface, magnification: 1000x

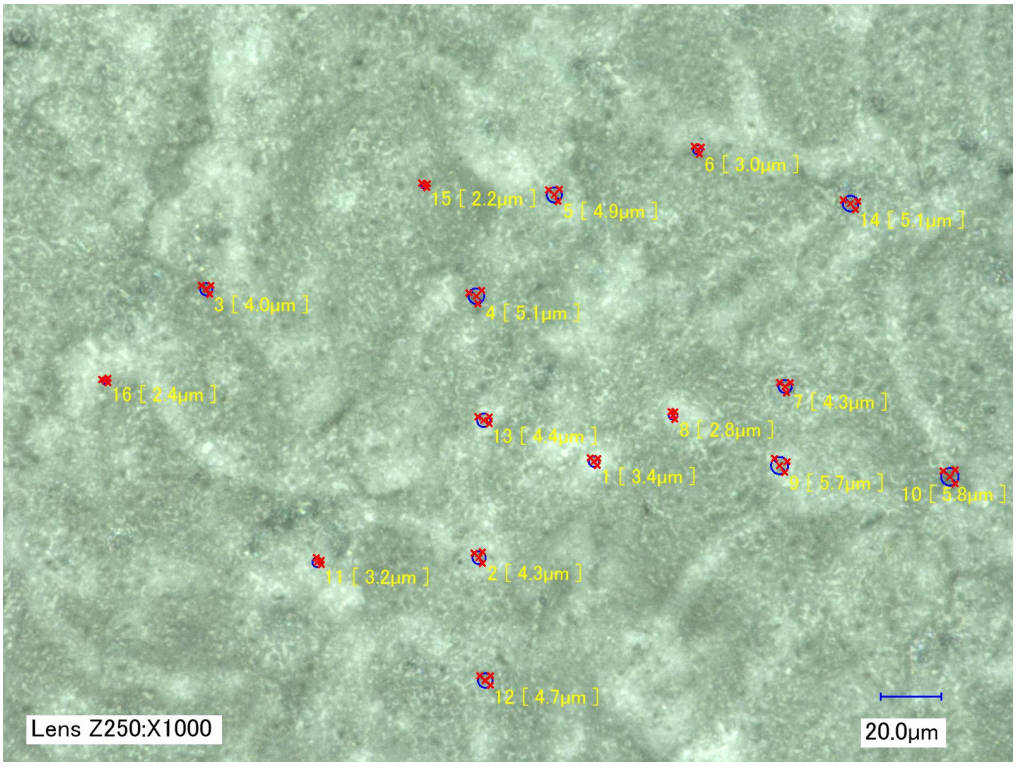

(B) 3D image and a section of the surface, magnification: 1000x

FIGURE A.10: P surface after the PEO treatment

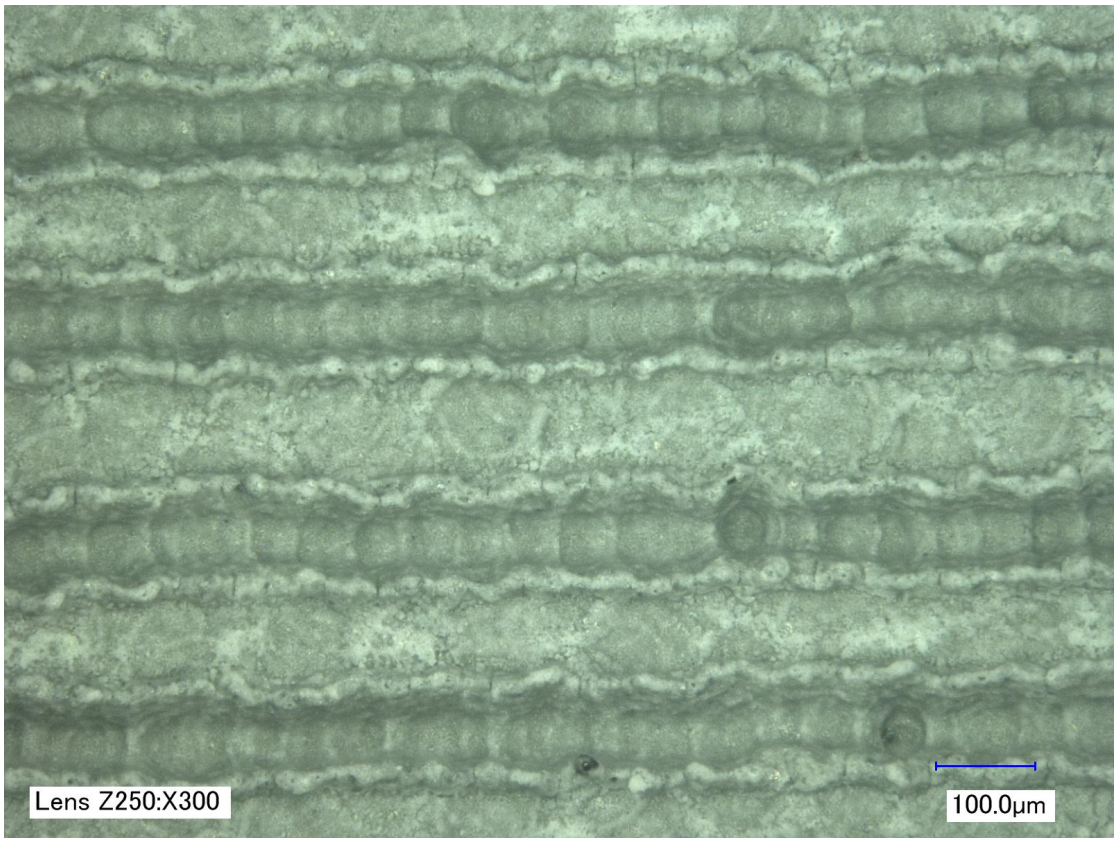

(A) Image of the surface, magnification: 300x

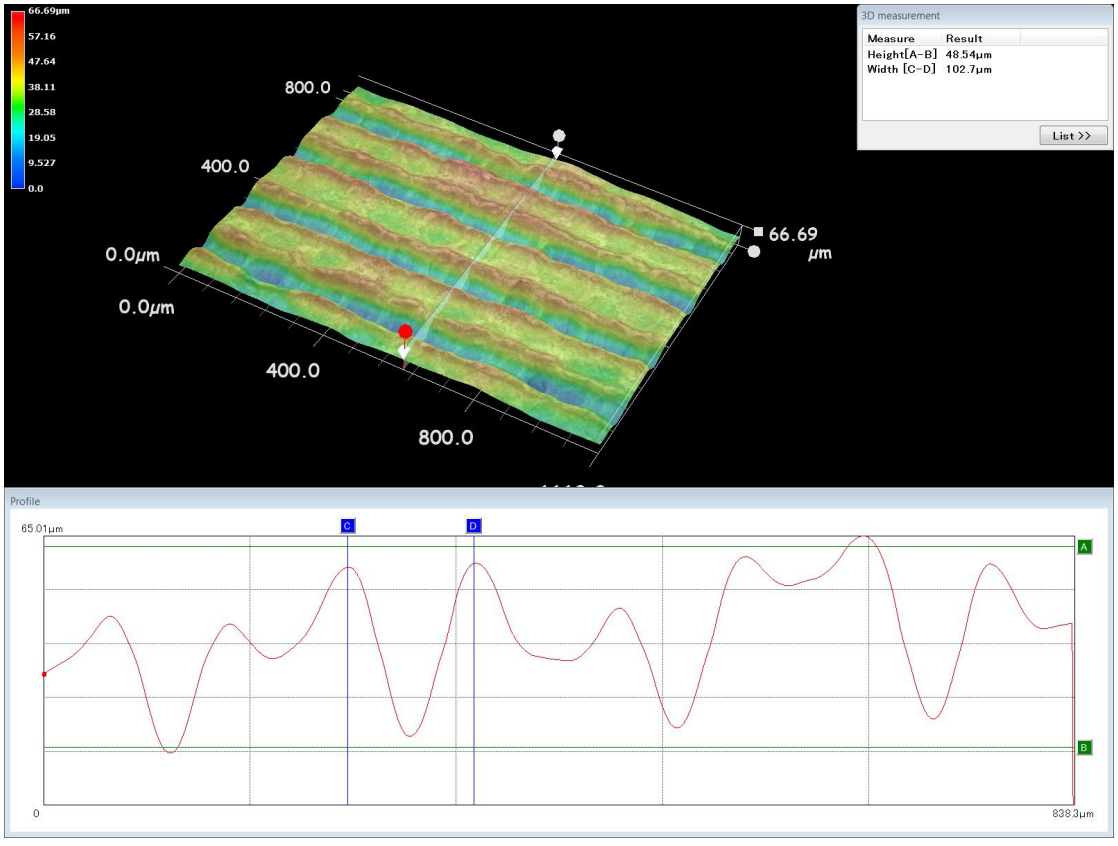

(B) 3D image and a section of the surface, magnification: 300x

FIGURE A.11: T1 surface after the PEO treatment

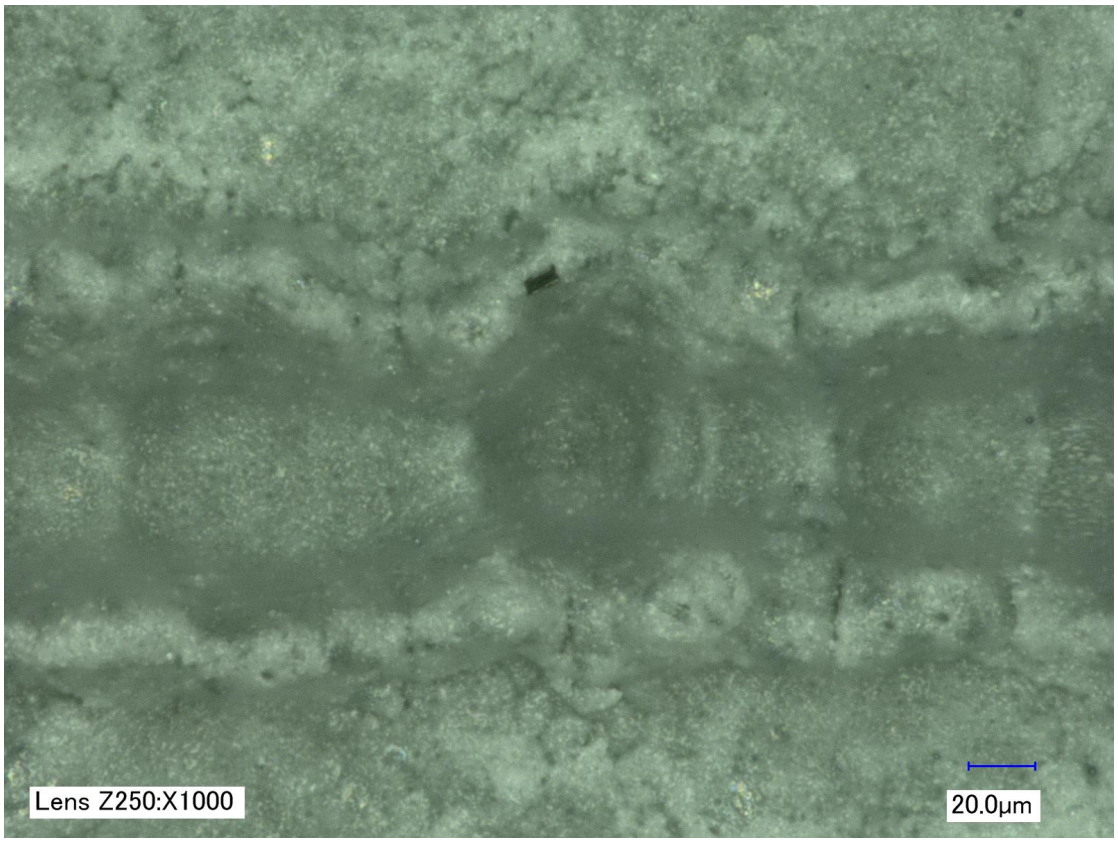

(A) Image of the surface, magnification: 1000x

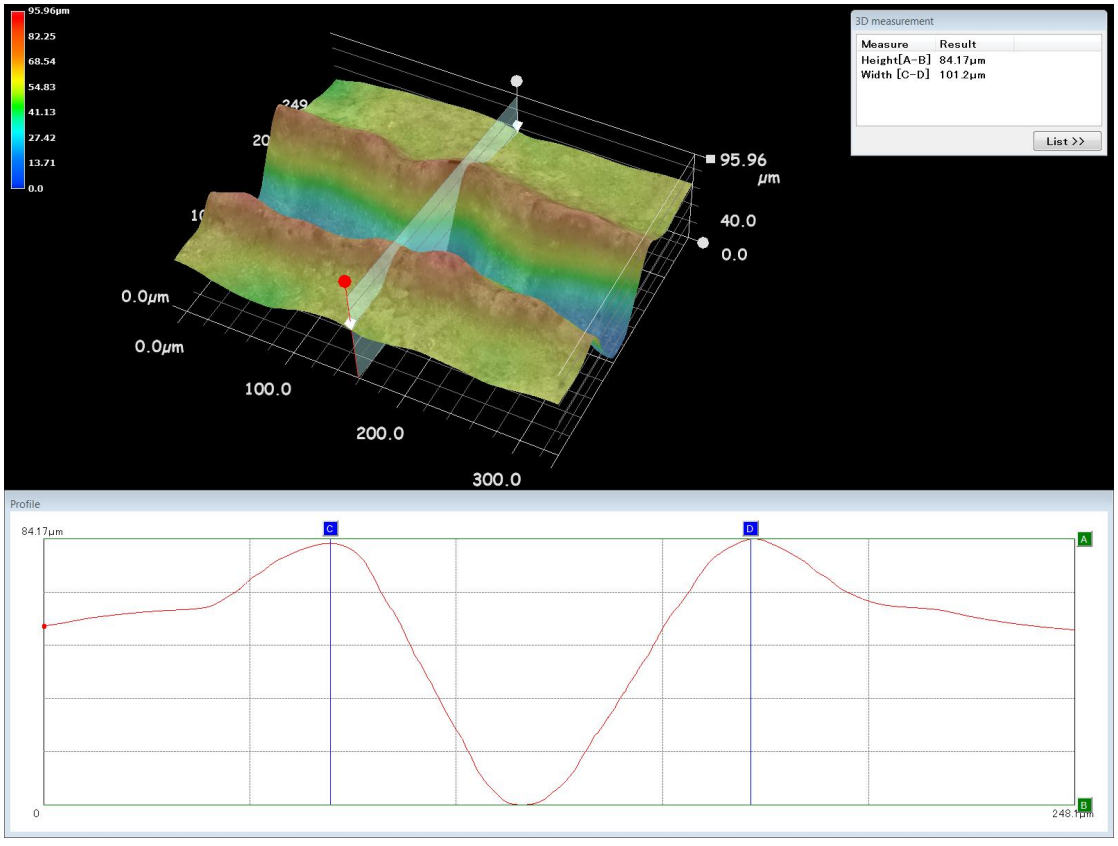

(B) 3D image and a section of the surface, magnification: 1000x

FIGURE A.12: T1 surface after the PEO treatment

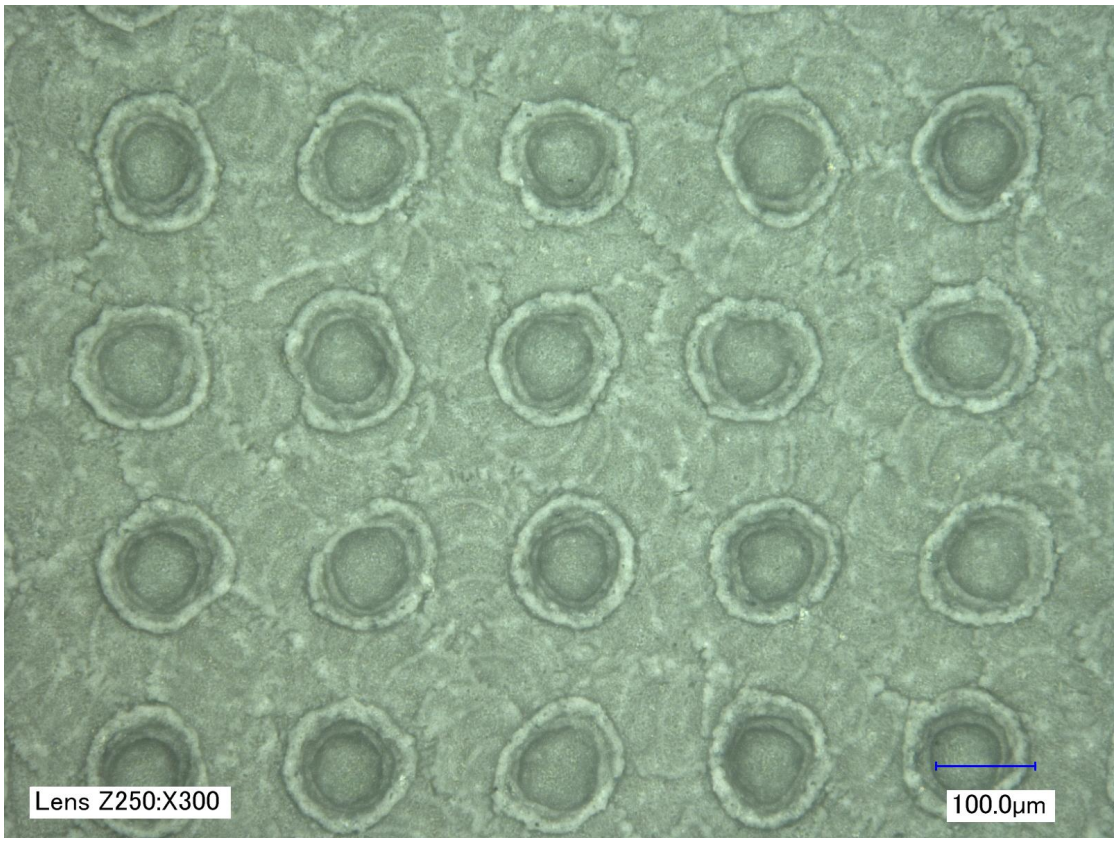

(A) Image of the surface, magnification: 300x

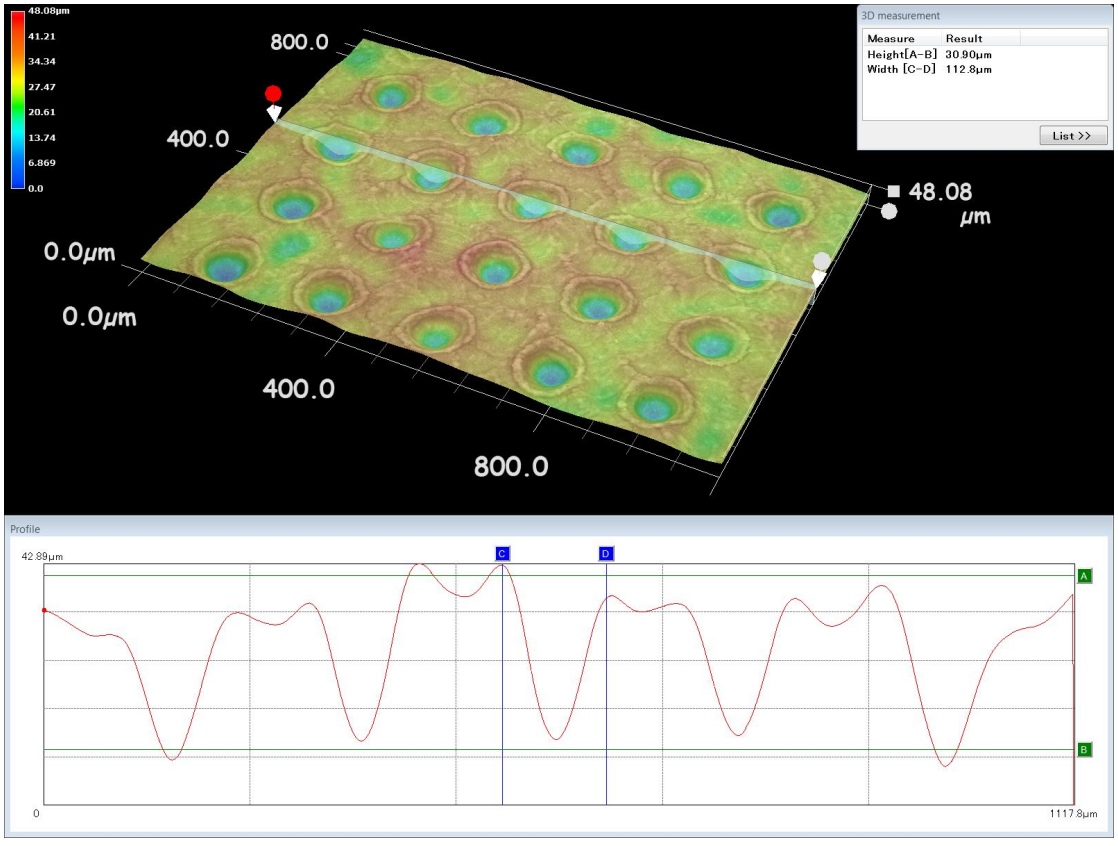

(B) 3D image and a section of the surface, magnification: 300x

FIGURE A.13: T2 surface after the PEO treatment

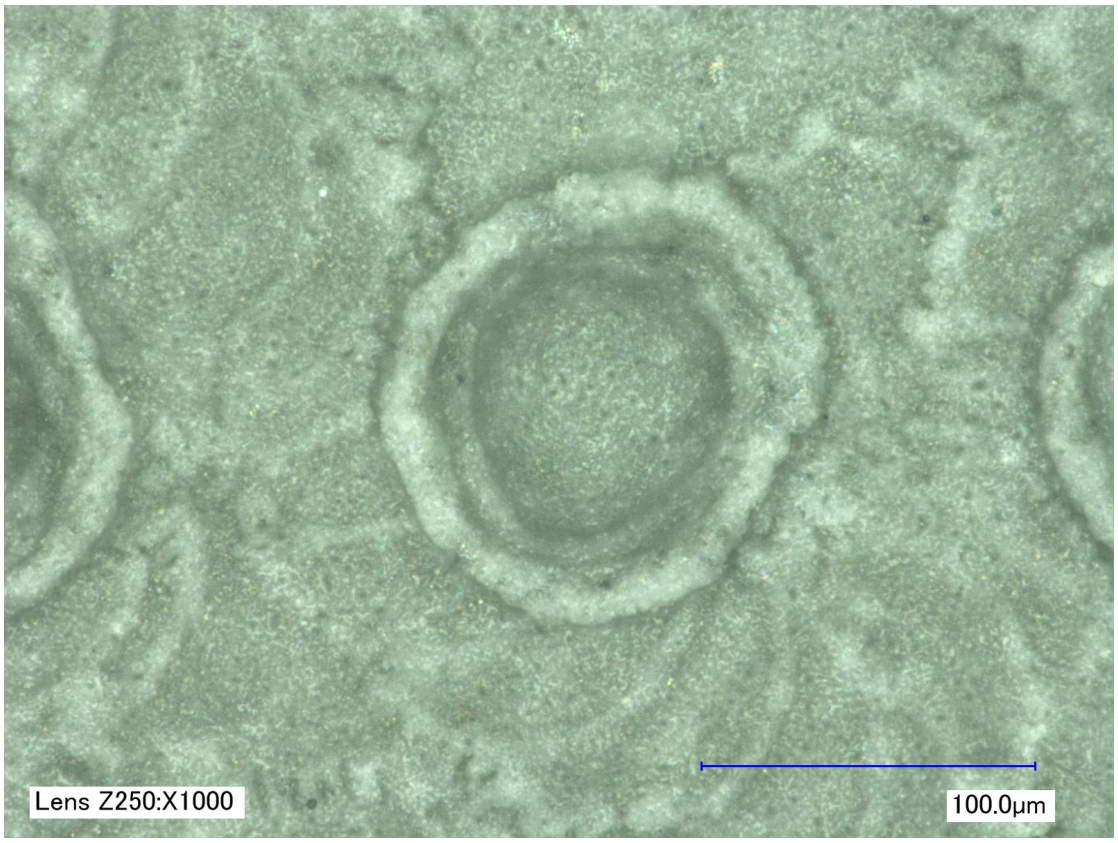

(A) Image of the surface, magnification: 1000x

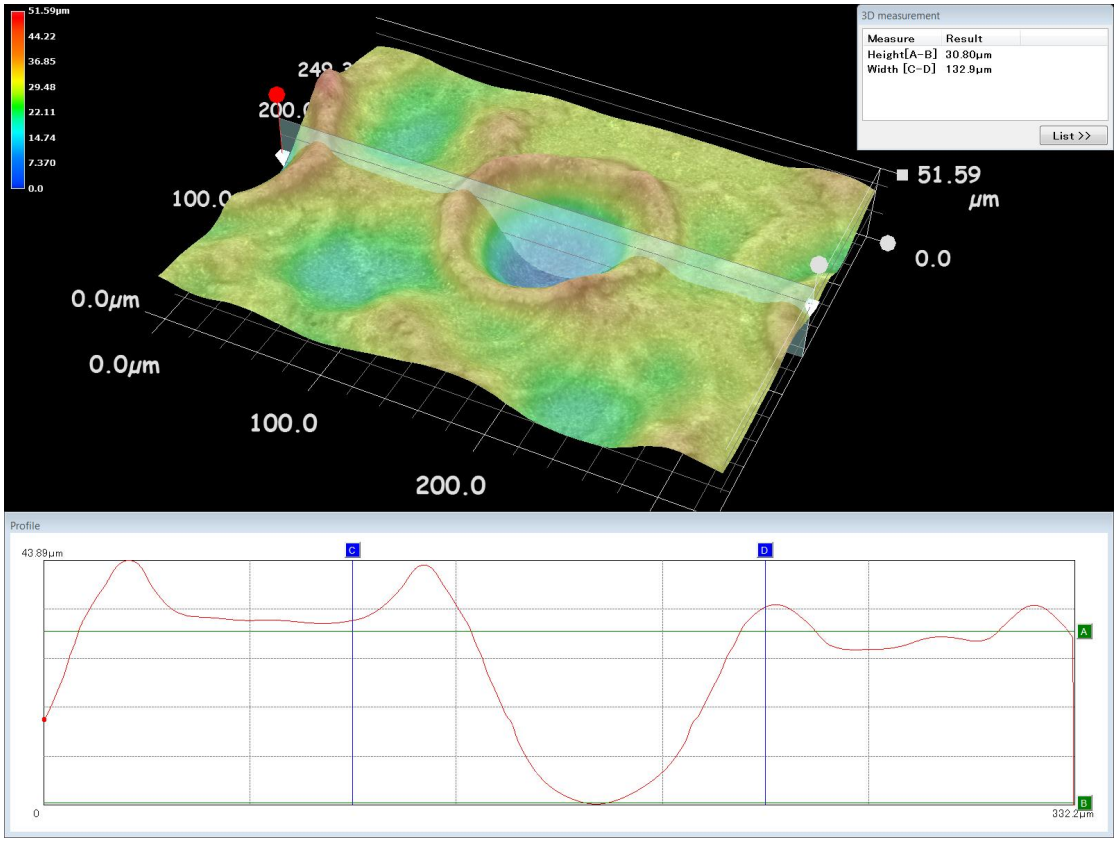

(B) 3D image and a section of the surface, magnification: 1000x

FIGURE A.14: T2 surface after the PEO treatment

Appendix B

SEM images and EDS diagrams

The SEM and EDS measurements were performed on a Philips XL 30 equipment.

B.1 C samples

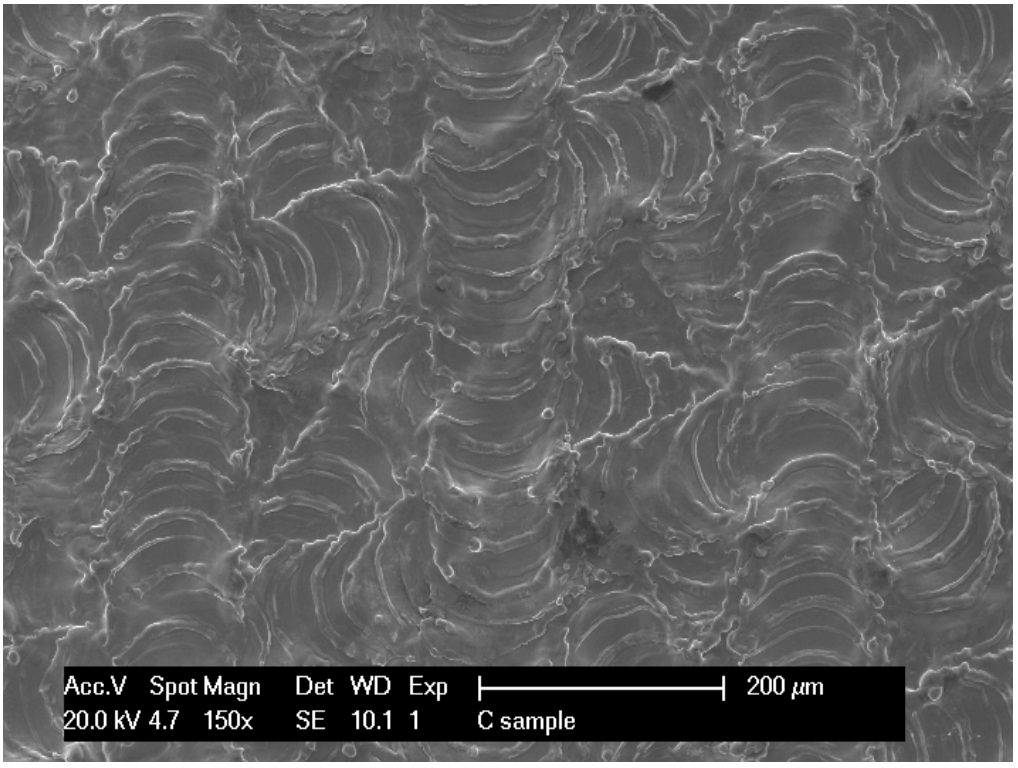

(A) Magnification: 150x

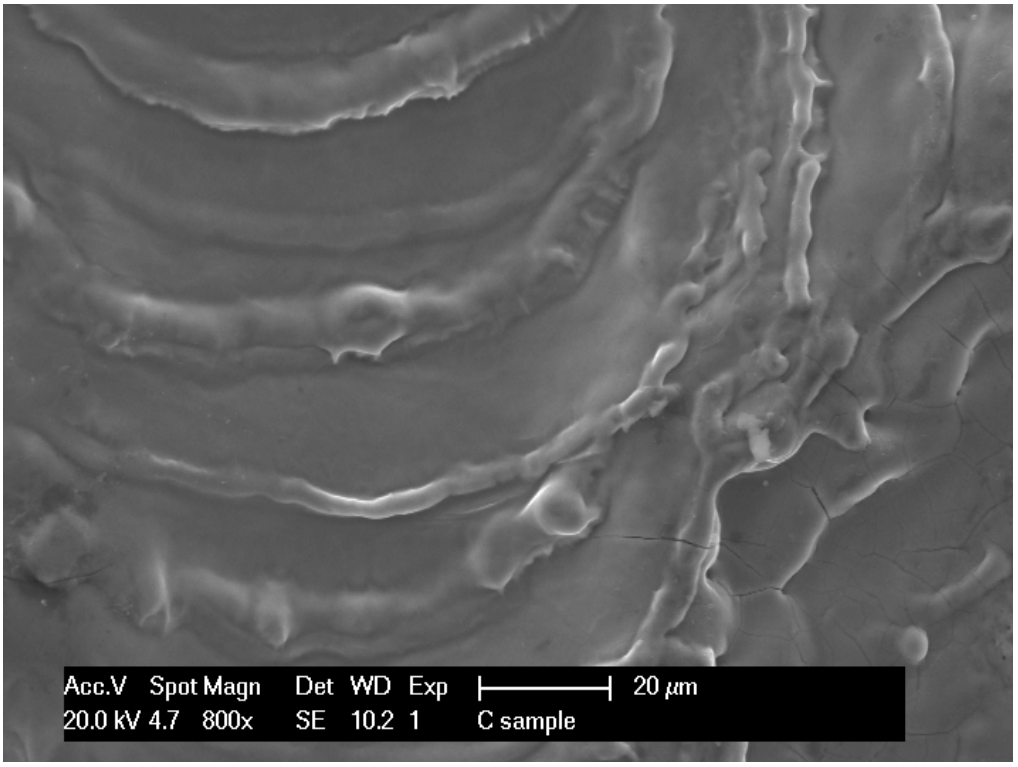

(B) Magnification: 800x. Micro-cracks are visible on the right side.

FIGURE B.1: SEM images of sample C

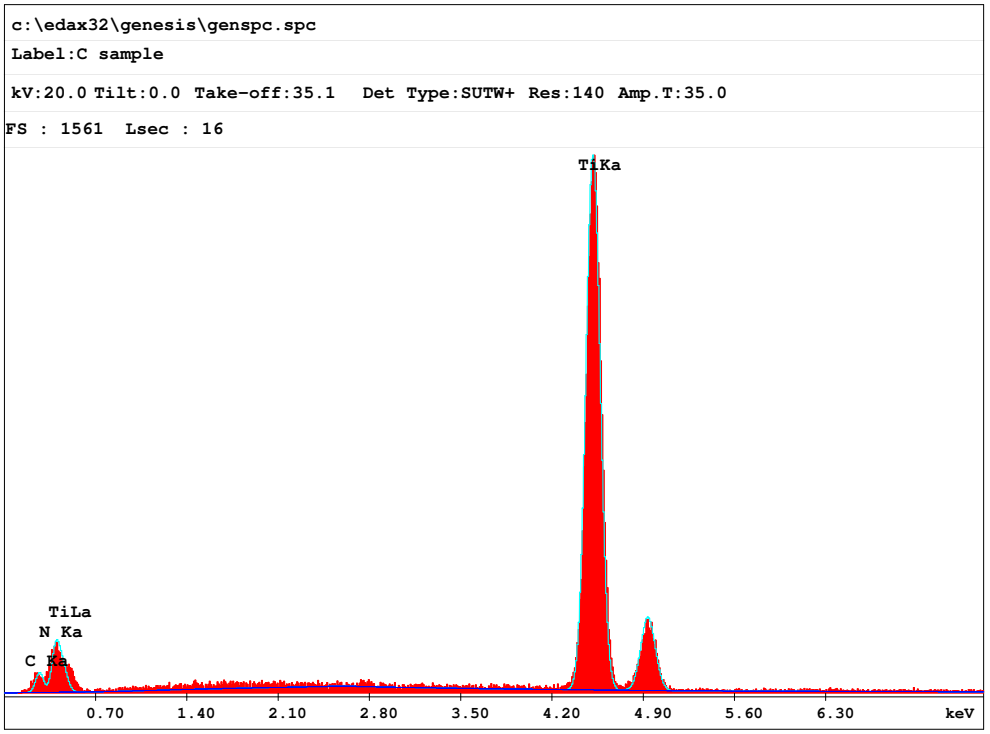

EDAX ZAF Quantification (Standardless)
Element Normalized
SEC Table : Default

Element	Wt %	At %
C K	8.99	25.24
N K	6.29	15.15
TiK	84.71	59.61
Total	100.00	100.00

Element	Net Inte.	Bkgd Inte.	Inte. Error	P/B
C K	21.99	0.48	5.34	45.77
N K	19.51	0.54	5.70	36.10
TiK	980.24	6.67	0.79	147.06

FIGURE B.2: EDS measurement of sample C

B.2 P samples

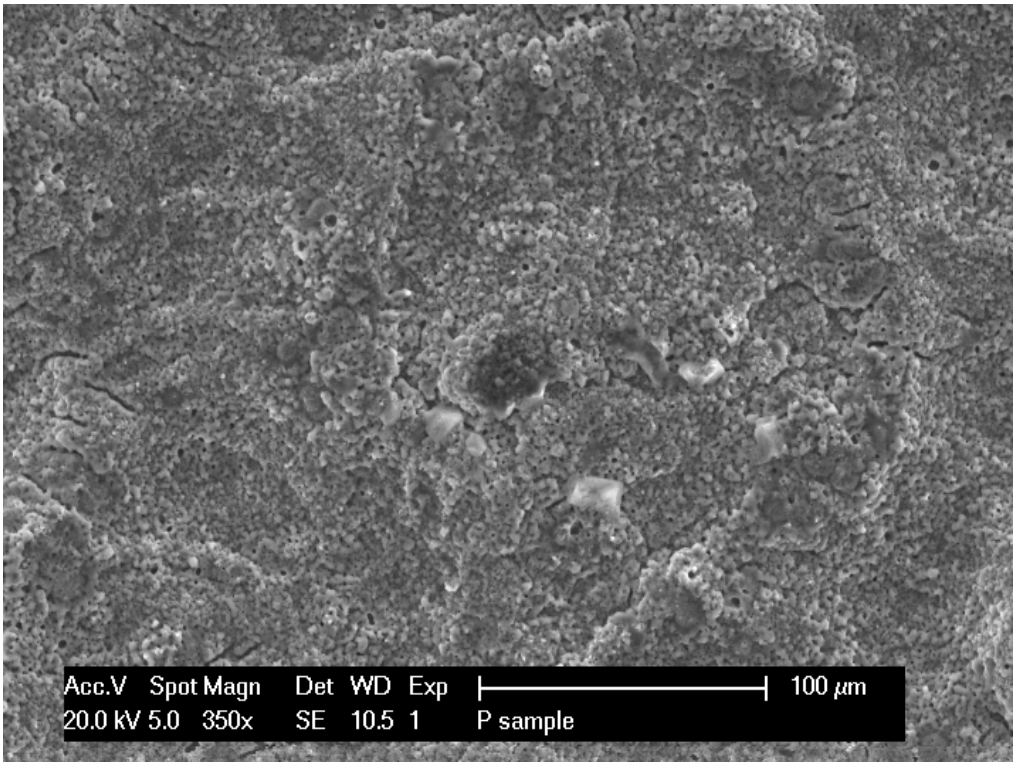

(A) Magnification: 350x

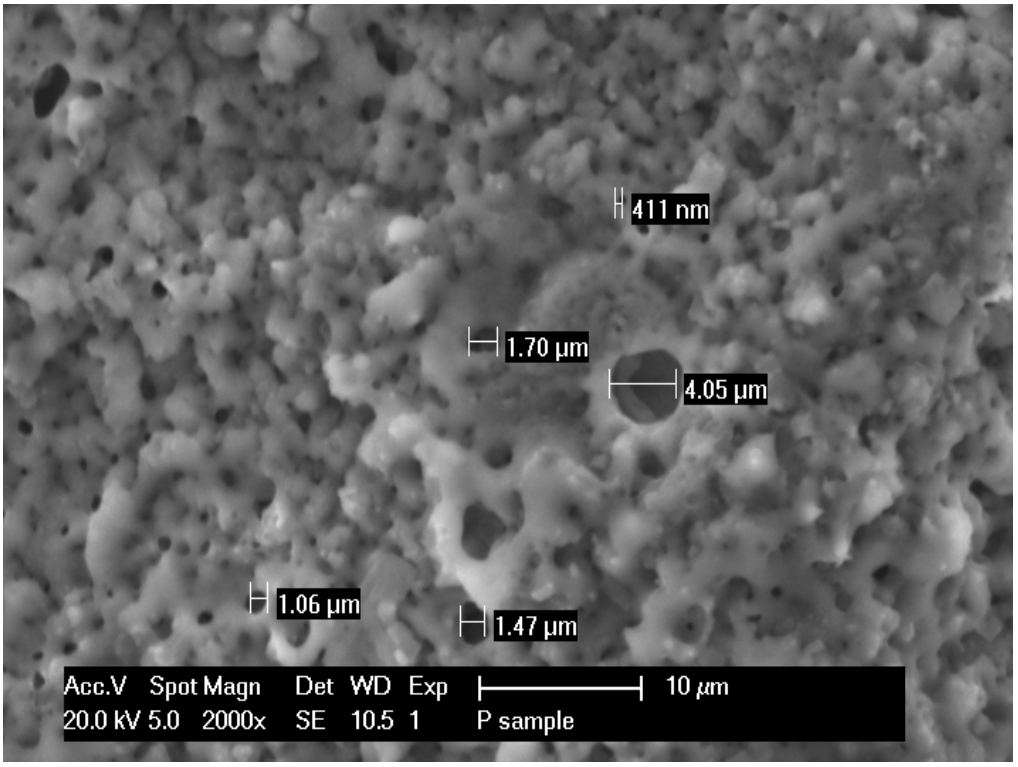

(B) Magnification: 2000x

FIGURE B.3: SEM images of sample P

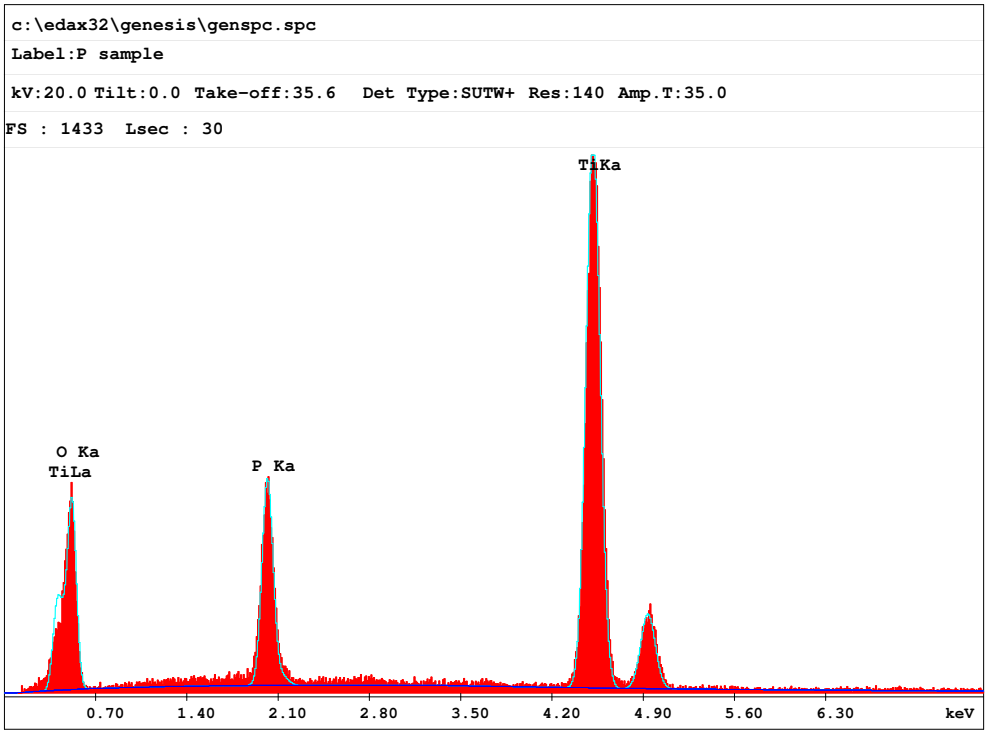

EDAX ZAF Quantification (Standardless)
Element Normalized
SEC Table : Default

Element	Wt %	At %
O K	42.64	67.12
P K	9.50	7.72
TiK	47.86	25.16
Total	100.00	100.00

Element	Net Inte.	Bkgd Inte.	Inte. Error	P/B
O K	101.59	2.26	1.84	44.90
P K	154.88	7.21	1.52	21.47
TiK	501.13	5.64	0.82	88.85

FIGURE B.4: EDS measurement of sample P's regular area

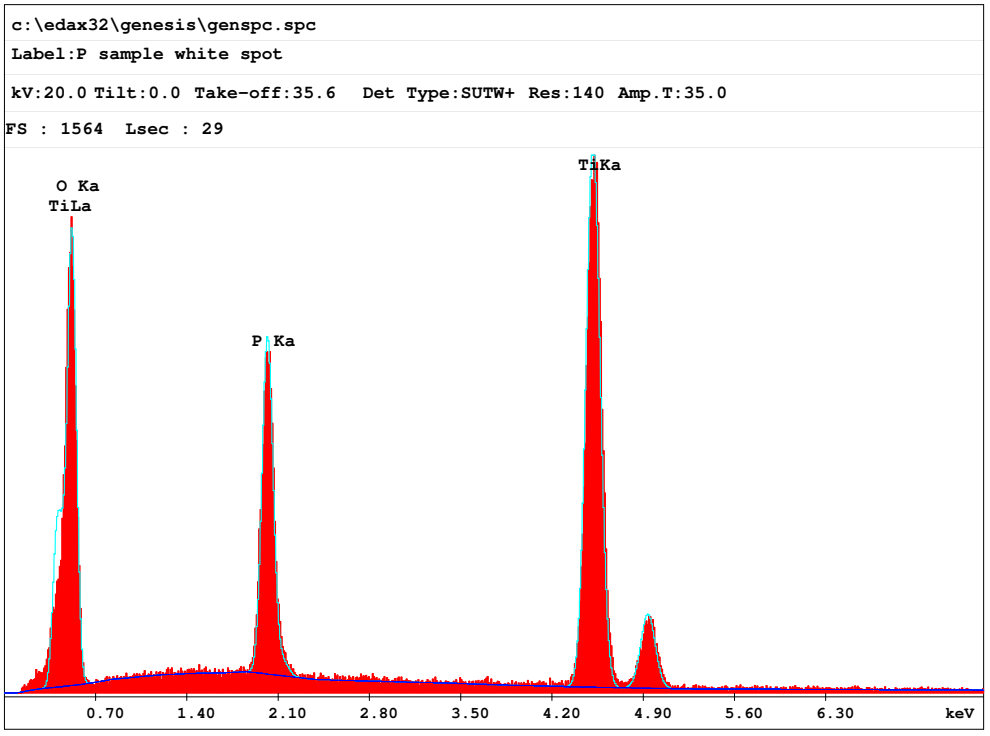

EDAX ZAF Quantification (Standardless)
Element Normalized
SEC Table : Default

Element	Wt %	At %
O K	55.61	76.81
P K	10.77	7.68
TiK	33.62	15.51
Total	100.00	100.00

Element	Net Inte.	Bkgd Inte.	Inte. Error	P/B
O K	274.22	5.77	1.13	47.52
P K	281.97	20.26	1.17	13.92
TiK	554.55	7.28	0.79	76.18

FIGURE B.5: EDS measurement of a white spot on sample P

B.3 T1 samples

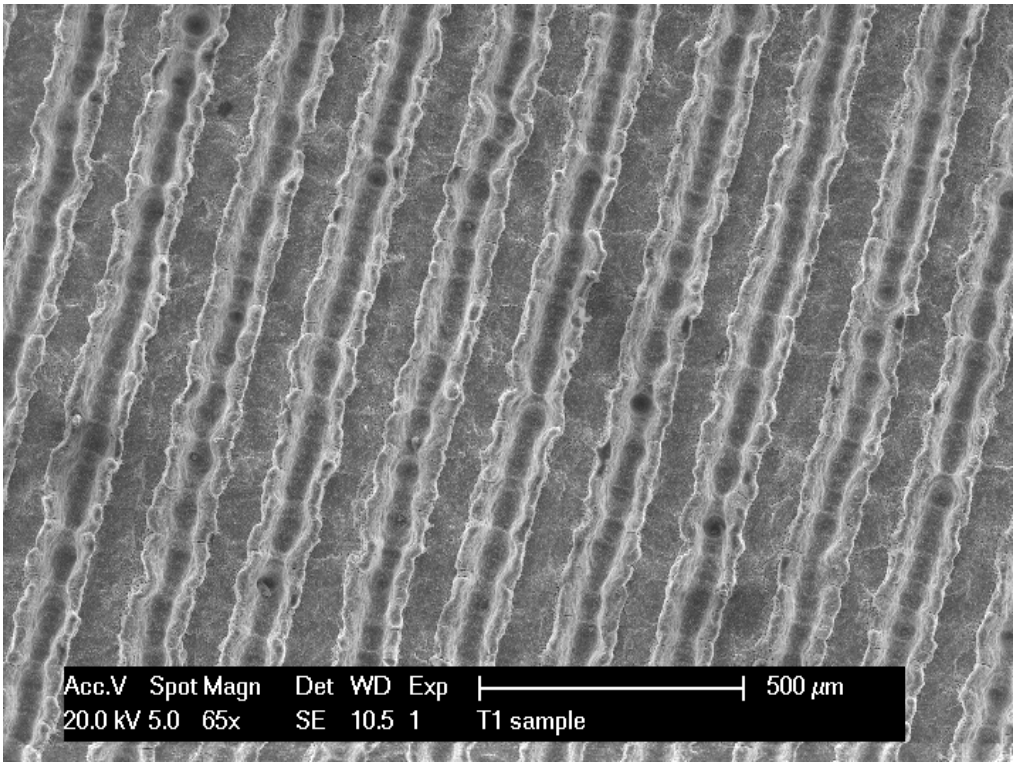

(A) Magnification: 65x

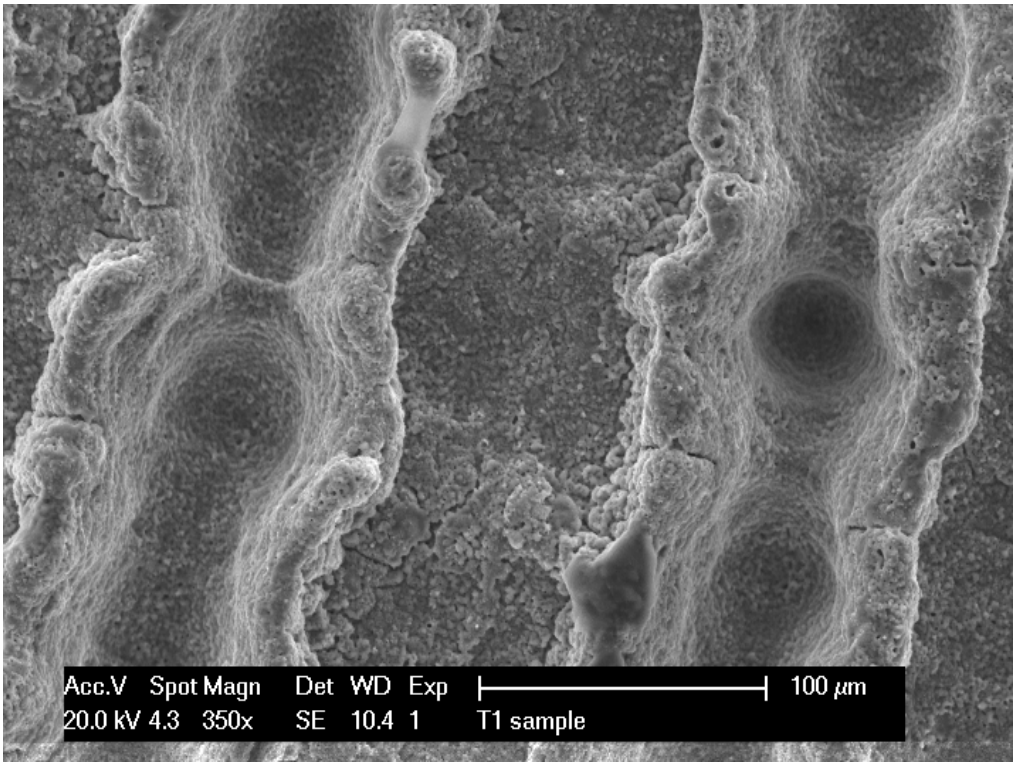

(B) Magnification: 350x

FIGURE B.6: SEM images of sample T1

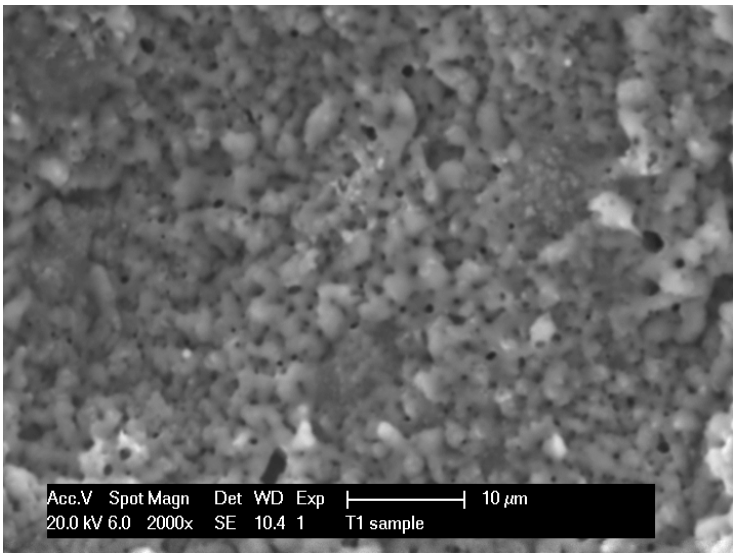

(A) Area between two grooves. Magnification: 2000x

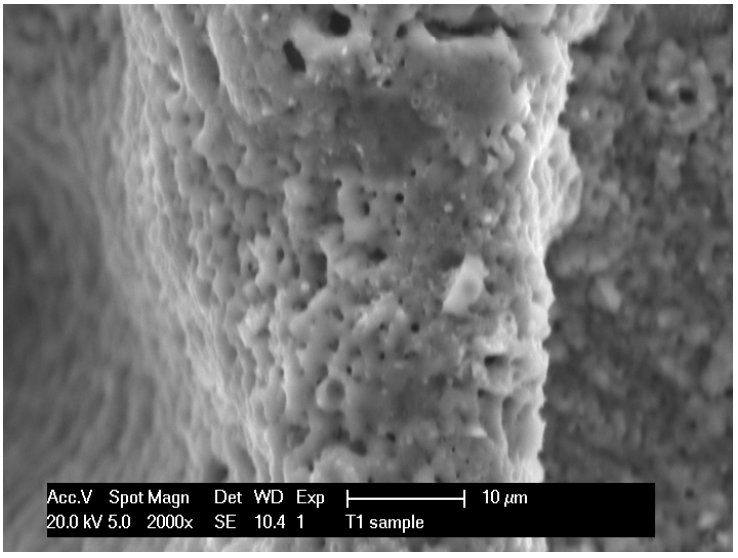

(B) A barbed part. Magnification: 2000x

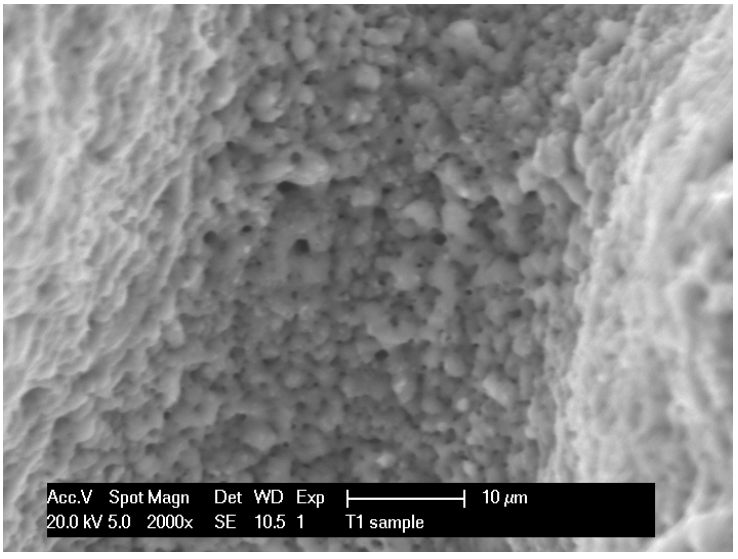

(C) Surface of a groove. Magnification: 2000x

FIGURE B.7: SEM images of sample T1 showing porosity

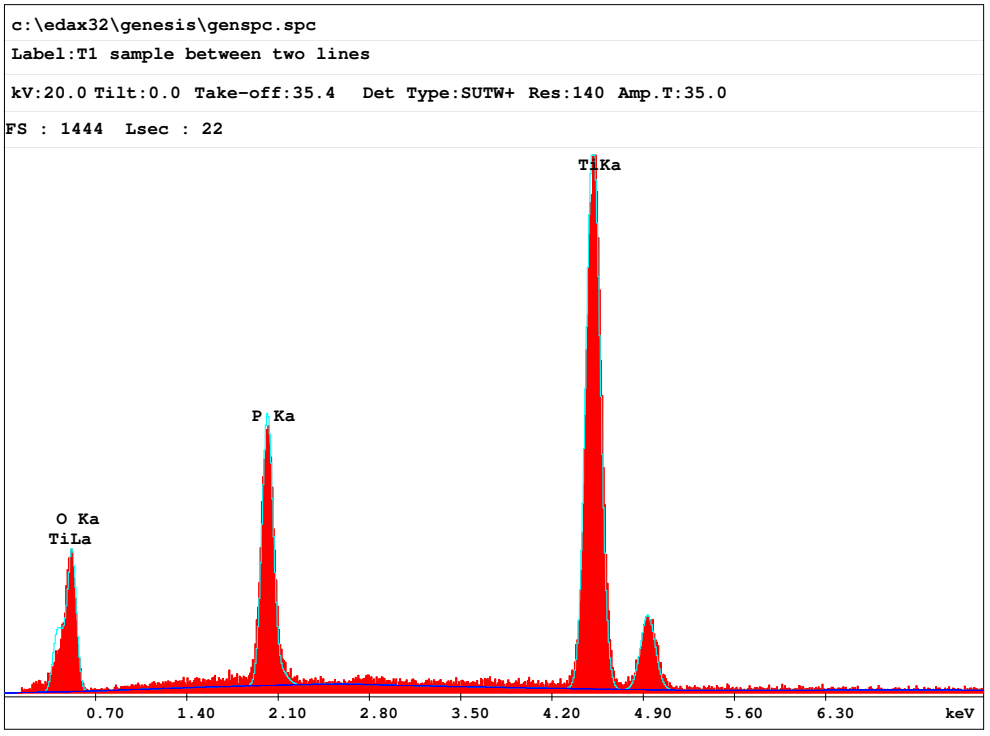

EDAX ZAF Quantification (Standardless)
Element Normalized
SEC Table : Default

Element	Wt %	At %
O K	36.25	60.48
P K	13.11	11.30
TiK	50.64	28.22
Total	100.00	100.00

Element	Net Inte.	Bkgd Inte.	Inte. Error	P/B
O K	102.54	1.27	2.09	80.79
P K	274.05	9.63	1.31	28.46
TiK	674.40	6.00	0.81	112.48

FIGURE B.8: EDS measurement of sample T1 on area between two grooves

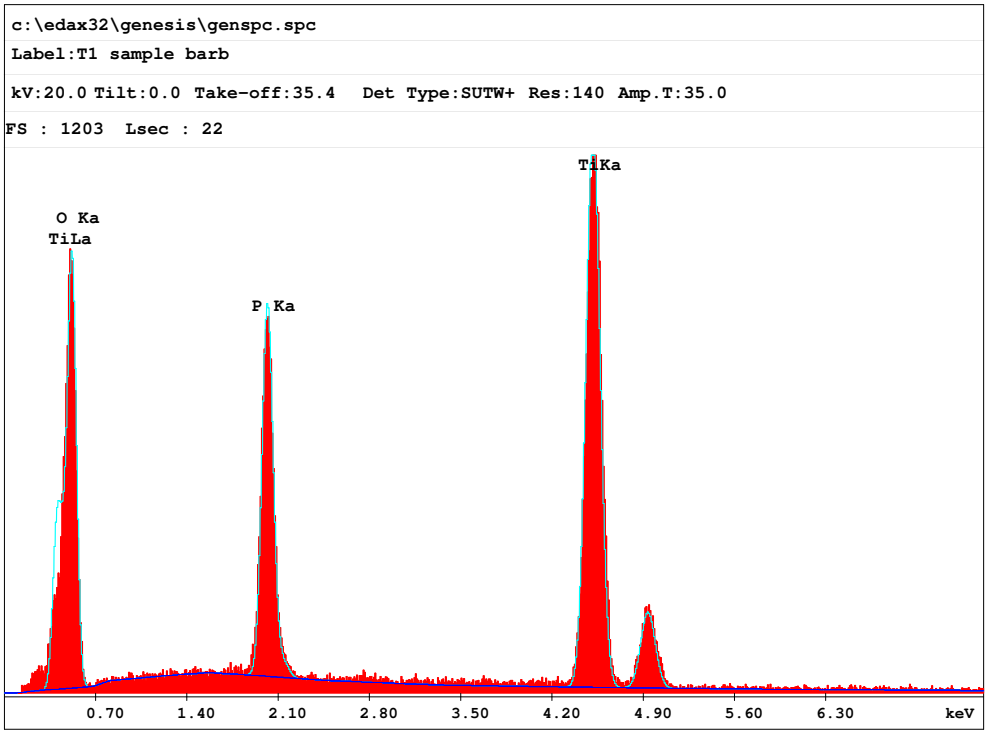

EDAX ZAF Quantification (Standardless)
Element Normalized
SEC Table : Default

Element	Wt %	At %
O K	53.93	75.46
P K	11.82	8.54
TiK	34.25	16.00
Total	100.00	100.00

Element	Net Inte.	Bkgd Inte.	Inte. Error	P/B
O K	265.51	3.73	1.31	71.19
P K	317.54	18.11	1.25	17.53
TiK	578.65	7.19	0.89	80.45

FIGURE B.9: EDS measurement of sample T1 on a barbed part

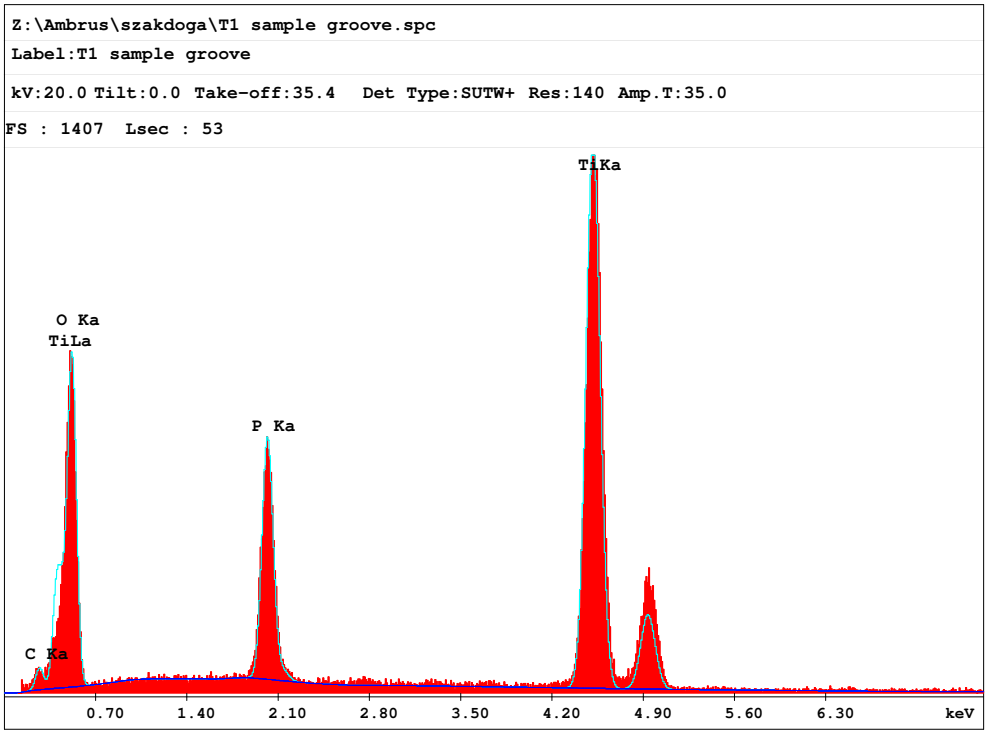

EDAX ZAF Quantification (Standardless)
Element Normalized
SEC Table : Default

Element	Wt %	At %
C K	5.33	9.69
O K	49.55	67.64
P K	8.41	5.93
TiK	36.70	16.73
Total	100.00	100.00

Element	Net Inte.	Bkgd Inte.	Inte. Error	P/B
C K	6.77	1.22	6.13	5.56
O K	101.38	2.30	1.39	44.02
P K	101.74	7.30	1.45	13.93
TiK	280.40	2.92	0.83	95.99

FIGURE B.10: EDS measurement of sample T1 in a groove

B.4 T2 samples

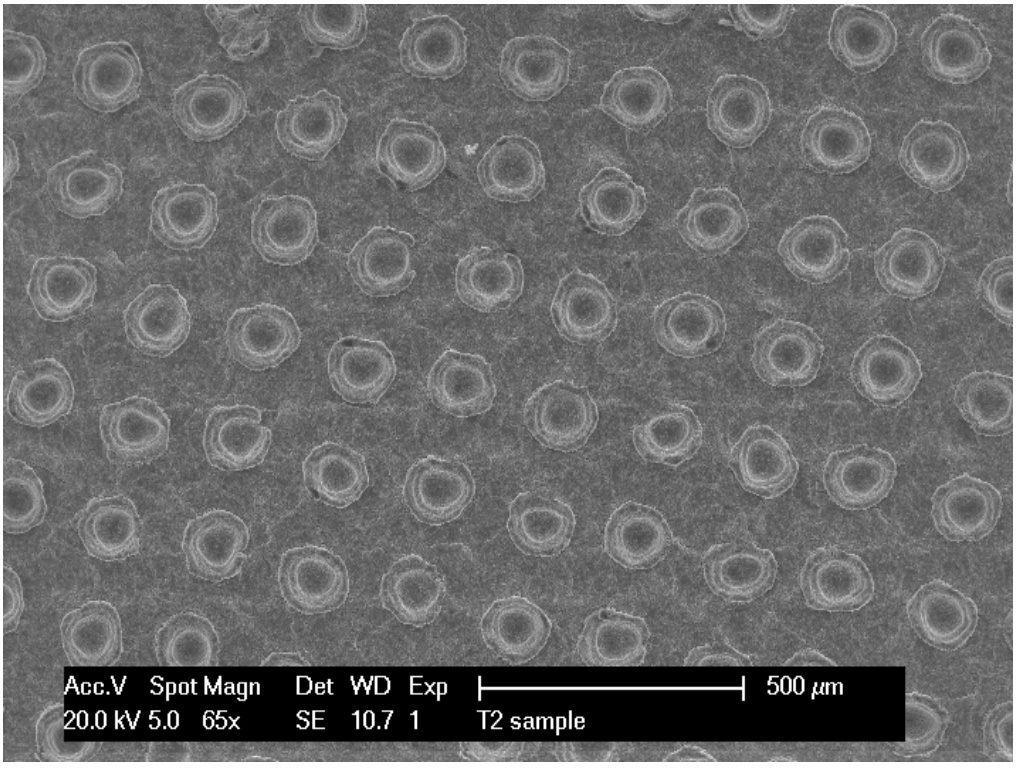

(A) Magnification: 65x

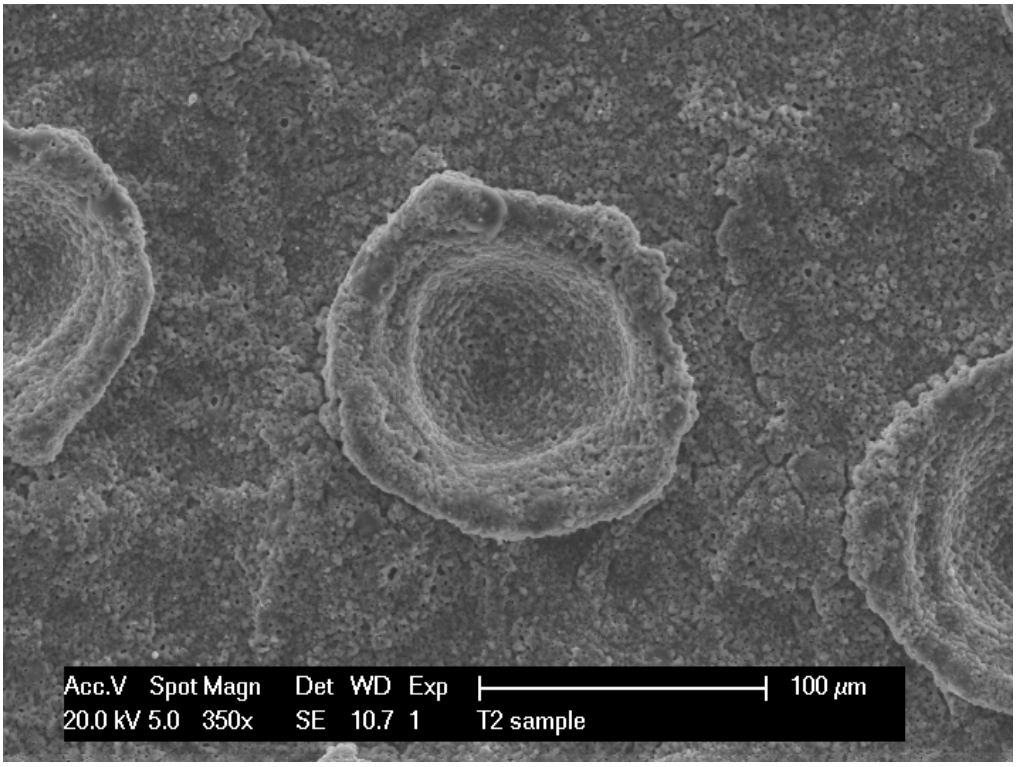

(B) Magnification: 350x

FIGURE B.11: SEM images of sample T2

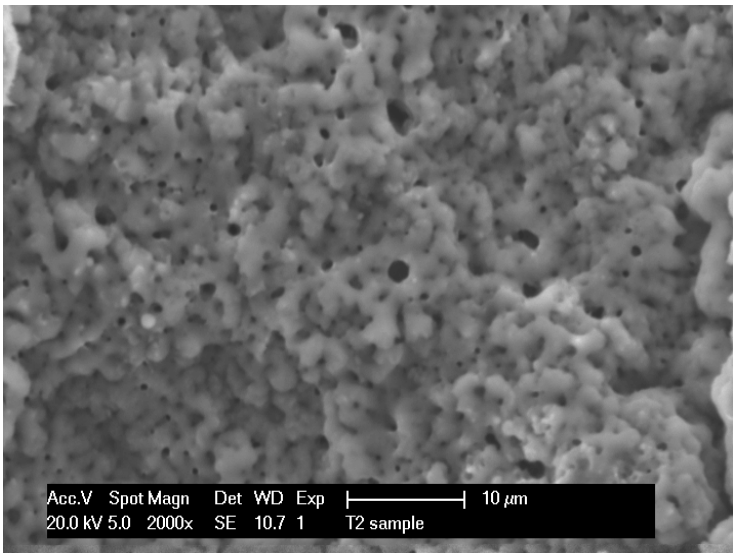

(A) Area between two dimples. Magnification: 2000x

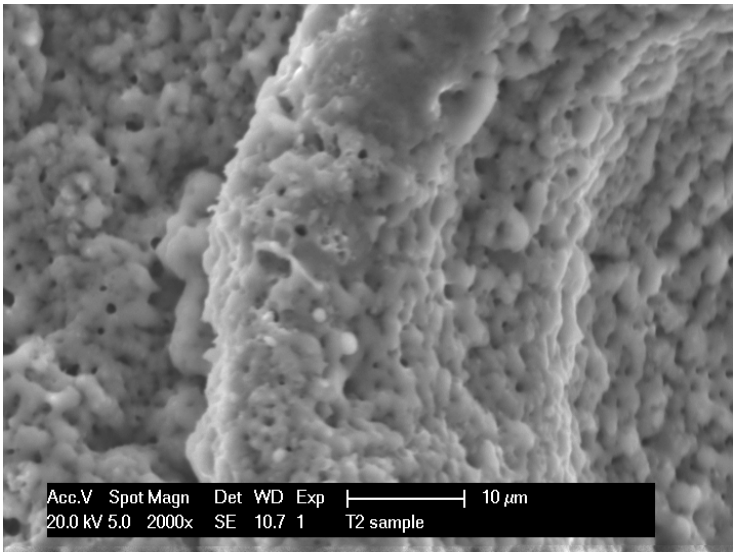

(B) A barbed part. Magnification: 2000x

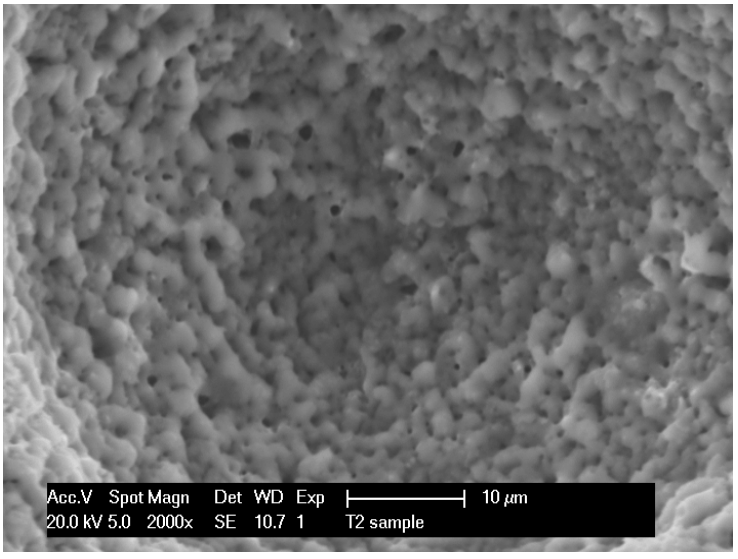

(C) Surface of a dimple. Magnification: 2000x

FIGURE B.12: SEM images of sample T2 showing porosity

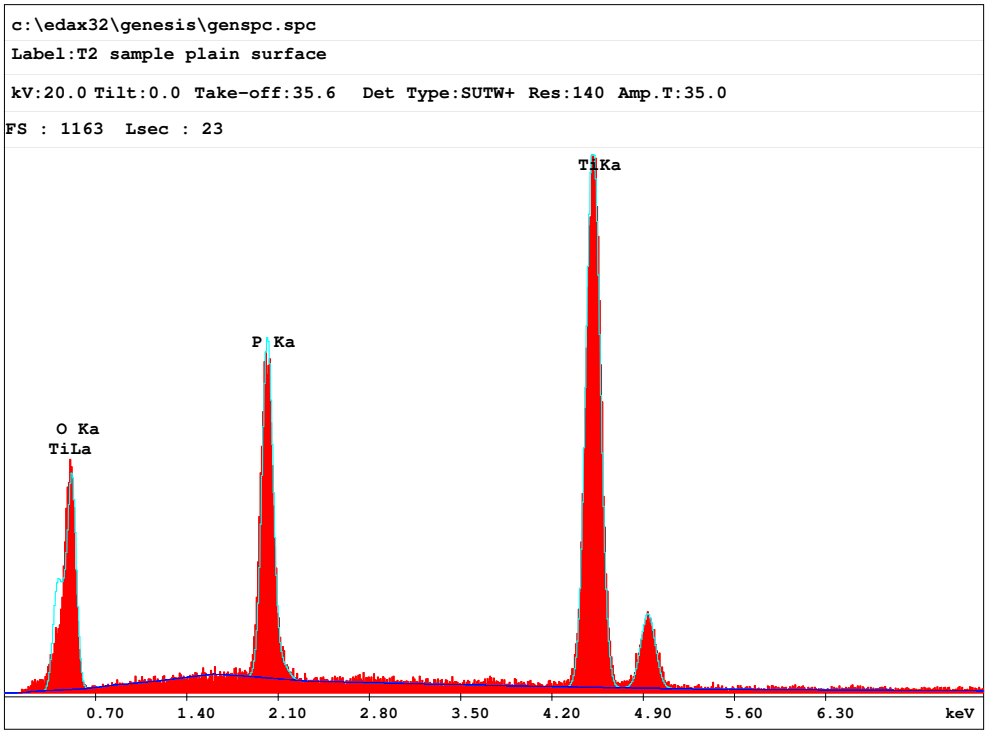

EDAX ZAF Quantification (Standardless)
Element Normalized
SEC Table : Default

Element	Wt %	At %
O K	42.07	65.75
P K	14.06	11.35
TiK	43.86	22.90
Total	100.00	100.00

Element	Net Inte.	Bkgd Inte.	Inte. Error	P/B
O K	120.22	2.55	1.92	47.20
P K	267.91	15.16	1.33	17.68
TiK	525.90	6.62	0.91	79.41

FIGURE B.13: EDS measurement of sample T2 on area between two dimples

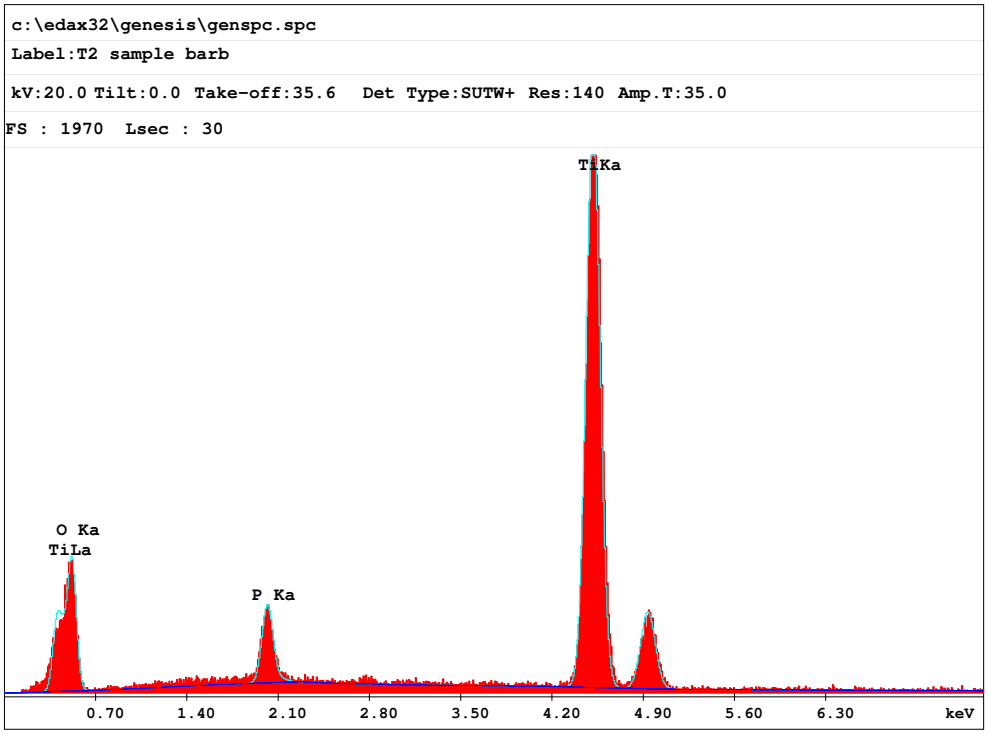

EDAX ZAF Quantification (Standardless)
Element Normalized
SEC Table : Default

Element	Wt %	At %
O K	38.70	64.55
P K	4.28	3.69
TiK	57.02	31.77
Total	100.00	100.00

Element	Net Inte.	Bkgd Inte.	Inte. Error	P/B
O K	97.36	1.72	1.87	56.67
P K	81.04	13.41	2.33	6.04
TiK	711.77	8.42	0.69	84.49

FIGURE B.14: EDS measurement of sample T2 on a barbed part

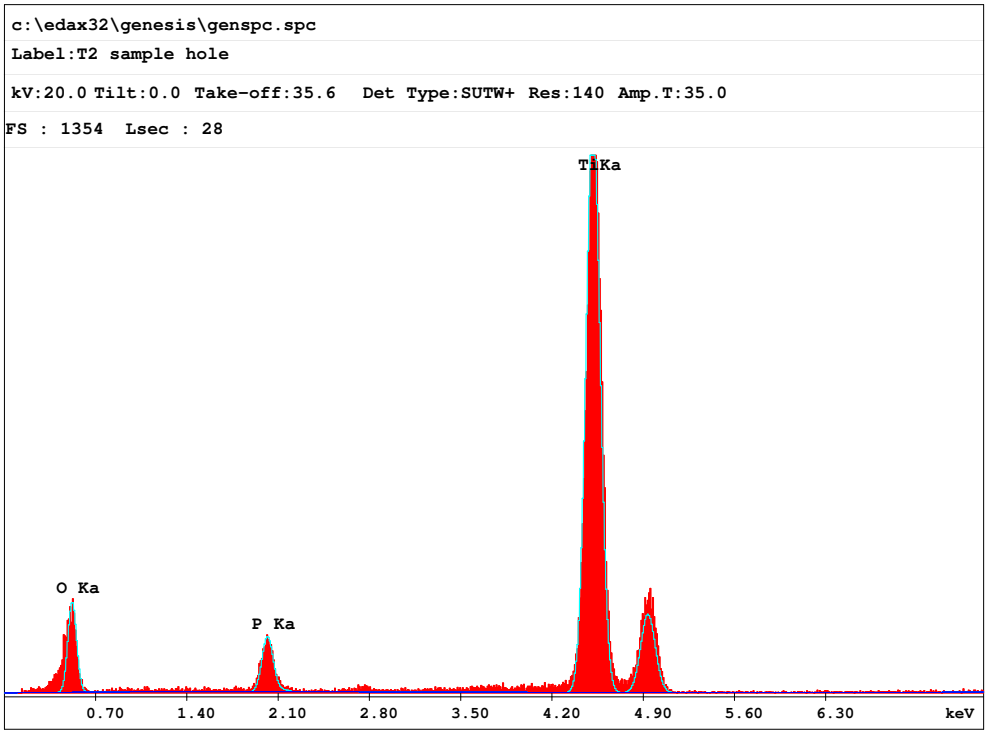

EDAX ZAF Quantification (Standardless)
Element Normalized
SEC Table : Default

Element	Wt %	At %
O K	33.30	59.27
P K	3.33	3.06
TiK	63.37	37.67
Total	100.00	100.00

Element	Net Inte.	Bkgd Inte.	Inte. Error	P/B
O K	50.95	0.42	2.63	122.08
P K	41.46	1.15	2.98	36.12
TiK	525.93	0.45	0.81	1163.23

FIGURE B.15: EDS measurement of sample T2 in a dimple

Appendix C

XRD diffractograms

The XRD measuring equipment was a Bruker AXS D8 Discover diffractometer.

- wavelength: CuK_{α}=0.15418 nm
- scanning range: 10...90°
- stepping angle 0.02°
- stepping time: 3 seconds

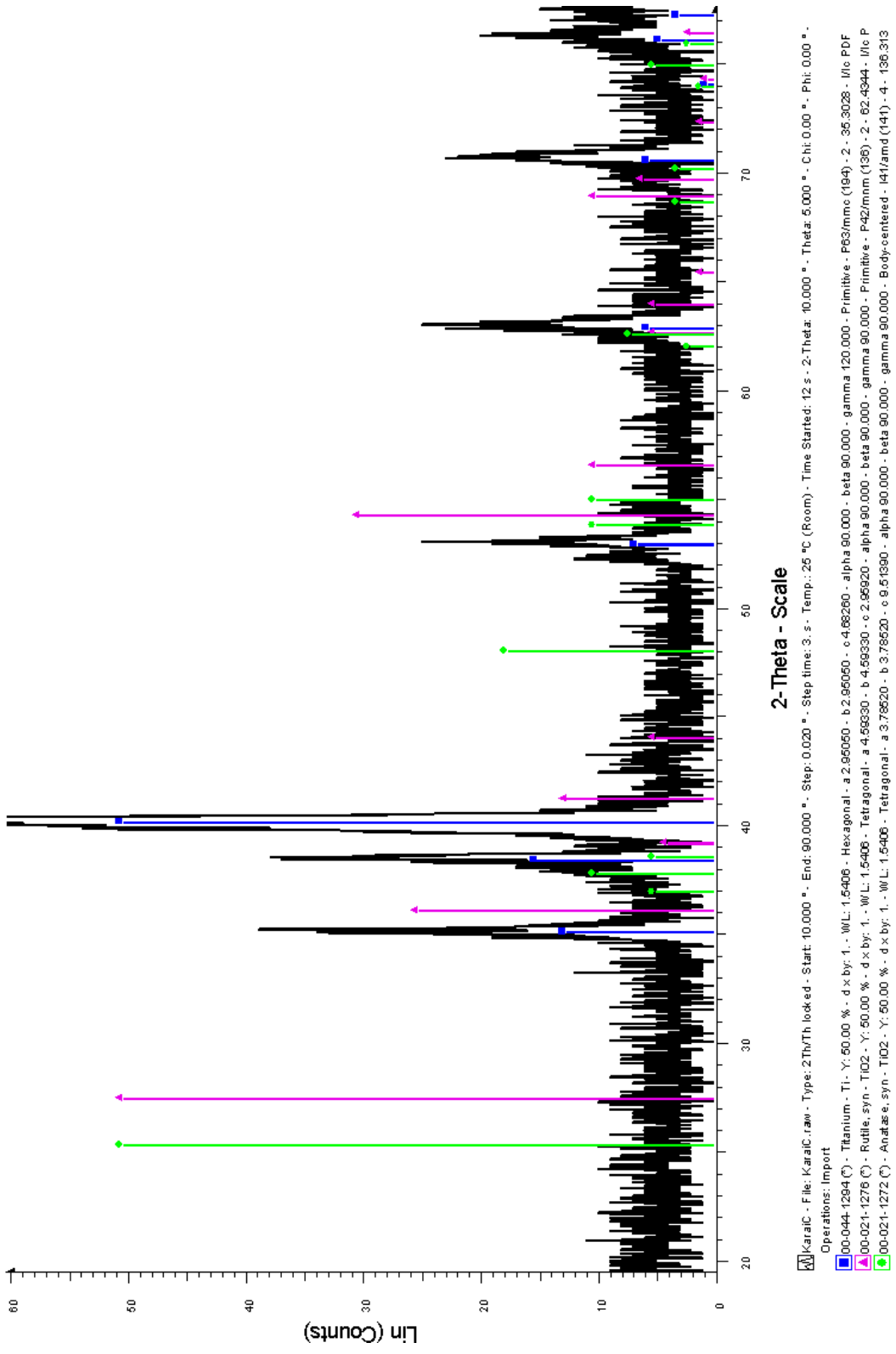

FIGURE C.1: XRD diffractogram of sample C. ■: α-Ti, ▲: rutile, ●: anatase.

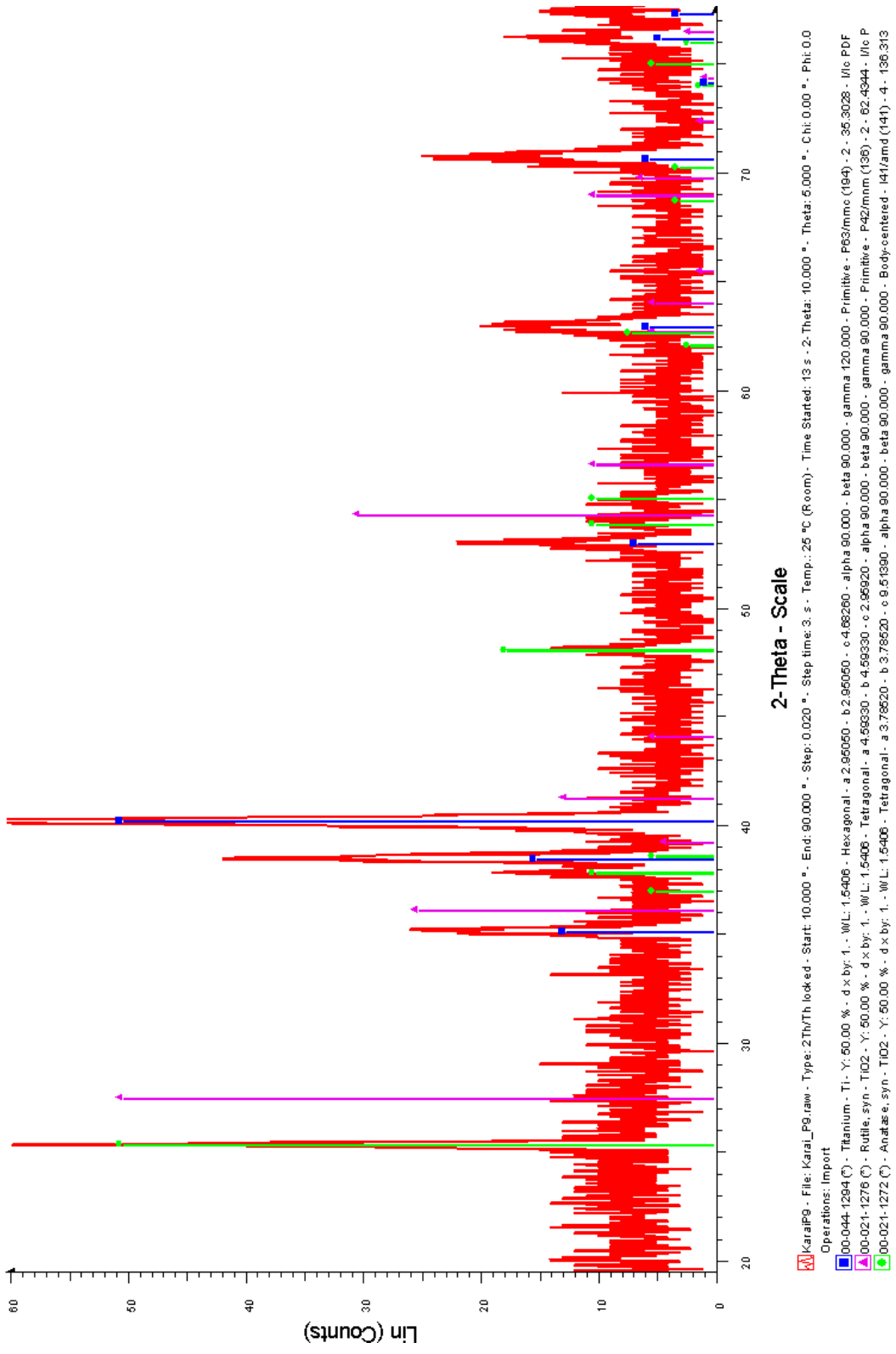

FIGURE C.2: XRD diffractogram of sample P. ■: α-Ti, ▲: rutile, ●: anatase.

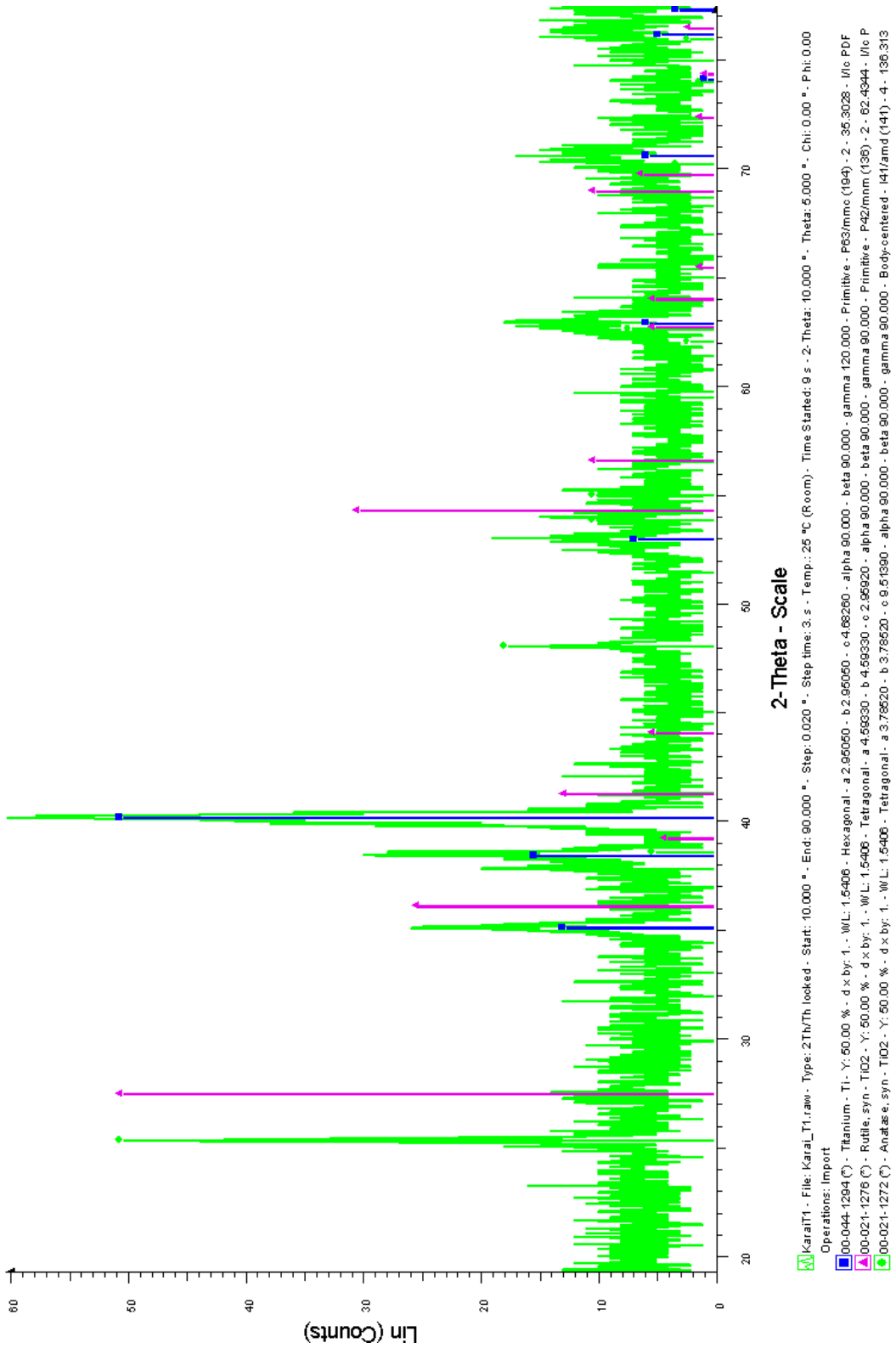

FIGURE C.3: XRD diffractogram of sample T1. ■: α-Ti, ▲: rutile, ●: anatase.

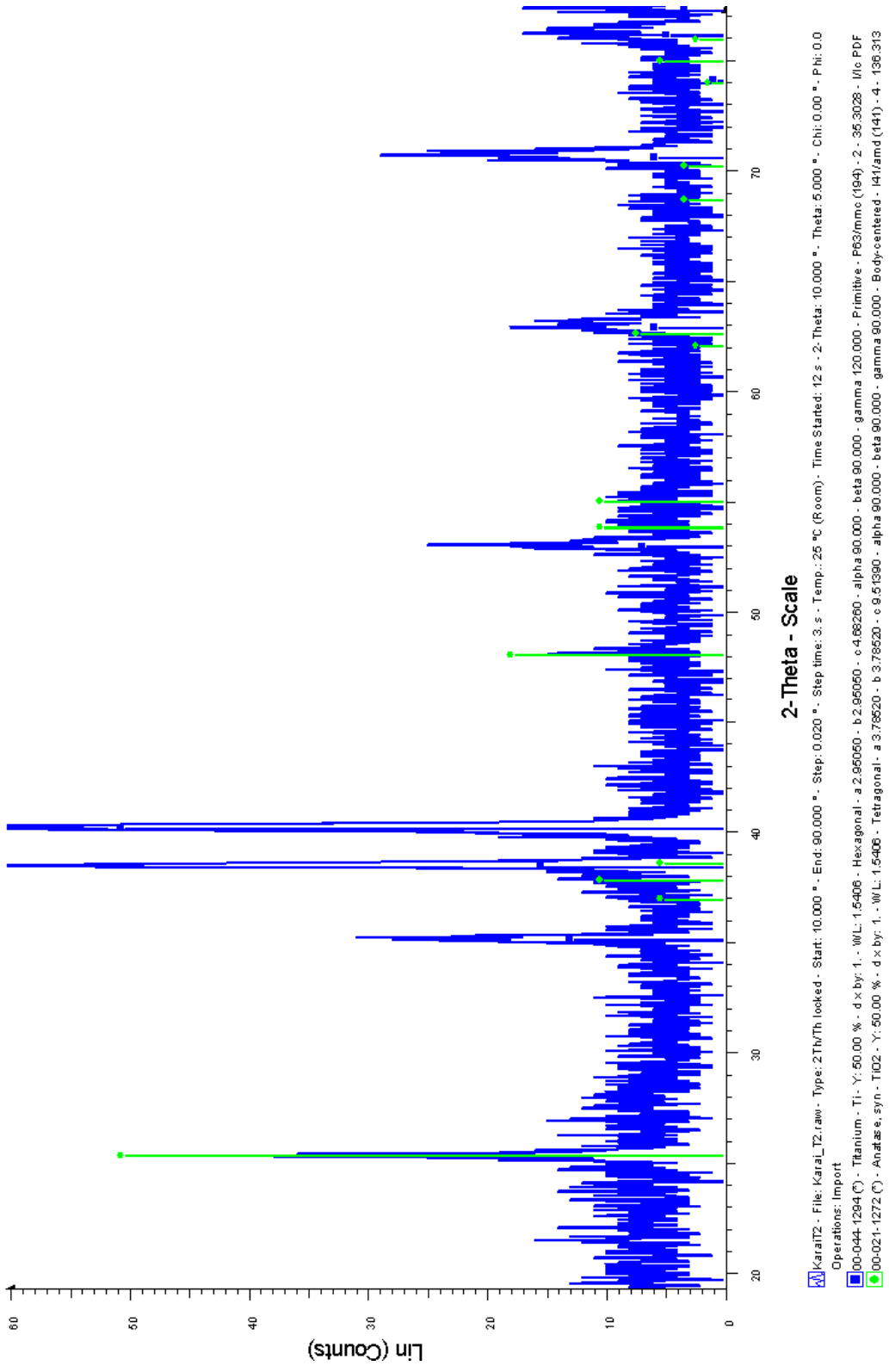

FIGURE C.4: XRD diffractogram of sample T2. ■: α-Ti, ●: anatase.

Appendix D

Diagrams of EIS measurements

The electrochemical measurements were controlled by a VoltaLab PGZ 301 equipment. Scribner Zview 2 software was used for the data evaluation.

D.1 C samples

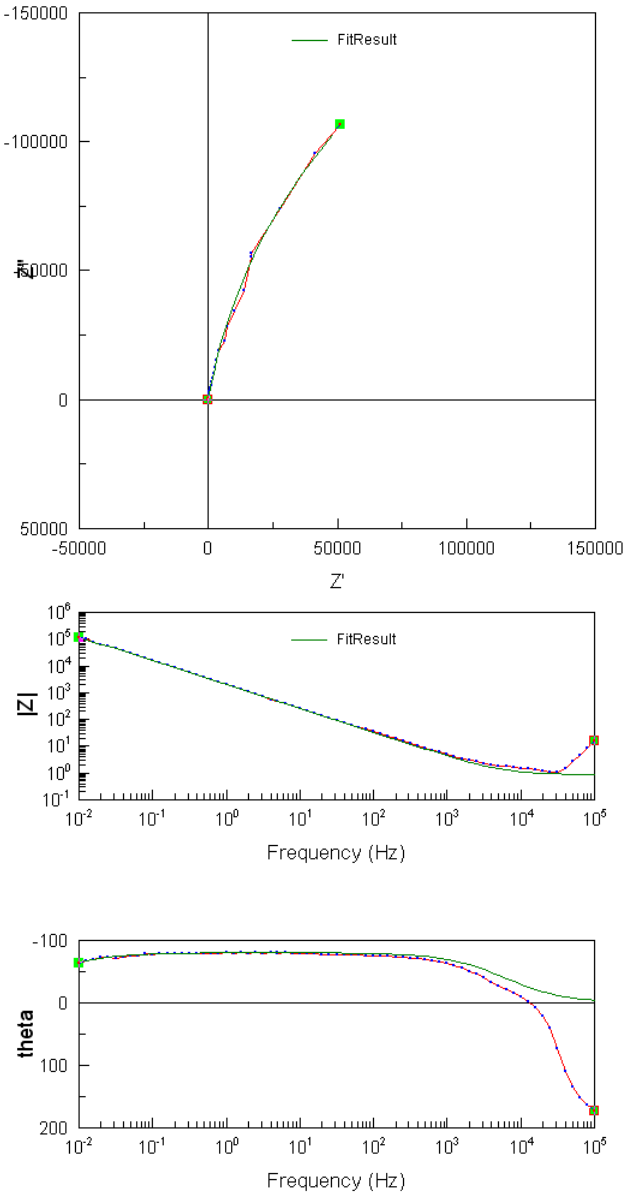

FIGURE D.1: Nyquist and Bode plot of sample C

FIGURE D.2: Equivalent circuit of sample C

D.2 P samples

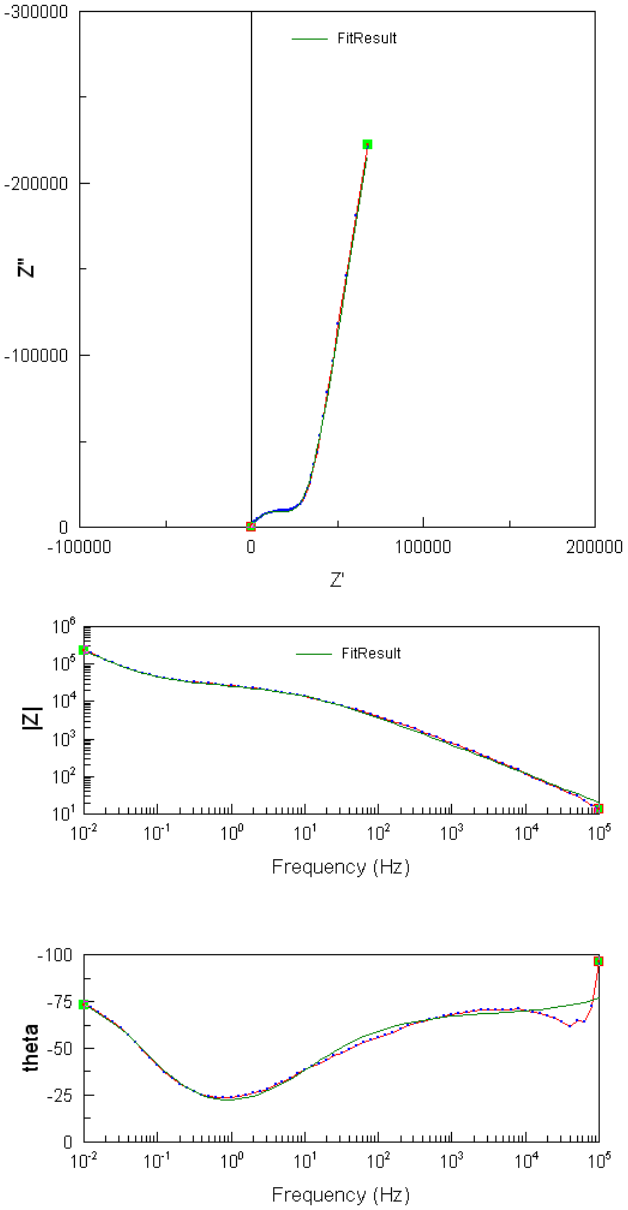

FIGURE D.3: Nyquist and Bode plot of sample P

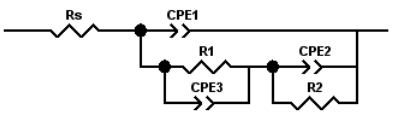

Element	Freedom	Value	Error	Error%
Rs	Fixed	-3,037	N/A	N/A
CPE1-T	Fixed	1,7437E-6	N/A	N/A
CPE1-P	Fixed	0,76659	N/A	N/A
R1	Free(±)	2,656E+11	6,4156E17	2,4158E8
CPE3-T	Free(±)	3,0435E-5	8,7242E-6	28,665
CPE3-P	Free(±)	0,08517	0,021832	25,633
CPE2-T	Free(±)	5,7113E-5	3,8494E-6	6,74
CPE2-P	Free(±)	0,91907	0,024275	2,6413
R2	Free(±)	1,385E+20	2,7888E12	2,0136E-6

FIGURE D.4: Equivalent circuit of sample P

D.3 T1 samples

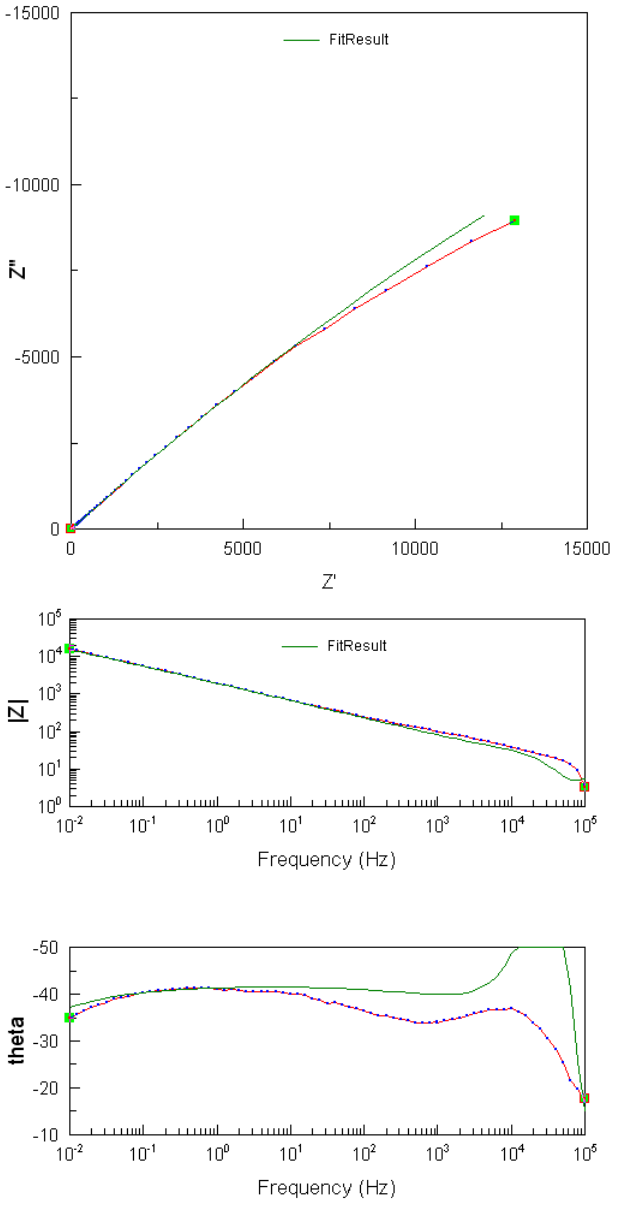

FIGURE D.5: Nyquist and Bode plot of sample T1

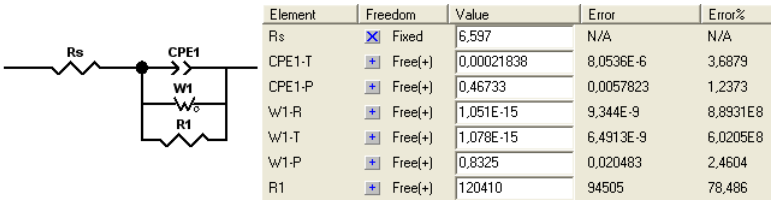

Element	Freedom	Value	Error	Error%
Rs	Fixed	6,597	N/A	N/A
CPE1-T	Free(+)	0,00021838	8,0536E-6	3,6879
CPE1-P	Free(+)	0,46733	0,0057823	1,2373
W1-R	Free(+)	1,051E-15	9,344E-9	8,8931E8
W1-T	Free(+)	1,078E-15	6,4913E-9	6,0205E8
W1-P	Free(+)	0,8325	0,020483	2,4604
R1	Free(+)	120410	94505	78,486

FIGURE D.6: Equivalent circuit of sample T1

D.4 T2 samples

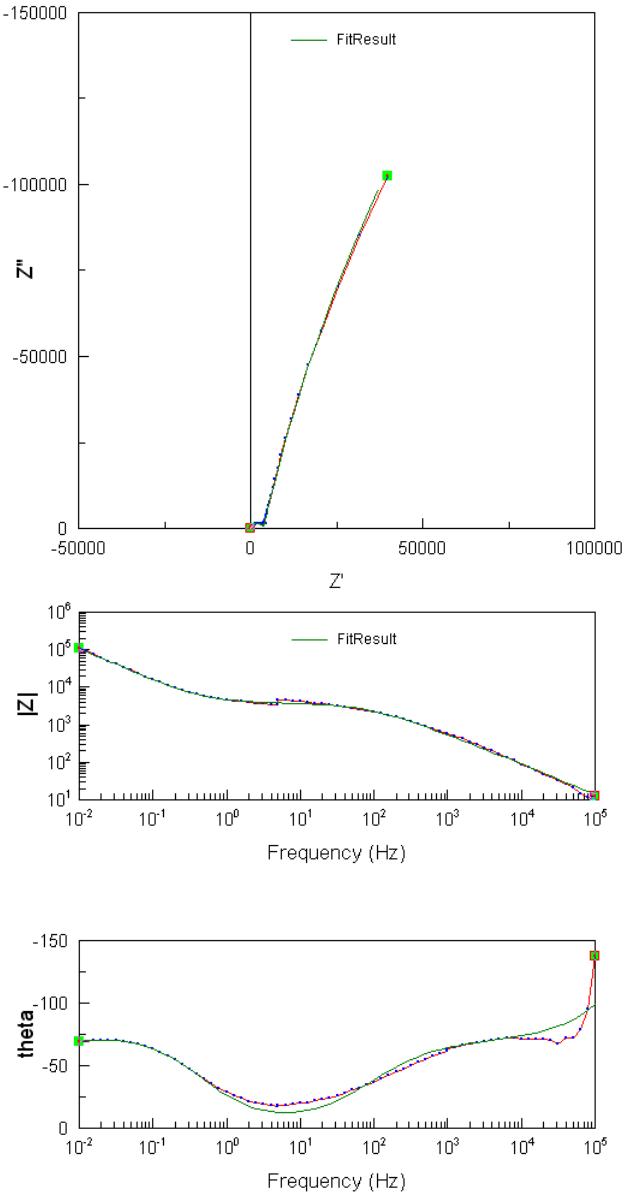

FIGURE D.7: Nyquist and Bode plot of sample T2

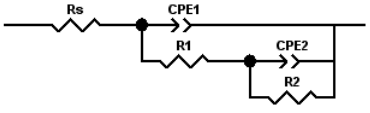

Element	Freedom	Value	Error	Error%
Rs	Free(±)	-7,153	0,94098	13,155
CPE1-T	Free(±)	1,7974E-6	1,5682E-7	8,7248
CPE1-P	Free(±)	0,78856	0,0088734	1,1253
R1	Free(±)	3933	106,22	2,7007
CPE2-T	Free(±)	9,9015E-5	2,8485E-6	2,8768
CPE2-P	Free(±)	0,86201	0,01777	2,0615
R2	Free(±)	956960	6,7911E5	70,965

FIGURE D.8: Equivalent circuit of sample T2

Bibliography

[1] Myer Kutz, editor. *Biomedical Engineering and Design Handbook Vol. 1.* McGraw-Hill, New York, NY, 2nd edition, 2009.

[2] Richard V. Curtis and Timothy F. Watson, editors. *Dental biomaterials - Imaging, testing and modelling.* Woodhead Publishing, Cambridge, England, 1st edition, 2008.

[3] Kenneth J. Anusavice, Chiayi Shen, and H. Ralph Rawls, editors. *Phillips' science of dental materials.* Elsevier, St. Louis, MO, 12th edition, 2013.

[4] Sebastian Bauer, Patrik Schmuki, Klaus von der Mark, and Jung Park. Engineering biocompatible implant surfaces - part 1: Materials and surfaces. *Progress in Materials Science*, 58:261–326, 2013.

[5] David F. Williams. On the mechanisms of biocompatibility. *Biomaterials*, 29: 2941–2953, 2008.

[6] Árpád Joób-Fancsaly. *Fogászati implantátumok felületi morfológiájának vizsgálata.* PhD thesis, Semmelweis University, 2003.

[7] Ashi Chug, Sagrika Shukla, Lanka Mahesh, and Sanjay Jadwani. Osseointegration—molecular events at the bone–implant interface: A review. *Journal of Oral and Maxillofacial Surgery, Medicine, and Pathology*, 25:1–4, 2013.

[8] T. Albrektsson, P.-I. Brånemark, H.-A. Hansson, and J. Lindström. Osseointegrated titanium implants. *Acta Orthopaedica*, 52:155–170, 1981.

[9] Robert B. Heimannand and Hans D. Lehmann, editors. *Bioceramic Coatings for Medical Implants.* Wiley-VCH, Weinheim, Germany, 1st edition, 2015.

[10] Xuanyong Liu, Paul K. Chu, and Chuanxian Ding. Surface modification of titanium, titanium alloys, and related materials for biomedical applications. *Materials Science and Engineering R*, 47:49–121, 2004.

[11] Gerd Lütjering and James C. Williams, editors. *Titanium (Engineering Materials and Processes).* Springer-Verlag, Berlin, Germany, 2nd edition, 2007.

[12] Yi Wang, Huijun Yu, Chuanzhong Chen, and Zhihuan Zhao. Review of the biocompatibility of micro-arc oxidation coated titanium alloys. *Materials and Design*, 85:640–652, 2015.

[13] Balakrishnan Munirathinam and Lakshman Neelakantan. Titania nanotubes from weak organic acid electrolyte: Fabrication, characterization and oxide film properties. *Materials Science and Engineering C*, 49:567–578, 2015.

[14] F.C. Campbell, editor. *Elements of Metallurgy and Engineering Alloys.* ASM International, Materials Park, OH, 1st edition, 2008.

[15] Shijuan Daia, Yu Wang, and Feng Chen. Effects of annealing on the microstructures and mechanical properties of biomedical cold-rolled ti–nb–zr–mo–sn alloy. *Materials Characterization*, 104:16–22, 2015.

[16] Ivana Kopova, Josef Stráský, Petr Harcuba, Michal Landa, and Lucie Bačákova Miloš Janeček. Newly developed ti–nb–zr–ta–si–fe biomedical beta titanium alloys with increased strength and enhanced biocompatibility. *Materials Science and Engineering C*, 60:230–238, 2016.

[17] M.A. Khan, R.L. Williams, and D.F. Williams. The corrosion behaviour of ti–6al–4v, ti–6al–7nb and ti–13nb–13zr in protein solutions. *Biomaterials*, 20(7): 631–637, 1999.

[18] M.C. Bottinoa, P.G. Coelho, M. Yoshimoto, B. König Jr., V.A.R. Henriquese, A.H.A. Bressiani, and J.C. Bressiani. Histomorphologic evaluation of ti–13nb–13zr alloys processed via powder metallurgy. a study in rabbits. *Materials Science and Engineering C*, 28:223–227, 2008.

[19] ASTM Designation: B265. Standard specification for titanium and titanium alloy strip, sheet, and plate, 2002.

[20] Madhav Prasad Neupane, Il Song Park, Tae Sung Bae, Ho Keun Yi, Fumio Watari, and Min Ho Lee. Biocompatibility of TiO_2 nanotubes fabricated on ti using different surfactant additives in electrolyte. *Materials Chemistry and Physics*, 134:536–541, 2012.

[21] L. Le Guéhennec, A. Soueidan, P. Layrolle, and Y. Amouriq. Surface treatments of titanium dental implants for rapid osseointegration. *Dental Materials*, 23:844–854, 2007.

[22] Bengt Wälivaara, Ingemar Lundström, and Pentti Tengvall. An in-vitro study of h2o2-treated titanium surfaces in contact with blood plasma and a simulated body fluid. *Clinical Materials*, 12:141–148, 1993.

[23] Yingmin Su, Satoshi Komasa, Tohru Sekino, Hiroshi Nishizaki, and Joji Okazaki. Nanostructured ti6al4v alloy fabricated using modified alkali-heat treatment: Characterization and cell adhesion. *Materials Science and Engineering C*, 59:617–623, 2016.

[24] M. Catauro, F. Bollino, and F. Papale. Preparation, characterization, and biological properties of organic–inorganic nanocomposite coatings on titanium substrates prepared by sol–gel. *Journal of Biomedical Materials Research Part A*, 102(2): 392–399, 2014.

[25] M. Catauro, F. Bollino, F. Papale, R. Giovanardi, and P. Veronesi. Corrosion behavior and mechanical properties of bioactive sol-gel coatings on titanium implants. *Materials Science and Engineering C*, 43:375–382, 2014.

[26] Sam Zhang, Zeng Xianting, Wang Yongsheng, Cheng Kui, and Weng Wenjian. Adhesion strength of sol–gel derived fluoridated hydroxyapatite coatings. *Surface & Coatings Technology*, 200:6350–6354, 2006.

[27] Takamitsu Mano, Yoshiya Ueyama, Kunio Ishikawa, Tomohiro Matsumura, and Kazuomi Suzuki. Initial tissue response to a titanium implant coated with apatite at room temperature using a blast coating method. *Biomaterials*, 23:1931–1936, 2002.

[28] Christian Leinenbach and Dietmar Eifler. Fatigue and cyclic deformation behaviour of surface-modified titanium alloys in simulated physiological media. *Biomaterials*, 27:1200–1208, 2006.

[29] Juanli Guo, Ricardo J. Padilla, Wallace Ambrose, Ingeborg J. De Kok, and Lyndon F. Cooper. The effect of hydrofluoric acid treatment of tio2 grit blasted titanium implants on adherent osteoblast gene expression in vitro and in vivo. *Biomaterials*, 28:5418–5425, 2007.

[30] Kuo-Yung Hung, Sung-Cheng Lo, Chung-Sheng Shih, Yung-Chin Yang, Hui-Ping Feng, and Yi-Chih Lin. Titanium surface modified by hydroxyapatite coating for dental implants. *Surface & Coatings Technology*, 231:337–345, 2013.

[31] R. Palanivelu, S. Kalainathan, and A. Ruban Kumar. Characterization studies on plasma sprayed (at/ha) bi-layered nano ceramics coating on biomedical commercially pure titanium dental implant. *Ceramics International*, 40:7745–7751, 2014.

[32] Wilhelm Pfleging, Renu Kumari, Heino Besser, Tim Scharnweber, and Jyotsna Dutta Majumdar. Laser surface textured titanium alloy (ti–6al–4v): Part 1 – surface characterization. *Applied Surface Science*, 355:104–111, 2015.

[33] Steven Mwenifumbo, Mingwei Li, Jianbo Chen, Aboubaker Beye, and Wolé Soboyejo. Cell/surface interactions on laser micro-textured titanium-coated silicon surfaces. *Journal of Materials Science: Materials in Medicine*, 18:9–23, 2007.

[34] Renu Kumari, Tim Scharnweber, Wilhelm Pfleging, Heino Besser, and Jyotsna Dutta Majumdar. Laser surface textured titanium alloy (ti–6al–4v) – part ii – studies on bio-compatibility. *Applied Surface Science*, 357:750–758, 2015.

[35] Jianguo Li, Hailhong Liao, Bahaman Fartash, Leif Hermanssoni, and Thomas Johnsson. Surface-dimpled commercially pure titanium implant and bone ingrowth. *Biomaterials*, 18:691–696, 1997.

[36] J. Chen, J.P. Ulerich, E. Abelev, A. Fasasi, C.B. Arnold, and W.O. Soboyejo. An investigation of the initial attachment and orientation of osteoblast-like cells on laser grooved ti-6al-4v surfaces. *Materials Science and Engineering C*, 29:1442–1452, 2009.

[37] D. Capek, M.-P. Gigandet, M. Masmoudi, M. Wery b, and O. Banakh. Long-time anodisation of titanium in sulphuric acid. *Surface & Coatings Technology*, 202: 1379–1384, 2008.

[38] Yonghao Gao. *Investigation of Plasma Electrolytic Oxidation of Commercially Pure Magnesium For Biomedical Applications*. PhD thesis, University of Sheffield, 2014.

[39] A.R. Rafieerad, M.R. Ashra, R. Mahmoodian, and A.R. Bushroa. Surface characterization and corrosion behavior of calcium phosphate-base composite layer on titanium and its alloys via plasma electrolytic oxidation: A review paper. *Materials Science and Engineering C*, 57:397–413, 2015.

[40] Long-Hao Li, Young-Min Kong, Hae-Won Kim, Young-Woon Kim, Hyoun-Ee Kim, Seong-Joo Heo, and Jai-Young Koak. Improved biological performance of ti implants due to surface modification by micro-arc oxidation. *Biomaterials*, 25: 2867–2875, 2004.

[41] T. Mi, B. Jiang, Z. Liu, and L. Fan. Plasma formation mechanism of microarc oxidation. *Electrochimica Acta*, 123:369–377, 2014.

[42] Jian zhi Chen, Yu long Shi, Lei Wang, Feng ying Yan, and Fu qiang Zhang. Preparation and properties of hydroxyapatite-containing titania coating by micro-arc oxidation. *Materials Letters*, 60:2538–2543, 2006.

[43] M. Shokouhfar, C. Dehghanian, M. Montazeri, and A. Baradaran. Preparation of ceramic coating on ti substrate by plasma electrolytic oxidation in different electrolytes and evaluation of its corrosion resistance: Part ii. *Applied Surface Science*, 258:2416–2423, 2012.

[44] S. Aliasghari, P. Skeldon, and G.E. Thompson. Plasma electrolytic oxidation of titanium in a phosphate/silicate electrolyte and tribological performance of the coatings. *Applied Surface Science*, 316:463–476, 2014.

[45] ISO 10993-15:2000. Biological evaluation of medical devices - part 15: Identification and quantification of degradation products from metals and alloys, 2000.

[46] Andrej M. Kielbassa, Rafael Martinez de Fuentes, Moshe Goldstein, Christoph Arnhart, Alberto Barlattani, Jochen Jackowski, Marko Knauf, Martin Lorenzoni, Carlo Maiorana, Regina Mericske-Stern, Eric Rompen, and Mariano Sanz. Randomized controlled trial comparing a variable-thread novel tapered and a standard tapered implant: Interim one-year results. *The Journal of Prosthetic Dentistry*, 101(5): 293–305, 2009.

[47] Ralf J. Kohal, Maria Bächle, Wael Att, Saad Chaar, Brigitte Altmann, Alexander Renz, and Frank Butz. Osteoblast and bone tissue response to surface modified zirconia and titanium implant materials. *Dental Materials*, 29:763–776, 2013.

[48] Pasqualina Naddeo, Luigi Laino, Marcella La Noce, Adriano Piattelli, Alfredo De Rosa, Giovanna Iezzi, Gregorio Laino, Francesca Paino, Gianpaolo Papaccio, and Virginia Tirino. Surface biocompatibility of differently textured titanium implants with mesenchymal stem cells. *Dental Materials*, 31:235–243, 2015.

[49] Guang Han and Zhijian Shen. Microscopic view of osseointegration and functional mechanisms of implant surfaces. *Materials Science and Engineering C*, 56:380–385, 2015.

[50] Byung-Soo Kang, Young-Taeg Sul, Se-Jung Oh, Hyun-Ju Lee, and Tomas Albrektsson. Xps, aes and sem analysis of recent dental implants. *Acta Biomaterialia*, 5: 2222–2229, 2009.

[51] ISO 5832-2:1999. Implants for surgery. metallic materials. part 2: Unalloyed titanium, 1999.